The Pennsylvania State University

The Graduate School

College of Earth and Mineral Sciences

STATE OF WATER IN PERFLUOROSULFONIC ACID MEMBRANES STUDIED BY MICROWAVE DIELECTRIC RELAXATION SPECTROSCOPY

A Thesis in

Materials Science and Engineering

by

Zijie Lu

Submitted in Partial Fulfillment
of the Requirements
for the Degree of

Doctor of Philosophy

December 2005

The thesis of Zijie Lu was reviewed and approved* by the following:

Digby D. Macdonald
Distinguished Professor of Materials Science and Engineering
Thesis Co-Advisor
Co-Chair of Committee

Evangelos Manias
Associate Professor of Materials Science and Engineering
Thesis Co-advisor
Co-Chair of Committee

Harry R. Allcock
Evan Pugh Professor of Chemistry

Michael T. Lanagan
Associate Professor of Engineering Science and Mechanics and Materials Science and Engineering

Gary Messing
Distinguished Professor of Materials Science and Engineering
Head of the Department of Materials Science and Engineering

*Signatures are on file in the Graduate School

ABSTRACT

The physical state of water in perfluosulfonic acid membranes (e.g., Nafion 117 and Flemion SH150) has been studied by the water sorption isotherms, DSC, ^{2}H NMR, and microwave dielectric relaxation spectroscopy. Different water states have been discriminated in these membranes: 1) the first few water molecules upon absorption from water vapor ($\lambda \sim 3$, where λ denotes the number of water molecules per sulfonic acid group) are tightly bound to the sulfonic acid group to form the first hydration water; 2) beyond this water content, water molecules form the second hydration layer of the sulfonic acid group. The amount of this water increases with water content, but reaches a constant value at higher water contents. The microwave DRS measurements showed a relaxation time of about 30 ps for this type of water; 3) the free water, locating at the center of the ion cluster regions where the ion-water interaction is negligible, is present when $\lambda \geq 6$. The free water, with relaxation time $\tau \approx 8$ ps at $25^{o}C$, shows the characteristic dynamics of bulk water; and 4) finally, as water content increases further, water molecules start to be associated with the perfluorinated side chains and even with the fluorocarbon backbone. A much longer relaxation time, $\tau \approx 90$ ps, is observed for this part of water due to the hydrophobic confinement by the polymer. Microwave DRS measurements showed markedly different dynamics, i.e., negligible activation enthalpy and large negative activation entropy, for the dielectric relaxation of this type of water. The presence of the hydrophobically confined water is found to correspond to the clustering of water and to the appearance of the freezing water in these membranes.

The equivalent weight (EW) of the PSA membrane has been found to have considerable influence on the dielectric response of the membranes. Flemion SH150, which has an EW value of 909, shows higher static permittivity than Nafion 117, which has an EW of 1100. This is consistent with the higher water sorption by Flemion SH150 at the same water activity. The “free” and “hydrophobically confined” water are found to start to appear at lower water content in Flemion than in Nafion. These results may suggest that Flemion SH150 membrane is likely to form larger and/or more numerous ionic cluster regions.

The free water provides a pathway to the fast proton conduction in the membranes. Optimization of the proton conductivity requires maximization of the free water content. Dimethyl sulfoxide was found to increase the fraction of “free water” in PSA membranes due to its strong ability to form hydrogen bonding with water molecules. This increase leads to increasing conductivity of Nafion/DMSO at lower water content. However, the Nafion/DMSO membrane showed lower conductivity at high water contents. This can be explained by the longer relaxation times for the solvent mixture, compared to pure water.

TABLE OF CONTENTS

LIST OF FIGURES

LIST OF TABLES

ACKNOWLEDGEMENTS

The author would like to express his sincere gratitude to his thesis advisors, Dr. Digby D. Macdonald and Dr. Evangelos Manias, for their guidance, encouragement, and patience throughout this work. Sincere gratitude is also extended to Dr. Michael Lanagan for his kind help and valuable suggestions in overcoming the numerous problems of microwave dielectric measurement. The author especially thanks Dr. Harry R. Allcock for his suggestions on this work and careful review of this manuscript.

Special appreciation is also extended to S. Perini for his help in the experimentation, to Rajah Kalid for assistance in software, and to Dr. Georgios Polyzos for assistance in data fitting. Furthermore, the author is indebted to all the members of the Center for Electrochemical Science and Technology for their help and suggestions.

A special thanks is given to my wife for all her love, support, and encouragement, which is so valuable to my life and my work. And finally, great thanks are given to my new-born daughter who has brought extra joy into my life.

Chapter 1

Introduction

Increasing interest in studies of solid electrolytes, mostly perfluorosulfonic acid (PSA) membranes, is inspired by their active application in proton exchange membrane (PEM) fuel cells, which are considered to be the most promising power sources for future automotive and stationary applications [1]. In fuel cell applications, the perfluorosulfonic acid membranes function as ion-conductive media and also as separators of gaseous reactants. In their ion conduction mode, PSA membranes have sufficiently high conductivity (0.06 S/cm at 30 ^{o}C for highly hydrated Nafion [2]) to find application in fuel cells. In separation technologies, PSA membranes work as molecular sieves letting through water molecules and blocking the transport of organic contaminants and gas reactants.

In this chapter, the structure and morphology of perfluorosulfonic acid (PSA) membranes is first introduced. The physical state and importance of water in these membranes are then reviewed. Finally, the proton conduction mechanisms in PSA and in liquid water are introduced.

1.1 Perfluorosulfonic acid (PSA) membrane

Nearly all of the currently commercially available PEM membranes are perfluorosulfonic acid membranes, e.g., Nafion produced by du Pont de Nemours & Co.

[3]. PSA membranes are composed of a polytetrafluoroethylene backbone and perfluorinated pendant side chains terminated by a sulfonate ionic group. The reported chemical structure of Nafion for PEM membranes is shown in Fig. 1.1. The polymeric composition is conventionally expressed in terms of equivalent weight (EW), which is defined as the mass of dry polymer (in grams) that contains 1 mole of sulfonate ion exchange groups. For example, Nafion 117 has an EW of 1100, which corresponds to an x value of around 6.5.

In theory, the ion content can be varied by changing the ratio of x to y, as seen in Fig. 1.1. Nafion has been commercially available in 900, 1100, 1200, and other equivalent weights. However, Nafion 1100 EW in thicknesses of 2, 5, and 7 mil (Nafion 112, 115, and 117, respectively) seem to be the only grades of Nafion that are currently widely used. This equivalent weight provides high protonic conductivity and moderate swelling in water, which suits most current PEM fuel cell applications. Other perfluorosulfonated ionomers with similar structures have also been developed by the Asahi Glass Company (under the name of Flemion) [4] and the Dow Chemical Company [5].

Perfluorosulfonic acid membranes have been described as a three-region structure: a hydrophobic domain formed by the fluorocarbon matrix, a hydrophilic domain containing sulfonic groups, counter-ions, and water, and an interfacial region of intermediate hydrophilicity [6]. One important feature of such a microstructure is that the hydrophobic part provides relatively good mechanical stability, even in the presence of water, while the hydrophilic aqueous domains provide high proton conductivity.

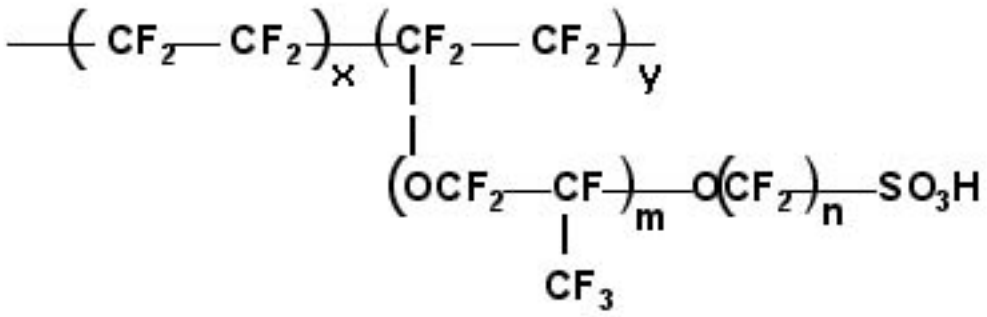

Fig. **1.1**: Chemical structure of perfluorosulfonic acid polymers. Nafion: x=5–13.5, y=1, m≥1, n=2.

Many models have been proposed for the morphology of these materials [7]. During the early efforts to understand the morphology of Nafion, a cluster-network model was proposed by Gierke *et al.* [8,9]. Based on Small-Angle X-ray Scattering (SAXS) studies, this model suggests that the ion clusters were inverted micellar spheres with diameters ranging from 40-50Å, interconnected by channels with a diameter and length of 10-20Å. This model gained wide acceptance and had been serving as a conceptual basis for rationalizing the properties of Nafion membranes. However, there is no direct experimental evidence, so far, for the existence of channels, which were invoked to account for inter-cluster ion hopping.

Over the following period of about two decades, numerous models were proposed for the morphology of dry and hydrated Nafion based on information gathered from small- and wide-angle X-ray scattering, neutron scattering, and neutron diffraction studies. These models include a core-shell model proposed by Fujimura *et al*. [10], a lamellar model proposed by Litt [11], a sandwich-like model proposed by Haubold *et al*. [12], and a rod-like model proposed by Rubatat *et al*. [13]. Kreuer summarized most of these models and put forth a self-consistent picture for the morphology of Nafion membrane [14]. The nanoscopic view, depicted in Fig. 1.2, is described as an arrangement of low-dimensional polymeric objects (which can be termed “clusters”), the spaces between which are filled with water (channels). This picture is based on the SAXS experiments [15], pulsed-field-gradient (PFG)-NMR measurements, and on broadband dielectric spectroscopy studies [16,17]. It is worth noting that the nanoscale morphology seen in Fig. 1.2 is rather similar to that seen in the AFM images of McLean *et al*. [18].

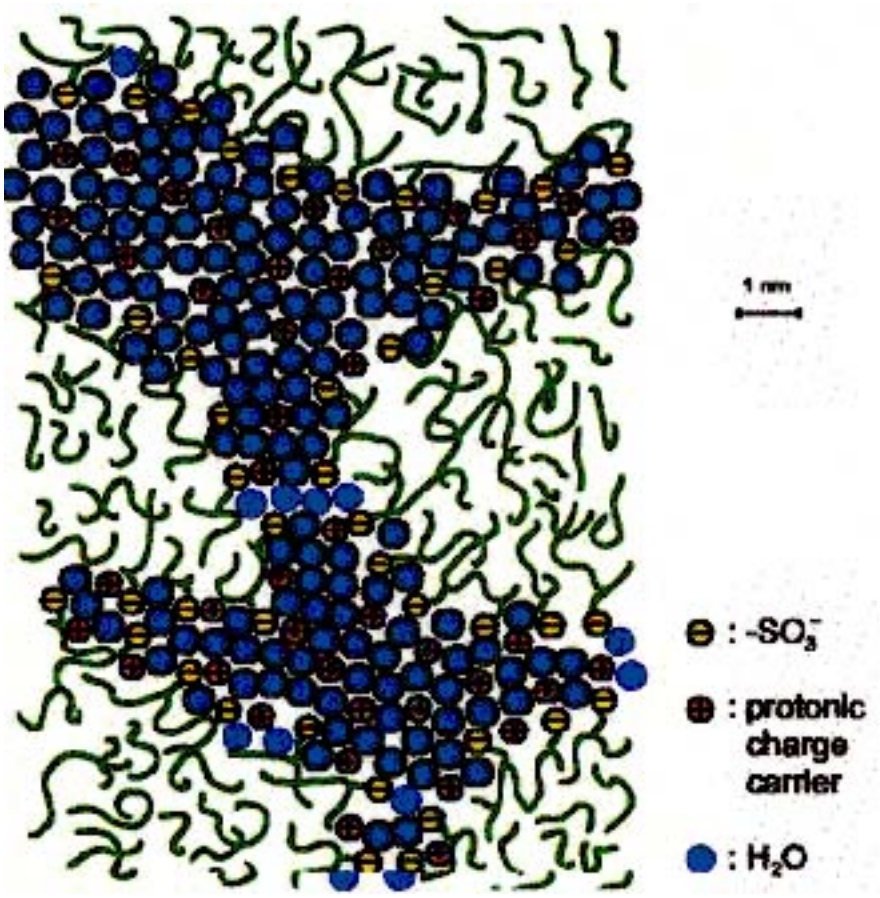

Fig. **1.2**: Schematic representation of the nano-phase separation in the hydrated morphology of Nafion [**14**]. This scheme illustrates the distinctions in the hydrophilic/hydrophobic separation, connectivity of the water and ion domains, and separation of the $-SO_3^-$ groups.

Based on a thorough analysis of Nafion over a wide range of water content, Gebel proposed a conceptual description for the swelling and dissolution process, shown schematically in Fig. **1.3** [**15**]. In this model, the isolated, spherical ionic clusters in the dry membrane swell with the absorption of water. As the water content increases to between $\phi_w = 0.3$ and 0.5 (volume fraction of water), structural inversion occurs and a normal micelle structure (polymer core surrounded by a counter-ion shell) is obtained, as in the model proposed by Rollet *et al*. [**19**]. At $\phi_w > 0.5$, the structure resembles a connected network of rods. Finally, as the membrane dissolves into the solution, the rodlike structures separate to yield a colloidal dispersion of isolated rods. The rodlike structure is prevalent for the morphology of Nafion solution in water and ethanol [**20**].This model offered a plausible mechanism for the evolution in structure as the water content increases. However, more experimental evidence is needed to support the phase inversion process occurred at $\phi_w = 0.5$.

From the above discussion, it is obvious that the morphology of hydrated Nafion has not been determined with certainty. The source of the debate results from the fact that this unique ionomer has a random chemical structure that is capable of organizing in a number of complex formations of ionic and crystalline domains with a significant distribution in dimensions over a wide range of length scales. Moreover, the microstructure and properties of Nafion are known to be quite sensitive to the history and details regarding preparation of samples for analysis.

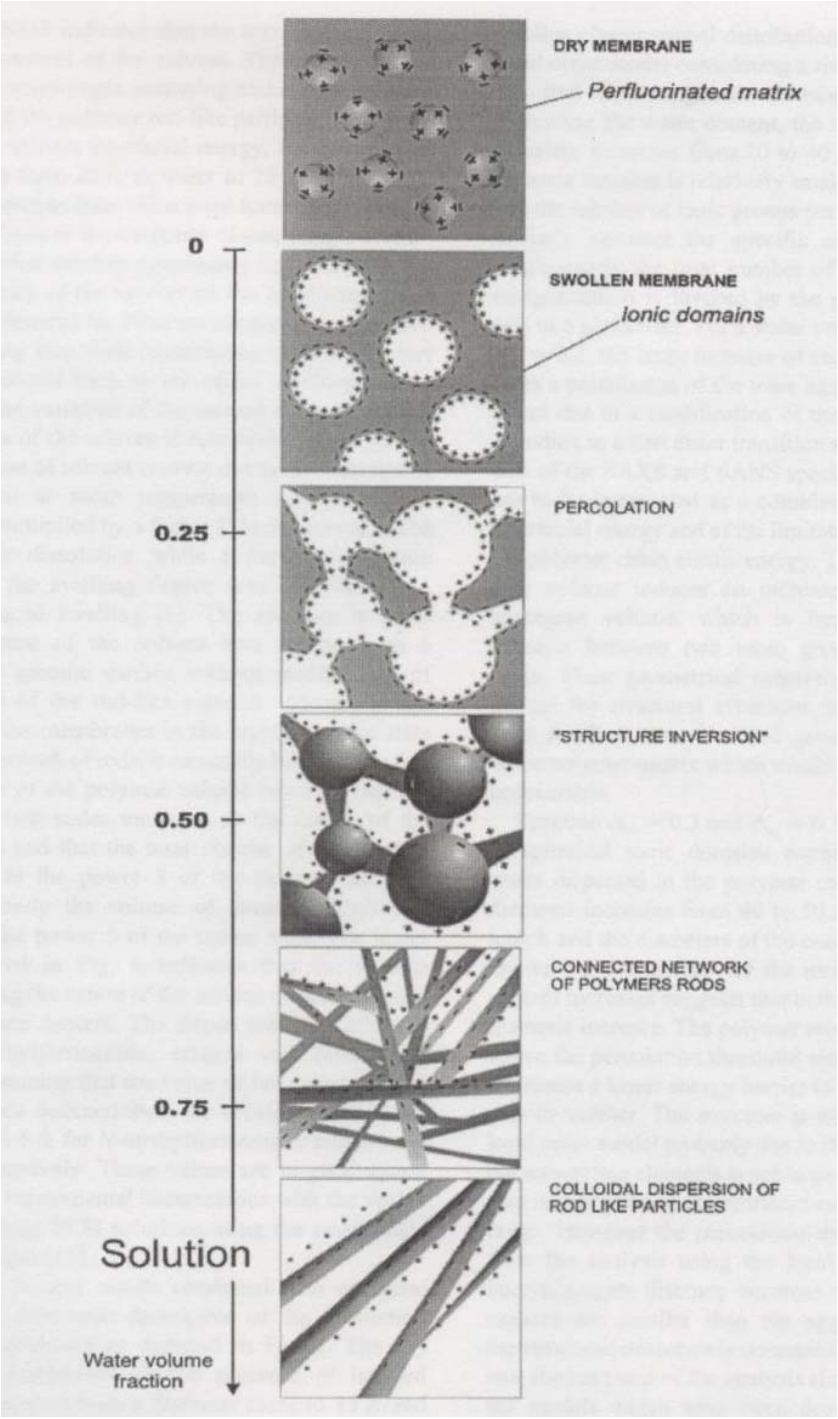

Fig. **1.3**: Conceptual model for the morphological reorganization and connection of the ionic domains in Nafion as the dry membrane is swollen with water to the state of complete dissolution [**15**].

1.2 The nature of water in PSA membranes

In hydrated PSA membranes, water and protons are confined to domains with dimensions of only nanometers. Because the water is confined, its structural and dynamical properties are distinct from bulk water, a trend that becomes even more significant as the water content is decreased and the density of anionic groups is increased. Thus, the state or nature of the water has direct consequences for the transport properties (dissociation, transfer, and transport) of the protons within the membranes.

The physical state of water in Nafion has been characterized by several techniques. Falk *et al*. [22,23] conducted FTIR studies of the structure of water in this ionomer, and their work served as an excellent resource for the various band assignments. The fundamental bands of the HDO isotope of water in Nafion were carefully studied. The O-H groups in water molecules were found to exist in two different molecular environments. The low frequency component was associated with hydrogen bonded O-H groups, while the high component reflected non-hydrogen bonded O-H groups, which are assumed to belong to H_2O molecules at the hydrophobic-hydrophilic interface. Falk concluded from the infrared studies that the hydrated clusters are highly nonspherical in shape, with a significant amount of water in the clusters associated with the fluorocarbon phase. This view is commensurate with the structures displayed in pictures by Kreuer [14]. Despite the considerable hydration capacity of Nafion, hydrogen bonding between water molecules in maximally hydrated membranes is considerably less extensive than that in liquid water [21,22]. This situation might be rationalized in terms of the large relative population of water molecules that reside at hydrophobic-hydrophilic interfaces,

as these surface water molecules have fewer hydrogen bonds. The specific water-polymer interaction will be further discussed in the following section.

The idea of rough interfaces suggested by the FTIR measurements [22,23] implies that water molecules are not entirely confined in a hydrophilic environment; instead, part of the water is associated with the hydrophobic side chains or polymer backbone. This is in contrast with the view of Rollet *et al*. [24], who concluded that the ionic domains are spherical and that interfaces between hydrophobic and hydrophilic phases are sharp. The recent FTIR/ATR studies by Cable *et al*. [25] suggested that parts of the perfluoronated side chains penetrate the ionic clusters rather than forming a neat inverted micelle as depicted in the Gierke model [8,9]. The near-IR (NIR) spectroscopy measurements for water in Nafion, conducted by Barnes *et al*. [26], also indicated that a fraction of water molecules reside close to the fluorocarbon backbone. The main advantage of using NIR is that band shifts due to hydrogen bonding are greater than the characteristic bands in the mid-IR range. Two types of water, non-hydrogen-bonded and hydrogen-bonded water, were observed in Nafion.

The molecular mobility of water in perfluorosulfonic acid membranes was investigated by nuclear magnetic resonance (NMR) spectroscopy [27-29]. The water in the ionomer was less mobile than in liquid water and showed a cooperative character with the mobility. This means that the water molecules strongly interacted with the ionic groups in the ionomers. The temperature dependences of the ^{1}H T_1 (spin-lattice) and T_2 (spin-spin) relaxations for water in Nafion in acid [30,31]] and in alkali ion forms [32] have been measured. The correlation time for water molecule motion in the membrane was found to be somewhat longer than that in supercooled liquid water but much shorter

than that in ice. A highly ordered, supercooled fluid of hydrogen bonded water was suggested to exist. These authors favored the idea of supercooled water whose structure is influenced by being in pores, as opposed to the idea of freezing water. The expressed explanation for this phenomenon was that water forms complex cage-like structures, or clathrates, of a number of molecules and groups.

The existence of different states for water in Nafion in acid and alkali metal forms was also observed by Differential Scanning Calorimetry (DSC) measurements [**33**,**34**]. The water molecules were classified into three categories: nonfreezing, freezing-bound, and free water. The freezing-bound water crystallizes at a lower temperature than free water. The heat of fusion of pure water and the areas under the exothermic peaks were used to calculate relative free versus freezing-bound water content. In plots of the amounts of the three types of water with increasing total water content, it is seen that a threshold must be exceeded before freezing water (including free water and freezing-bound water) can exist. Nonfreezing water molecules were considered to exist in hydration shells around the given counter-ions. Presumably, mobility restrictions placed on ion-contacting water molecules, imposed by the strong electric fields, prevent these water molecules from crystalline packing, as in the so-called “structure-breaking” effect in simple aqueous electrolytes.

The average heat of absorption per water molecule for 1200 EW acid Nafion has been measured with differential microcalorimeter analysis combined with the simultaneous water vapor isotherm (i.e., water uptake vs. relative humidity) [**35**]. Different heat of water absorption was obtained for different hydration states, indicating two types of water in Nafion. At low water content, up to 5 H_2O per SO_3H group, the

average heat of water absorption was exothermic and remained at a constant value of -50 kJ/mol, which was assumed to be associated with water of hydration. At higher water content, the heat of water absorption continuously decreased to about 17 kJ/mol, which is approximately the strength of a hydrogen bond in liquid water. The energy for the second type of water was found to be sensitive to the heat treatment. The amount of hydration water was found to be 5-6 H_2O per SO_3H group from the water vapor isotherm measurements [**35**,**36**].

In attempting to elucidate the connection between the hydration state and the nature of the water in the membrane, Paddison *et al*. [**16**,**17**] measured the dielectric spectrum of both Nafion and PEEK membranes in the microwave region (0.045–30 GHz). Their rationale for carrying out measurements with an oscillating electric field frequencies as high as 30 GHz was based on the observation that the principal absorption band attributed to a Debye-type relaxation of molecular origin in pure bulk water occurs at about 18 GHz [**37**]. Their results show a strong dependence in the dielectric constant and loss factor in the Nafion membranes with water content but a much weaker dependence in the PEEK membranes. The explanation is that, owing to the stronger confinement of water in the narrow channels of the PEEK membranes, the dielectric constant of hydrated PEEK is lower (i.e., the water molecules are more tightly bound to each other and to the fixed sulfonate groups) than that of Nafion. The drawback or limitation in such experiments is that the results reflect only the dielectric response of the bulk material (i.e., both the polymer and the water) and, thus, specific information concerning the water in the pores is somewhat obscured. In an effort to quantify the state of the water in the nanopores of hydrated PEMs on a more microscopic level, Paul and

Paddison [38,39] calculated the radial profiles of the relative permittivity for Nafion at various degrees of hydration. Their calculation was based on statistical thermodynamics and the assumption of a cylindrical PEM pore with a radially symmetric distribution of point charges (for the fixed $-SO_3^-$ groups). The dielectric constant as a function of radial position for Nafion membranes with water contents of λ = 6, 13, and 22.5 is plotted in Fig. 1.4. From these calculations, the permittivity of the water in the center of the pores at the higher two water contents reaches that of bulk water (ε = 80) and reduces to only about 60 at the lower water content λ = 6. Another important finding is that the permittivity of water decreases rapidly with increasing distance from the center of a pore. All of these plots show an ordering in the water (as witnessed in a reduction in dielectric constant) that occurs when one approaches the first two monolayers of water around the fixed anionic sites.

1.3 Hydrogen bonding of water in the confined environment

To study the structure and dynamics of water within PSA membranes, an important aspect is the interaction of water with the sulfonic acid groups (SO_3H), which is hydrophilic in nature. On the other hand, part of the water is closely associated with the perfluorinated side chains and even with the fluorocarbon backbone, as indicated by FTIR and DSC measurements [21-23,33,34]. Hence, the interactions of water with the hydrophobic polymer can not be excluded. It is known that the behavior of water can change radically in going from a hydrophilic environment to a hydrophobic one [40,41].

It is thus important to understand the differences between water confined in hydrophilic and hydrophobic environments [42,43].

The characteristic feature of water is its three-dimensional hydrogen bonding network [44], which has the following features: (a) a large number of “intact” intermolecular hydrogen bonds; (b) the directionality of the bonds strongly imposes a local tetrahedral structure; and (c) a short “lifetime” of the hydrogen bonds (i.e., in the picosecond range). In the following section, the meaning of these concepts and how they are modified by the hydrophilic and hydrophobic confinement will be discussed. Since little prior work has been done on PSA membranes, the discussion is given on a general basis.

A common structural effect of nanoconfinement on water is that water exhibits layering near pores, whether they are hydrophobic or hydrophilic [45-49]. However, the number and dynamics of water-water hydrogen bond are different when confined in hydrophilic or hydrophobic walls.

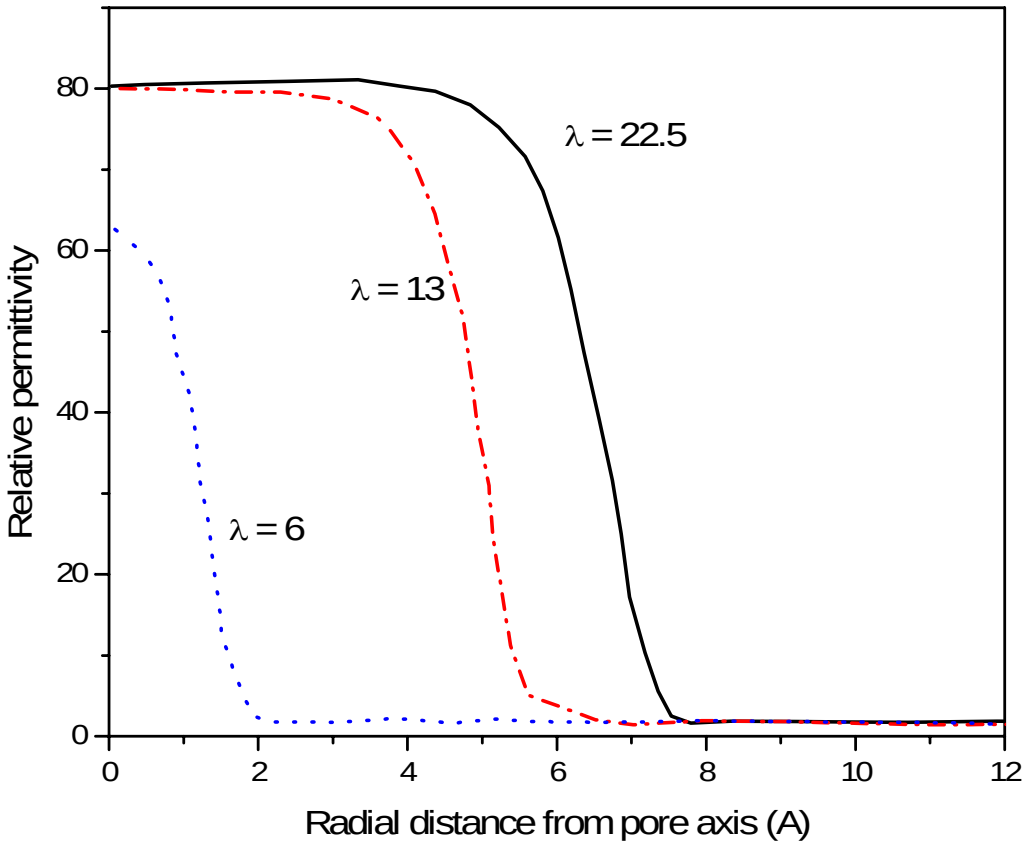

Fig. **1.4**: Computed radial dependence of the relative permittivity of the water in the pores of Nafion membranes with hydration levels (λ) of 6, 13, and 22.5 water molecules per sulfonic acid group [**39**].

Charged and hydrophilic pore surfaces interact with water through electrostatic forces, such as dipole-dipole or dipole-ion interactions, and direct hydrogen bonding [45,50]. Generally, these interactions between hydrophilic sites and water are stronger than that of water with itself. The breaking of the hydrogen bond network of water is thus expected, as observed in silica pores [50]. The strong attraction between water and hydrophilic groups significantly decreases the translational and orientational diffusion of these water molecules as compared to the bulk. In other words, these water molecules have a longer residence time than those solely formed between water molecules. The orientational correlation time decreases monotonically in moving away from the pore surfaces, as the effects of the fixed hydrogen bonding sites at the pore surfaces are felt only over a limited distance (in most case only one or two layers next to the interface). However, even in the centers of sizable pores the orientational correlation time can be modestly larger than in the bulk. Specially, the dynamic properties of the confined water within silica pores were found to be identical to those of bulk water at a temperature typically 30^{o}C below the real temperature [51].

At the surface of hydrophobic pores, the situation is markedly different and more complicated. The interaction between a hydrophobic molecule or surface and water is much less than the interaction of water with itself (due to hydrogen bonding). The “hydrophobic effect” of hydrophobic solutes in water is thus primarily a consequence of changes in clustering in the surrounding water rather than water-solute interactions [52]. Additionally, it is worth noting that the hydrophobic effects are associated with length scales [53]. For small apolar molecules (e.g., methane), the hydrogen bonding network deforms to accommodate such hydrophobic species. Then, the water reorganizes without

reducing the number of hydrogen bonds, and forms polyhedral structures, called clathrates [54]. In contrast, as the hydrophobic solutes grow in size, the physics become rather different. At the hydrophobic surfaces, two conflicting effects come into play to influence the dynamic behavior of water. On one hand, water try to cover the surface with clathrate-like clusters, so avoiding the loss of most of the hydrogen bonds. This necessitates an expanded low-density local structure and leads to a modest inhibition of the orientational dynamics of water [45,58]. On the other hand, water at a hydrophobic surface loses a hydrogen bond, therefore has increased enthalpy [55]. The hydrophobic surfaces have been found to act as a "lubricants" [56,57]. For example, the orientational dynamics of water confined in hydrophobic pores have been observed to be similar to those of the bulk liquid. Which of these effects wins out depends on both the chemical nature of the interfaces and the factors such as pore size and geometry.

As we have seen, the anomalies of water properties are essentially due to the hydrogen bond network, which is affected by the addition of a solute. Terms like "enhancement" (structure maker) and "breakdown" (structure breaker) of water structure have frequently been applied to different solutes. Polar solutes have the ability to destroy the hydrogen bonding of water (due to the strong interactions between polar solutes and water molecules), and are accordingly called "structure breakers". Similarly, apolar solutes are called "structure makers" because of the formation of clathrate structures of water in the vicinity. However, there is a degree of ambiguity in this terminology as the conclusions drawn depend upon which physical property is being observed. Actually, the effects are quite different when forming a bond with water than when disrupting the tetrahedral network or water-water hydrogen bonds.

1.4 Theoretical views of proton transport in aqueous systems and hydrated membranes

One of the most difficult hurdles facing the development of novel proton conducting membranes is the understanding of the proton transport mechanism. The perfluorosulfonic acid polymers are essentially strong polymer acids. Exposed to water, they dissociate upon hydration into the immobile ionomer (anionic) groups residing on side chains of the polymer and free mobile protons in the aqueous solution. Thus, the free protons move freely through the hydrogen-bonded network of water molecules inside the polymer.

Water is a perfect medium for proton transport. A donated excess proton becomes indistinguishable from other protons, and it gives birth to charged clusters in water. Present understanding concerning the transfer of proton in bulk water comes primarily from the qualitative evaluations of Agmon [**59**] and Kreuer [**60**,**61**] and from state-of-art molecular dynamics simulations of Marx *et al*. [**62**]and Kornyshev *et al*.[**63**]. These authors described the three main options for charged clusters: (1) an excess proton can be a part of an H_3O^+ ion in which all of the three protons are equivalent; (2) the proton is placed between the two water molecules in the hydrogen bond in an $H_5O_2^+$ grouping (Zundel ion); and (3) the proton is a part of an Eigen $H_9O_4^+$ cluster comprised of an H_3O^+ ion and three hydration H_2O molecules. Fig. **1.5** illustrates the important species and features involved in the transfer of an excess proton in bulk water along with the timescale for the transfer of the proton between two limiting structures, the Zundel ion ($H_5O_2^+$) and the Eigen ion ($H_9O_4^+$).

The most straightforward transport mechanism for any proton of an H_3O^+ donor is the hopping to a neighboring water molecule. For this to happen, a neighboring water molecule must approach one of the protons in the H_3O^+ ion in such a way that a Zundel complex is formed, where this proton is in the bridge position. If there is further charge transfer, then a new H_3O^+ acceptor state is formed and the water molecule of the former donor must fluctuate out of the $H_5O_2^+$ state. This process also carries over to mechanisms based on the $H_9O_4^+$ cluster. Here, charge transfer is triggered by shifting the charge center from the central H_3O^+ toward one of the hydration water molecules that serves as an acceptor.

A second pathway is the structural diffusion of $H_5O_2^+$. An attacking water molecule next to such a cluster fluctuates into a configuration where the proton charge is delocalized over more than just two molecules. Then, a new $H_5O_2^+$ cluster is formed. Subsequent fluctuations may move one of the original water molecules out of the proton cluster. This process is equivalent to proton tunneling through two hydrogen bonds.

Last, the H_3O^+ ion can drift classically as a whole, like a hydrated alkali ion. However, this is only one of the contributions to the proton transfer and is certainly not the dominating contribution in bulk water.

In all these elementary processes, the key step is associated with the making or breaking of a hydrogen bond, which allows a water molecule to either attach itself to the cluster or leave the cluster. This preorganization of the pertinent water molecules makes the proton transfer itself virtually barrierless, and it determines the time scale of an elementary process within several picoseconds.

The next level is concerned with the proton transport within “channels” in PEM. Several modifications must be taken into account in the membrane environment. First, near the pore surface (i.e., near the SO_3^- groups), if there is any pore, the structure of water may be significantly different from the bulk water. Water is pretty much “frozen” near the pore surface due to the dielectric saturation effect [**64**]. As a consequence, higher barriers for molecular preorganization are expected, resulting in higher effective activation energies for proton transfer. Second, the large distance between the SO_3^- groups (0.7-1 nm for Nafion) prevents direct proton transfer between equivalent states. Thus, a Coulomb barrier exists, which the transferring proton has to overcome. One possible pathway is through a water molecule which bridges between these sites. Yet, the fluctuation of side chains might be also possible to help the proton transport: the side chains carrying the SO_3^- groups can move toward each other to facilitate symmetric proton transfer. Fig. **1.6** is a summary of these transport mechanisms.

The theoretical treatments of activated proton transfer in a single pore in hydrated Nafion have been carried out [**65**-**67**]. In these treatments, the proton transfer occurs throughout and between clusters of hydrogen bonded water, which involves intermolecular proton transfer and the breaking and re-forming of hydrogen bonds. Eikerling *et al*. [**68**] presented a phenomenological model for proton conductivity and mobility in hydrated Nafion channels. The mobility of protons is assumed to occur via two mechanisms: a surface mechanism where proton transport proceeds along the array of acid groups over the interface and a bulk mechanism where the protons are transported with the Grotthus mechanism. In this model, the surface mechanism has a higher activation energy but also a higher concentration of charge carriers, and the balance

between surface and bulk effects depends on the surface density of SO_3^- groups and pore size. The model accounts for the effect of proton localization sites, dependence on EW, and pore water content and overall swelling. Theoretical estimates of the membrane conductivity agree well with experimental data.

1.5 Objective of this work

As noted above, the objective of this work is to characterize the state of water in PSA membranes with the ultimate objective of developing tools to aid in the molecular design of advanced, high temperature proton exchange fuel cells that would operate at much higher temperatures than those currently available. The specific tasks in the proposed work are as follows:

- Explore the structural properties of water in PSA membranes over a wide range of water content using the dielectric relaxation technique.
- Correlate the dielectric relaxation data with proton conductivity to ascertain the nature of any relationship between these parameters.
- Develop a phenomenological model of water in PSA membranes and identify promising molecular engineering routes for designing superior PEMs.

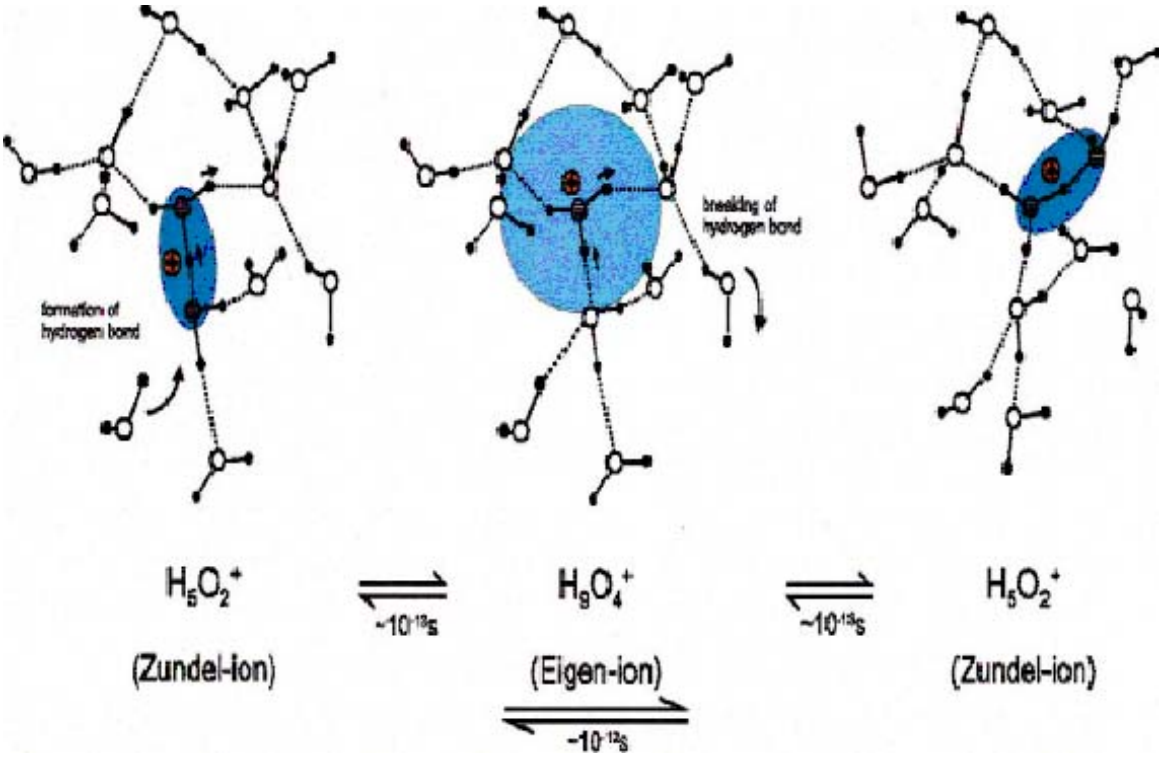

Fig. **1.5**: The proton transport mechanism in bulk water. Taken from reference [**61**].

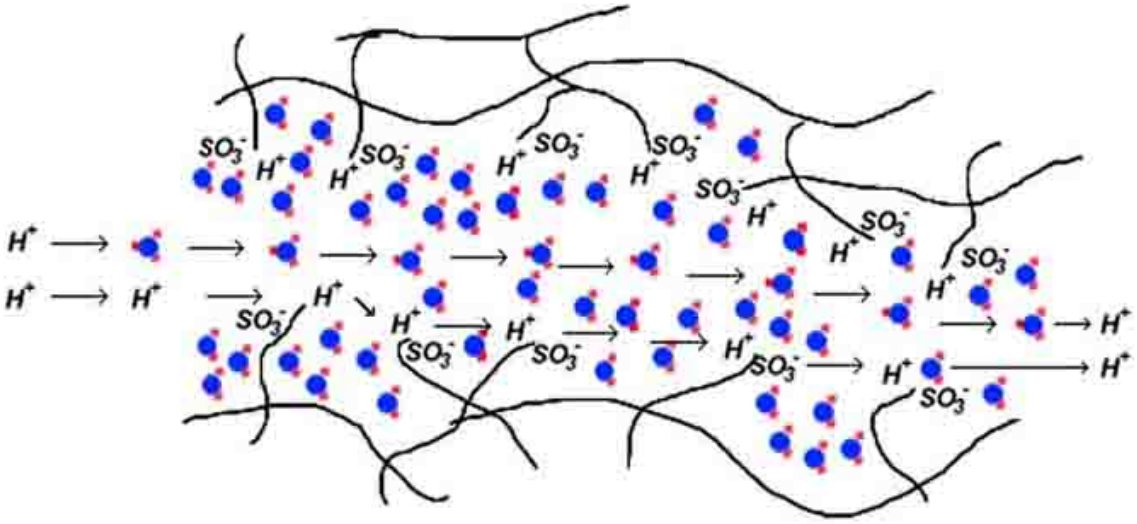

Fig. **1.6**: Proton transport in Nafion membranes

1.6 References

1. L. Carrette, K.A. Friedrich, U. Stimming, *Fuel Cells*, **1**, 1 (2001)

2. T.A. Zawodzinski Jr., T.E. Springer, F. Uribe, S. Gottesfeld, *Solid State Ionics*, **60**, 199 (1993)

3. S.M. Ibrahim, E.H. Price, R.A. Smith, of E.I. du Pont de Nemours, *Proc. Electrochem. Soc.*, 1983, 83-6

4. M. Rikukawa and K. Sanui, *Prog. Polym. Sci.*, **25**, 1463 (2000)

5. M.R. Tant, K.P. Darst, K.D. Lee, C.W. Martin, *ACS Symp. Ser.*, **395**, 370 (1989)

6. T.A. Davis, J.D. Genders, D. Pletcher, *In a first course in ion-exchange membranes*, Electrochemical Consultancy, Romsey, UK, 1997, Chapter 3

7. K.A. Mauritz, In *ionomers: synthesis, structure, properties and applications*, M.R. Tamt, K.A. Mauritz, G.L. Wilkes, Eds, Blackie academic and professional, London, 1997, Chapter 3

8. T.D. Gierke, G.E. Munn, F.C.J. Wilson, *J. Poly. Sci., Polym. Phys.*, **19**, 1687 (1981)

9. W.Y. Hsu and T.D. Gierke, *J. Membr. Sci.*, **13**, 307 (1983)

10. M. Fujimura, T. Hashimoto, H. Kawai, *Macromolecules*, **15**, 136 (1982)

11. M.H. Litt, *Polym. Prepr.*, **38**, 80 (1997)

12. H.G. Haubold, T. Vad, H. Jungbluth, P. Hiller, *Electrochim. Acta*, **46**, 1559 (2001)

13. L. Rubatat, A.L. Rollet, G. Gebel, O. Diat, *Macromolecules*, **35**, 4050 (2002)

14. K.D. Kreuer, *J. Membr. Sci.*, **185**, 29 (2001)

15. G. Gebel, *Polymer*, **41**, 5829 (2000)

16. S.J. Paddison, D.W. Reagor, T.A. Zawodzinski Jr., *J. Electroanal. Chem.*, **459**, 91 (1998)

17. S.J. Paddison, G. Bender, K.D. Kreuer, N. Nicoloso, T.A. Zawodzinski Jr., *J. New Mater. Electrochem. Syst.*, **3**, 291 (2000)

18. R.S. McLean, M. Doyle, B.B. Sauer, *Macromolecules*, **33**, 6541 (2000)

19. A.L. Rollet, O. Diat, G. Gebel, *J. Phys. Chem. B*, **106**, 3033 (2002)

20. P. Aldebert, B. Dreyfus, M. Pineri, *Macromolecules*, **19**, 2651 (1986)

21. E.E. Boakye and H.L. Yeager, *J. Membrane Sci.*, **69**, 155 (1992)

22. M.Falk, in *Structure and Properties of Ionomers*, M. Pineri and A. Eisenberg, Eds, D. Reidel Publishing Co., Dordrecht, Holland, 1987

23. M. Falk, *Can. J. Chem.*, **58**, 1495 (1980)

24. A.L. Rollet, G. Gebel, J.P. Simonin, P. Turq, *J. Polym. Sci., Part B: Polym. Phys.*, **39**, 548 (2001)

25. K.M. Cable, K.A. Mauritz, R.B. Moore, *J. Polym. Sci., Part B: Polym. Phys.*, **33**, 1065 (1995)

26. D.J. Barnes, in *Structure and Properties of Ionomers*, M. Pineri, A. Eisenberg, Eds.,D. Reidel Publ. Co., Dordrecht, 1987, p501.

27. H.W. Starkweather and J.J. Chang, *Macromolecules*, **15**, 752 (1982)

28. N.G. Boyle, V.J. McBrierty, D.C. Douglass, *Macromolecules*, **16**, 75 (1983)

29. N.J. Bunce, S.J. Sondheimer, C.A. Fyfe, *Macromoleucles*, **19**, 333 (1986)

30. B. MacMillan, A.R. Sharp, R.L. Armstrong, *Polymer*, **40**, 2471 (1999)

31. B. MacMillan, A.R. Sharp, R.L. Armstrong, *Polymer*, **40**, 2481 (1999)

32. N. Sivashinsky and G.B. Tanny, *J. Appl. Polym. Sci.*, **26**, 2625 (1981)

33. M. Pineri, F. Volino, M. Escoubes, *J. Polym. Sci., Polym. Phys. Ed*., **23**, 2009 (1985)

34. H. Yoshida, Y. Miura, *J. Membr. Sci.*, **68**, 1 (1992)

35. R. Duplessix, M. Escoubes, B. Rodmacq, F. Volino, E. Roche, A. Eisenberg, M. Pineri, in *Water in Polymers*, S.P. Rowland, Ed., ACS Symposium Series No. 127, American Chemical Society, Washington, DC, 1980, p469

36. T.A. Zawodzinski, M. Neeman, O.L. Sillerud, S. Gottesfeld, *J. Phys. Chem.*, **95**, 6040 (1991)

37. R. Buchner, J. Barthel, J. Stauber, *Chem. Phys. Letters*, **306**, 57 (1999)

38. R. Paul and S.J. Paddison, *J. Chem. Phys.*, **115**, 7762 (2001)

39. S.J. Paddison, *Ann. Rev. Mater. Res.*, **33**, 289 (2003)

40. S.H. Lee and P.J. Rossky, *J. Chem. Phys.*, **100**, 3334 (1994)

41. A. Scodinu and J.T. Fourkas, *J. Phys. Chem. B*, **106**, 10292 (2002)

42. T.W.Allen, S. Kuyucak, S.H. Chung, *J. Chem. Phys.*, **111**, 7985 (1999)

43. O. Beckstein, P.C. Biggin, M.S.P. Sansom, *J. Phys. Chem. B*, **105**, 12902 (2001)

44. http://www.lsbu.ac.uk/water/intro.html and the references cited

45. S.H. Lee and P.J. Rossky, *J. Chem. Phys*., **100**, 3334 (1994)

46. C.Y. Lee, J.A. McCammon, P.J. Rossky, *J. Chem. Phys*., **80**, 4448 (1994)

47. C. Hartnig, W. Witschel, E. Spohr, P. Gallo, A. Ricci, M. Rovere, *J. Mol. Liq*., **85**, 127 (2000)

48. P. Gallo, M.A. Ricci, M. Rovere, *J. Chem. Phys*., **116**, 342 (2002)

49. A. Fouzri, R.D. Sridi, M. Oumezzine, *J. Chem. Phys*., **116**, 791 (2002)

50. A.K. Soper, F. Bruni, M.A. Ricci, *J. Chem. Phys*., **109**, 1486 (1998)

51. J. Teixeira, J.M. Zanotti, M.C. Bellissent Funel, S.H. Chen, *Physica B*, **234-236**, 370 (1997)

52. L.R. Pratt and A. Pohorille, *Chem. Rev.*, **102**, 2671 (2002)

53. B.J. Berne, *Proc. Natl. Acad. Sci. USA*, **93**, 8800 (1996)

54. F. Frank, in *Water – A Comprehensive Treatise*, F. Frank, Ed, Plenum Press, New York, 1975, Vol. 4

55. Q. Du, E. Freysz, Y.R. Shen, *Science*, **264**, 826 (1994)

56. V. Crupi, D. Majolino, P. Migliardo, V. Venuti, *J. Phys. Chem. A*, **104**, 11000 (2000)

57. M. Arndt, R. Stannarius, H. Groothues, E. Hempel, F. Kremer, *Phys. Rev. Lett.*, **79**, 2077 (1997)

58. A. Scodinu and J.T. Fourkas, *J. Phys. Chem. B*, **106**, 10292 (2002)

59. N. Agmon, *Chem. Phys. Lett.*, **244**, 456 (1995)

60. K.D. Kreuer, *Chem. Mater.*, **8**, 610 (1997)

61. K.D. Kreuer, *Solid State Ionics*, **136-137**, 149 (2000)

62. D. Marx, M.E. Tuckerman, J. Hutter, M. Parrinelo, *Nature*, **397**, 601 (1999)

63. A.A. Kornyshev, A.M. Kuznetsov, E. Spohr, J. Ulstrup, *J. Phys. Chem. B*, **107**, 3351 (2003)

64. M. Spaeth, K. Kreuer, J. Maier, C. Cramer, *J. Solid State Chem.*, **148**, 169 (1999)

65. M. Eikerling and A.A. Kornyshev, *J. Electroanalytical Chem.*, **502**, 1 (2001)

66. E. Spohr, P. Commer, A.A. Kornyshev, *J. Phys. Chem. B*, **106**, 10560 (2002)

67. S.J. Paddison, R. Paul, T.A. Zawodzinski Jr., *J. Chem. Phys.*, **115**, 7753 (2001)

68. M. Eikerling, A.A. Kornyshev, A.M. Kuznetsov, J. Ulstrup, S. Walbran, *J. Phys. Chem. B*, **105**, 3646 (2001)

Chapter 2

Microwave Dielectric Relaxation Spectroscopy

Dielectric relaxation spectroscopy (DRS) probes the response of the total dipole moment of a system, $M(t) = \sum \mu_j(t)$, to a time-dependent external electrical field. This inherent ability to monitor the cooperative motion of a molecular ensemble makes it a powerful tool for investigation of liquids whose structure and dynamics are dominated by intermolecular hydrogen bonds. In the first part of this chapter, the theories of the dielectric relaxation are reviewed. The measurement technique, focused in the microwave frequency range, and error analysis are then discussed. Finally, the validity of this method of determining the dielectric response of the hydrated PEM samples over the broadband frequency range is assessed.

2.1 Fundamental aspects of dielectric theory

An important result of the imposition of an external electric field (static or periodically changed) on a material is the production of polarization, which arises from the perturbation of the arrangement of the constituent charge. At the limit of the static electric field the relation between the polarization, P, and the external electric field, E, can be expressed as

$$P = \varepsilon_0(\varepsilon_s - 1)E \qquad (2.1)$$

where $\varepsilon_0 = 8.85 \times 10^{-12}\ F/m$ is the absolute permittivity of a vacuum and ε_s is the static (relative) permittivity.

At a fundamental level, the polarization is built up from an enormous number of elementary dipoles induced in the molecules of the dielectric. The so-defined equilibrium polarization, P_{eq}, relates the specific dielectric permittivity to the molecular properties, such as dipole moment, μ, and polarizability, α, [**1**]

$$P^{eq} = \frac{\sum_{i=1}^{N}[(\alpha_d)_i (E_{\text{int}})_i + \frac{\mu_i^{\,2}}{3k_B T}(E_{dir})_i]}{V} = P_d^{eq} + P_\mu^{eq} \qquad \textbf{(2.2)}$$

where N is the number of dipoles, and V is the volume of the dielectric. E_{int} is the internal field which governs the induced intramolecular charge distortion and, hence, the distortional polarization, P_d^{eq}. E_{dir} is the average local field which aligns the permanent dipole moment against the thermal motion, producing the orientational polarization, P_μ^{eq}.

For a variable electric field, E(t), the fluctuation rates of both contributions are markedly different. P_d, associated with the displacement of the atoms and electronic clouds in the molecules, is always in equilibrium with the external field. On the other hand, the orientational polarization, P_μ, determined by the intermolecular interactions, relaxes to equilibrium after an external perturbation. This process is manifested by a dispersion of permittivity from ε_s down to a value ε_∞ at frequencies where the dipoles are

unable to follow the external field, yielding the dispersion curve, ε′(ω). Simultaneously, dissipation of energy over a broad range of frequencies is observed and characterized by the dielectric loss spectrum, ε″(ω). ε′ and ε″ together define the complex permittivity spectrum of the sample,

$$\varepsilon^*(\omega) = \varepsilon'(\omega) - i\varepsilon''(\omega) \tag{2.3}$$

The relaxation of the orientational polarization is characterized by a time-correlation function (TCF) [**1**, **6**], which gives information on the dynamics of the intermolecular processes. The time-correlation function is generally defined as:

$$F_\mu(t) = \frac{< P_\mu(0) \cdot P_\mu(t) >}{< P_\mu(0) \cdot P_\mu(0) >} = \frac{< \mu(0) \cdot \mu(t) >}{< \mu(0) \cdot \mu(0) >} \tag{2.4}$$

where P and μ represent the orientational polarization and dipole moment, respectively. According to linear-response theory, the permittivity in the frequency domain is related to the time-correlation function via the Laplace transformation:

$$\varepsilon^*(\omega) - \varepsilon_\infty = (\varepsilon_s - \varepsilon_\infty) \int_0^\infty (-\frac{\partial F_\mu(t)}{\partial t}) \exp(-i\omega t) dt \tag{2.5}$$

For a simple case where $F_\mu(t)$ is given by a single exponential function a linear system is expressed as:

$$F_\mu(t) = \exp(-t/\tau) \quad (2.6)$$

On the molecular level, this process can be used to describe a small-step rotational diffusion of molecules with a rotational diffusion coefficient, D_r. The time-correlation function decays exponentially with $\tau_\mu = (2D_r)^{-1}$:

$$F_\mu(t) = \exp(-2D_r t) \quad (2.7)$$

Eq. **2.7** is identical to Eq. **2.6** with only τ_μ replacing τ in Eq. **2.8**. Then, Eq. **2.6** and Eq. **2.7** yield the result

$$\varepsilon^*(\omega) = \varepsilon_\infty + \frac{\varepsilon_s - \varepsilon_\infty}{1 + i\omega\tau} \quad (2.8)$$

T

his equation is known as the Debye relaxation, which produces a single relaxation time. Fig. **2.1** shows plots of $\varepsilon'(\omega)$ and $\varepsilon''(\omega)$ vs. $\log(\omega\tau)$, where ε_s and ε_∞ are chosen arbitrarily as 13 and 3, respectively. $\varepsilon'(\omega)$ falls with increasing frequency, and $\varepsilon''(\omega)$ shows a peak at $\omega\tau=1$. The peak height is $(\varepsilon_s-\varepsilon_\infty)/2$, and the "relaxation strength" is $(\varepsilon_s-\varepsilon_\infty)$. The area below the plot of $\varepsilon''(\omega)$ vs. $\log(\omega\tau)$ is given by $(\varepsilon_s-\varepsilon_\infty)\pi/2$, so that the total relaxation

strength, as given by this area, is directly related to the magnitude of the dielectric dispersion, (ε_s-ε_∞).

The Debye mode (Eq. **2.8**) has been used to explain the dielectric relaxation of dipolar molecules in the liquid and solid states [2-4]. However, no material precisely matches the plot shown in Fig. **2.1**. To overcome this difficulty, two approaches are usually used. One approach is to represent $\varepsilon^*(\omega)$ as a superposition of single relaxation-time processes each being described by a Debye equation with a relaxation time τ. Hence, Eq. **2.8** is generalized to [4]:

$$\frac{\varepsilon^*(\omega)-\varepsilon_\infty}{\varepsilon_s-\varepsilon_\infty}=\int\frac{f(\tau)}{1+i\omega\tau}d\tau \qquad (2.9)$$

The function $f(\tau)$ is called the relaxation-time distribution function, or simply the distribution function. $f(\tau)d\tau$ is a measure of the contribution to (ε_s-ε_∞) from those parts of the dielectric with relaxation times in the range from τ to $\tau+d\tau$. Through this approach one may be able to find a satisfactory explanation based on knowledge of the physical properties of the material. However, it is not easy to form the distribution function $f(\tau)$.

Traditionally, it has been customary to fit plots of ε' and ε'' vs. $\log(\omega)$ using empirical functions. The most versatile function is the Havriliak-Negami equation [5], which is an empirical modification of the single Debye equation:

$$\varepsilon^*(\omega)=\varepsilon_\infty+\frac{\varepsilon_s-\varepsilon_\infty}{[1+(i\omega\tau)^{1-\alpha}]^\beta}, \qquad 0\le\alpha<1;\ \ 0<\beta\le 1 \qquad (2.10)$$

where α and β are the shape parameters, representing asymmetric and symmetric distribution of relaxation, respectively. Three well-known models are limiting cases of this general equation: the Debye equation ($\alpha = 0, \beta = 1$), the Cole-Cole equation ($0 \le \alpha < 1, \beta = 1$), and the Davidson-Cole equation ($\alpha = 0, 0 < \beta \le 1$). Eq. **2.10** generates broad, asymmetric curves for ε″ vs. log(ω) that are skewed at high frequencies. For a multi-step dielectric relaxation, the following general form is often used to model the dielectric data:

$$\varepsilon^*(\omega) = \varepsilon_\infty + \sum_{j=1}^{n} \frac{\Delta\varepsilon_j}{[1 + (i\omega\tau_j)^{1-\alpha_j}]^{\beta_j}} \qquad \textbf{(2.11)}$$

$$\Delta\varepsilon_j = \varepsilon_{sj} - \varepsilon_{\infty j} \qquad 0 \le \alpha_j < 1: \;\; 0 < \beta_j \le 1$$

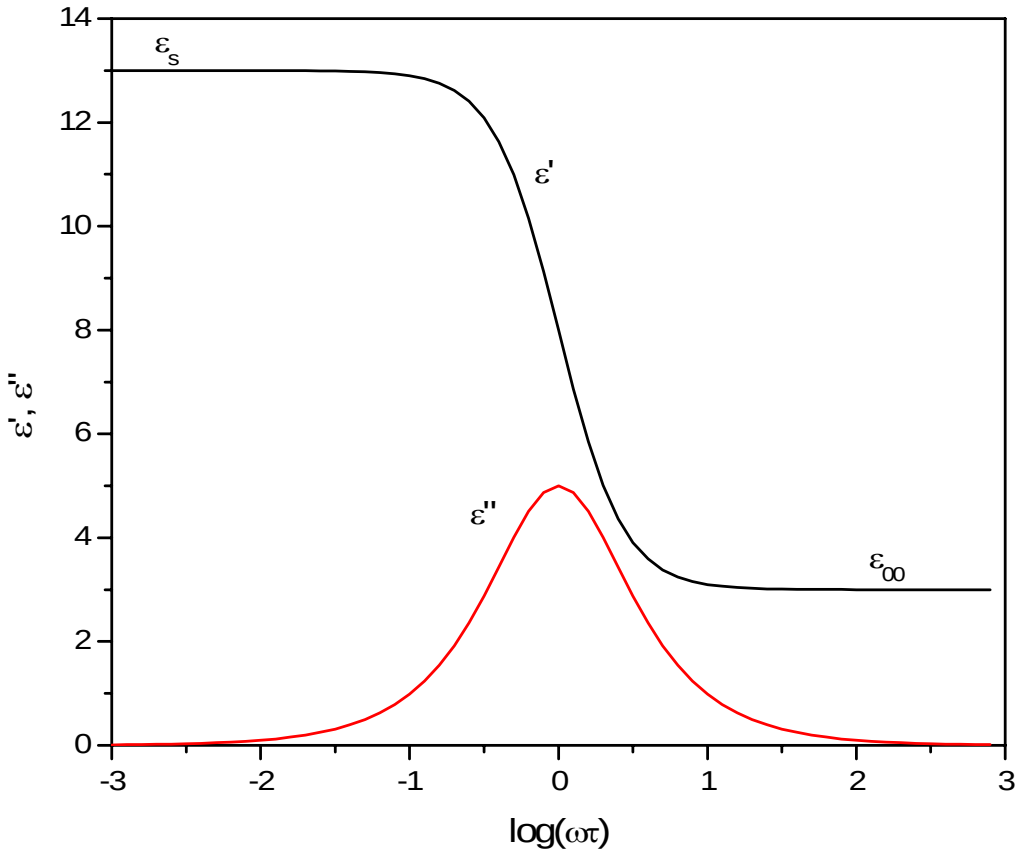

Fig. **2.1**: Plots of real permittivity, ε′, and loss factor, ε″, vs. log(ωτ) for a sample represented as Eq. **2.8**. ε_s and ε_∞ are chosen as 13 and 3, respectively.

where n is the number of separable dispersion steps, and ε_{sj} and $\varepsilon_{\infty j}$ are the low and high-frequency permittivity limits for the jth process from the lower frequency side, respectively. $\varepsilon_{n\infty} = \varepsilon_{\infty}$, ω is an angular frequency, and τ_j is the dielectric relaxation time for the jth process.

2.2 Measurement of ε*(ω)

2.2.1 Theory and apparatus [7,8]

Dielectric relaxation spectroscopy (DRS) investigates the interaction of electromagnetic radiation with matter in a very wide frequency range, from 10^{11} Hz down to 10^{-6} Hz. However, no single measurement can be made over such a large frequency range. The proper measurement technique depends on the dielectric properties, frequency range, and possible sample geometries. For frequencies lower than 10^7 Hz, it is convenient to use equivalent electrical circuits made up of resistors, capacitors, and inductors to represent the dielectric properties of a material. This “lumped circuit” representation assumes that the electric field is uniform throughout the sample. Measurement of dielectric properties at low frequencies (below 10 MHz) is usually carried out by conventional bridge techniques. This method has been widely used in the DRS of polymer materials and ionic materials [9-11].

For low molar mass materials, such as liquid water, the dielectric relaxation usually occurs at higher frequency, even in the microwave range [2]. Thus, dielectric measurement techniques at high frequencies are needed. For frequencies higher than 10^7

Hz and into the microwave range, lumped circuits are replaced by distributed circuits that describe the propagation of electromagnetic (EM) waves through a material. The measurement method for dielectrics at microwave range can be generally divided into two groups: transmission line methods and resonant methods. These two methods are distinguished by the boundary conditions. Resonant techniques are spatially defined in three directions, and the dielectric property measurements are limited to fixed frequencies. The resonant method usually assures very good accuracy, but is difficult and time consuming when applied in a broad range of frequencies.

The transmission line methods, on the other hand, have at least one spatial degree of freedom and typically measure dielectric properties through a broad frequency range. The transmission line methods can be further divided into the total reflection and total transmission methods [**12**]. The permittivity of the samples is expressed in terms of the measured values of the complex reflection and transmission coefficients, respectively.

The waveguide is the primary media for microwave propagation. A coaxial airline is used as a waveguide over a wide frequency range in this work. The fundamental propagation mode for waves in a coaxial system is the transverse electromagnetic wave (TEM). The structure in Fig. **2.2** represents a dielectric sample placed in the coaxial line. The sample can be viewed as a two-port device characterized by the scattering parameters, S_{11} and S_{21}, which represent the sum of reflected and transmitted waves, respectively. The S-parameters are defined in terms of a voltage ratio as described by the following equation:

$$S_{ij} = \frac{b_i}{a_j} \quad (2.12)$$

where b_i is the incident wave voltage on port i, and a_j is the wave voltage initiated from port j. For example, the transmission S-parameter, S_{21}, is described as the ratio of the incident wave voltage on port 2 divided by the voltage leaving port 1.

Reflected and transmitted waves are portrayed as vectors in Fig. **2.2** and are expressed in terms of complex reflection and transmission coefficients. The incident wave has an amplitude defined as unity, and the first reflected wave can be described in terms of a complex reflection coefficient ρ:

$$\rho = \frac{1-(\varepsilon^*)^{1/2}}{1+(\varepsilon^*)^{1/2}} \quad (2.13)$$

The remainder of the incident wave is transmitted through the dielectric material until the next dielectric discontinuity is reached.

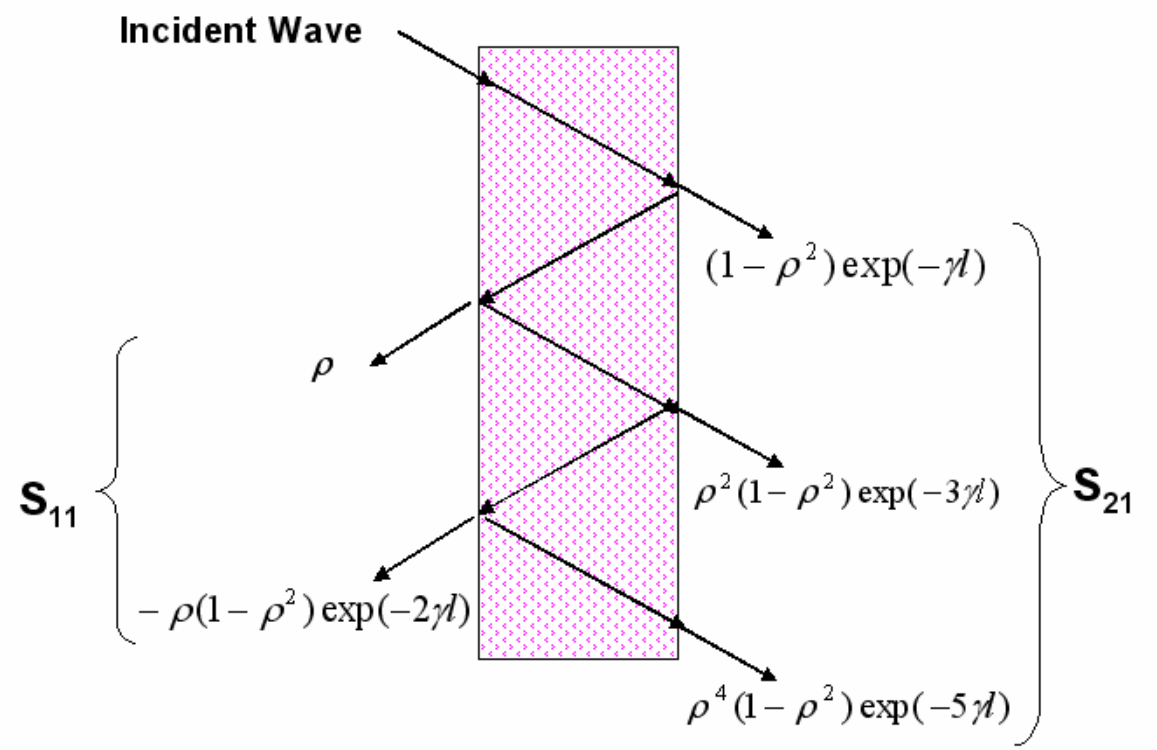

Fig. **2.2**: An electromagnetic wave passing through a dielectric slab. Multiple reflections occur at the air-dielectric boundary.

The transmitted wave can be described in terms of the propagation coefficient γ and the sample length l. According to von Hippel [7], the propagation coefficient γ(ω) is written as:

$$\gamma(\omega) = \alpha(\omega) + i\beta(\omega) \quad \textbf{(2.14)}$$

where α(ω) is the attenuation coefficient, and β(ω) is the phase factor for the material. For a material,

$$\beta(\omega) = \frac{2\pi}{\lambda_m} = \frac{2\pi\sqrt{\varepsilon'(\omega)}}{\lambda_0} \quad \textbf{(2.15)}$$

where λ_m and λ_0 are the wavelength in the sample and in a vacuum, respectively, for a given value of ω. The expression for the attenuation coefficient, α(ω), is more complicated; both the dielectric and the waveguide can cause attenuation of TEM waves.

The scattering parameters can be further expressed by the following equations [**12**]:

$$S_{11} = \rho \frac{1 - \exp(-2\gamma l)}{1 - \rho^2 \exp(-2\gamma l)} \quad \textbf{(2.16)}$$

$$S_{21} = \frac{(1-\rho^2)\exp(-\gamma l)}{1-\rho^2\exp(-2\gamma l)} \quad (2.17)$$

The values of the complex permittivity can therefore be calculated from Eq. **2.16** and Eq. **2.17**. However, the analytical solution for the permittivity is not available, and numerical methods are needed.

Both the reflected and transmitted waves allow for the determination of the complex permittivity of the sample. However, the transmission approach allows for higher accuracy for high dielectric loss material (e.g., Nafion membrane) [**8**]. In this work, the dielectric properties are determined by measuring the frequency dependence of transmission S-parameter S_{21}.

S_{21} are complex numbers and are expressed in terms of magnitude and phase:

$$S_{21} = Mag\angle\phi \quad (2.18)$$

The magnitude of the S-parameters is expressed in decibel (dB) units. The phase ϕ is expressed in degree and is related to the phase factor β by:

$$\phi = -\beta L = -\frac{2\pi\sqrt{\varepsilon'(\omega)}}{\lambda_0}L \quad (2.19)$$

With the difficulties to obtain accurate values of complex permittivity from Eq. **2.17**, an alternative approach is used in this work. The real part of the permittivity is calculated from Eq. **2.19**. The imaginary part is obtained by substituting ε' into Eq. **2.17** and via an iterative procedure. In this procedure, a value for dielectric loss is estimated and the S_{21} magnitude is calculated with this value. The estimated dielectric loss is then changed to minimize the difference between calculated and measured S_{21} values.

The apparatus for the dielectric measurements is shown in Fig. **2.3**. The HP8510 system, with a broad band sweep generator synthesizing signals from 45 MHz to 26 GHz, measures the complex transmission S_{21} precisely and quickly. The calibration standards, used to generate reference planes from which the real and imaginary parts of S_{21} were determined, consists of an open, a short, and a known load (50Ω). Calibration of S_{21} magnitude was made by performing a simple through connection.

For accurate measurements, the sample must be completely filled into the coaxial line. Air gaps between sample and waveguide could cause serious error in the S-parameter measurement. In the following section, the accuracy of this approach is briefly analyzed.

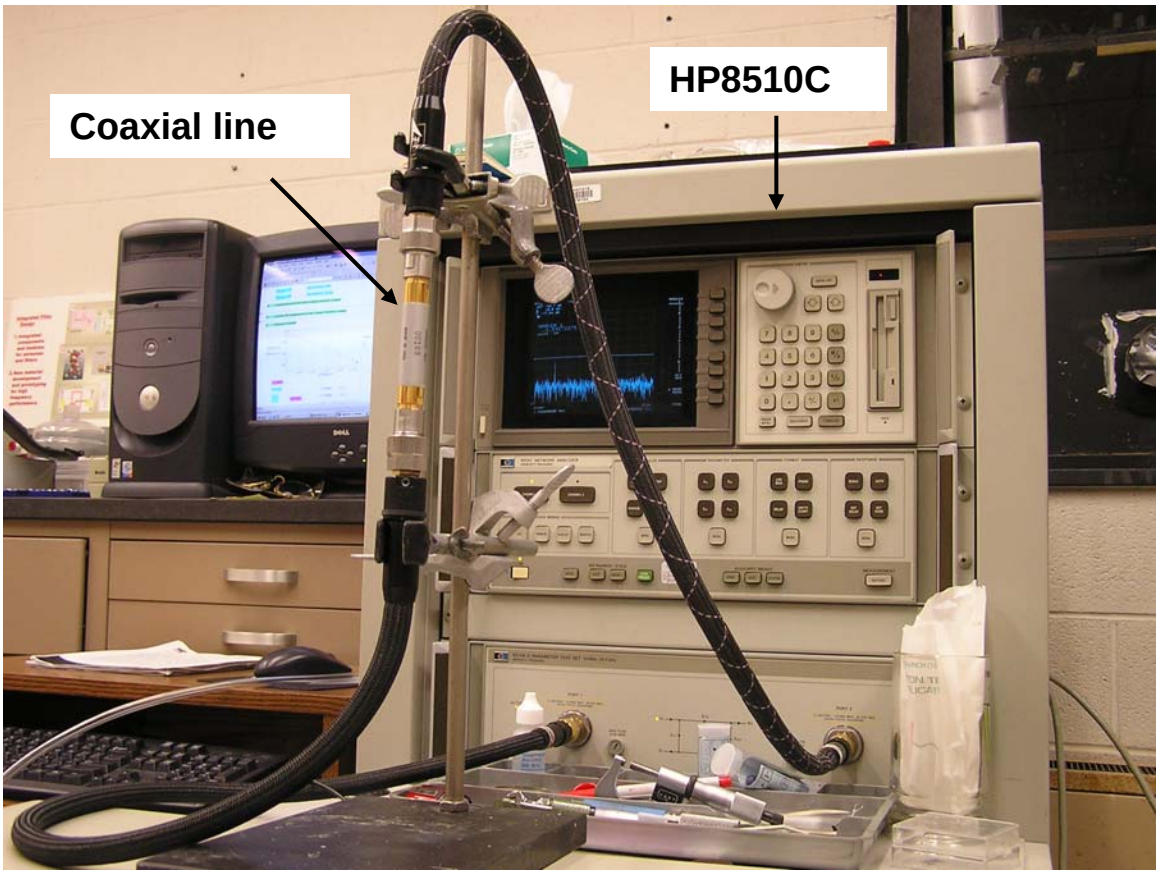

Fig. **2.3**: The experimental setup for the microwave DRS measurements.

2.2.2 Accuracy analysis

The accuracy of the technique is divided into two parts. The first regards the accuracy of the measured S-parameter, which is primarily dependent on the S_{21} magnitude and equipment precision. The error for S_{21} was taken as suggested by the manufacturer [13]. For S_{21} magnitude less than -30 dB, the error is better than 0.5%. But it increases quickly with S_{21} magnitude when its magnitude values are below -40 dB. For example, S_{21} values below -50 dB result in a measured error in excess of 5%. The second part is the accuracy of the calculated complex permittivity. In order to calculate the uncertainties in the permittivity ($\Delta\varepsilon'/\varepsilon'$) and the dielectric loss ($\Delta\varepsilon''/\varepsilon''$), it is necessary to calculate the partial derivative of the permittivity with respect to the S-parameter, $\partial\varepsilon^*/\partial S_{21}$. Detailed analysis of this procedure is given in the reference [8]. For static permittivity less than 100, which is the case of proton exchange membranes, typical errors for the complex permittivity are 2% for ε' and 3% for ε''. Other contributions to the error include sample length measurements, air gaps around the sample, and waveguide mismatch. These error terms were minimized by careful sample preparation and operation.

In principle, such transmission measurements using a coaxial device allow the determination of $\varepsilon^*(\omega)$ between approximately 50 MHz and 30 GHz from a single experiment. However, to achieve a good signal-to-noise ratio a set of samples with length adapted to the desired permittivity and frequency range is needed. Stuchly [14] obtained an empirical expression for the normalized sample length l/λ, which gives minimum experimental uncertainty,

$$\frac{l}{\lambda} = \frac{1}{4}\left|\varepsilon(\omega)\right|^{-1/2} \qquad (2.20)$$

A graphical representation of Eq. **2.20** is given in Fig. **2.4**. According to this figure, the optimum length for the operation is dependent on the dielectric properties and the frequency range. For example, for water and aqueous solutions with a permittivity around 80, the optimum length of the sample is calculated and shown in Table **2.1**. Variation of the sample length allow for absolute measurements over the entire frequency range.

Table **2.1**: The optimum sample length calculated according to Eq. **2.20** and Fig. **2.4**. Calculation was made for ε′= 80, ε″=20.

Frequency range (GHz)	Sample length
0.045 – 4	10 cm
3 – 9	20 mm
6 – 18	5 mm

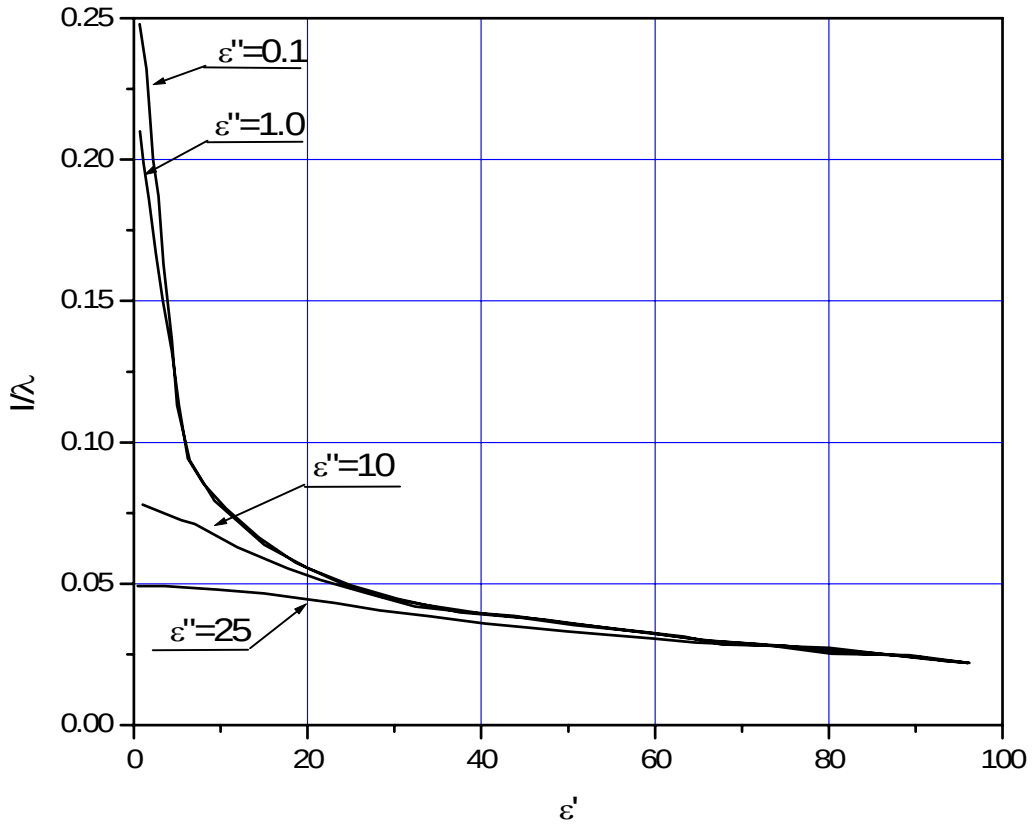

Fig. **2.4**: Optimum normalized length of the sample as a function of the static permittivity for different loss factors.

2.3 Data processing

After the measurement of S_{21} and calculation of ε*(ω), the next step was to analyze these data (ε′ and ε″) to obtain the dielectric parameters, including relaxation time and dielectric dispersion. From these parameters, the structural and dynamic behavior of the studied system can be investigated. The general form of the relaxation model used to fit the spectra is the Havrilliak-Negami function (Eq. **2.10**). For one-step H-N relaxation, Park [**15**] derived the corresponding ε′(ω) and ε″(ω) relationships as:

$$\varepsilon'(\omega) = \varepsilon_\infty + r^{-\beta/2}(\varepsilon_s - \varepsilon_\infty)\cos(\theta\beta) \qquad \textbf{(2.21)}$$

$$\varepsilon''(\omega) = r^{-\beta/2}(\varepsilon_s - \varepsilon_\infty)\sin(\theta\beta) \qquad \textbf{(2.22)}$$

where $$r = [1+(\omega\tau_0)^{1-\alpha}\sin(\alpha\pi/2)]^2 + [(\omega\tau_0)^{1-\alpha}\cos(\alpha\pi/2)]^2$$

and $$\theta = \arctan\left[\frac{(\omega\tau_0)^{1-\alpha}\cos(\alpha\pi/2)}{1+(\omega\tau_0)^{1-\alpha}\sin(\alpha\pi/2)}\right]$$

The experimental dielectric spectra were fitted to Eq. **2.21** and Eq. **2.22** simultaneously by a complex nonlinear least-square (CNLS) routine to obtain the absolute minimum value of the normalized variance, S_N^2, defined as:

$$s_N^2 = \frac{1}{N}\left[\frac{1}{\varepsilon'_{\max}}\sum_{i=1}^{N}\delta\varepsilon'(\omega_i)^2 + \frac{1}{\varepsilon''_{\max}}\sum_{i=1}^{N}\delta\varepsilon''(\omega_i)^2\right] \qquad \textbf{(2.23)}$$

where $\delta\varepsilon'(\omega_i)$ and $\delta\varepsilon''(\omega_i)$ are the residuals for the dispersion and absorption, respectively. N represents the number of measured points of permittivity. The data fittings were carried out using the software "Origin".

2.4 Calibration of the Microwave DRS

2.4.1 DRS of pure water

As a calibration, the dielectric spectra of liquid water were measured by this approach over frequency range of 45 MHz to 26.5 GHz and at temperatures ranging from 25 to 45^{o}C. Several sample lengths was then used, according to Table **2.1**. For instance, the dielectric spectra for liquid water at 25^{o}C are shown in Fig. **2.5**. From this figure, $\varepsilon'(\omega)$ falls with increasing frequency, and $\varepsilon''(\omega)$ shows a peak at around 18 GHz. The spectra were fitted using various models represented by Eq. **2.10**. The best fitting was obtained by a Debye relaxation model (j=1, α=0, and β=1). A faster process was recently reported to exist at around 1-2 ps for water [**16**], which was attributed to the rotation of single unbonded water molecule. However, this fast process is far outside of our accessible frequency range. A single Debye model thus suffices to fit the dielectric data in this frequency range [**17**]. The static permittivity obtained from the best fitting is 79.13, which agrees within 1% with ε_s data in the literature [**17**,**18**]. The relaxation time was obtained to be 8.31 ps. This value accords within 0.5% with the literature data [**17**,**19**].

The dielectric spectra of water at higher temperatures were also measured and are shown in Fig. **2.6**. Two important conclusions can be made based on this figure. First, the static permittivity decreases with increasing temperature. This can be interpreted by the fact that the dipole correlation decreases at higher temperatures. Moreover, the dielectric dispersion (ε_s-ε_∞) decreases accordingly with temperature. Second, the relaxation shifts to higher frequency as temperature increases, as shown by $\varepsilon''(\omega)$. This result may indicate the reduction of the number of hydrogen bonds in water, the decrease in the hydrogen bonding energy, or both. The dielectric parameters obtained from the best fitting of the dielectric data of water are collected in Table **2.2**.

Table **2.2**: Parameters of the Debye relaxation spectral function for water at different temperatures.

T, ^oC	ε_s	τ, ps	ε_∞	S_N^2
25	79.13	8.31	5.2	0.00651
35	74.95	6.50	3.8	0.00764
45	71.44	5.21	3.2	0.01119

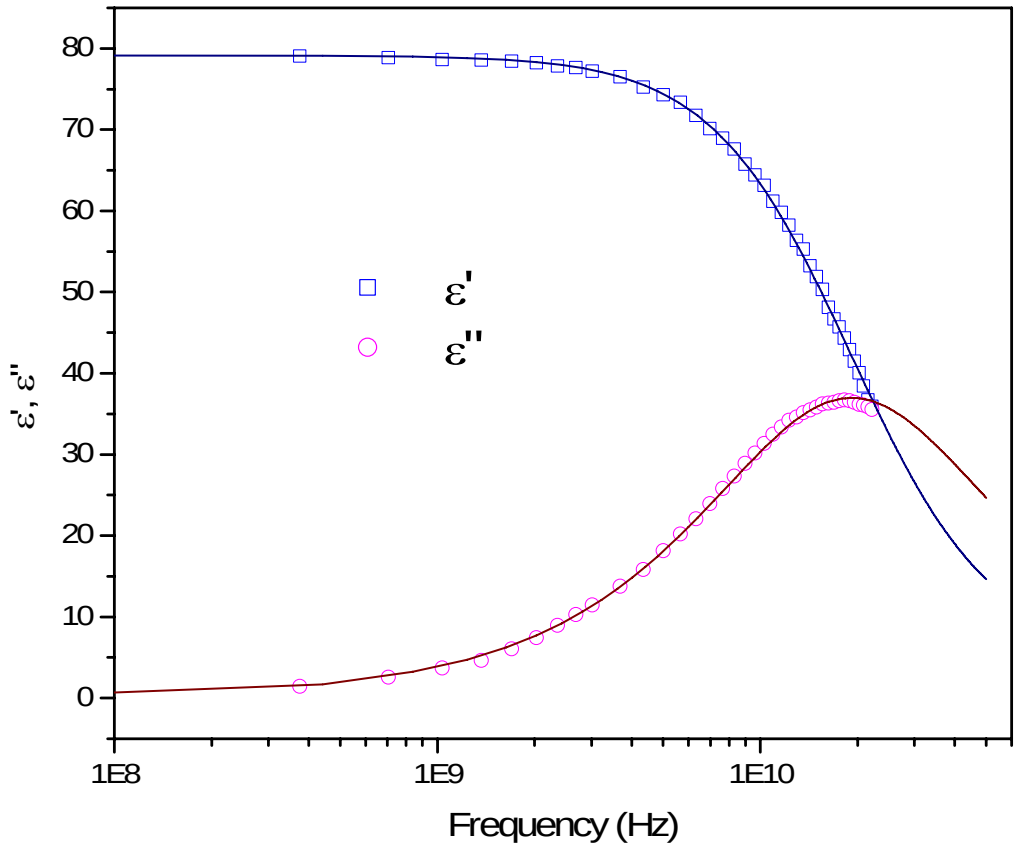

Fig. **2.5**: Frequency dependence of relative permittivity (ε′) and dielectric loss factor (ε″) for liquid water at 25 ^{o}C. The solid lines represent the Debye relaxation fitting.

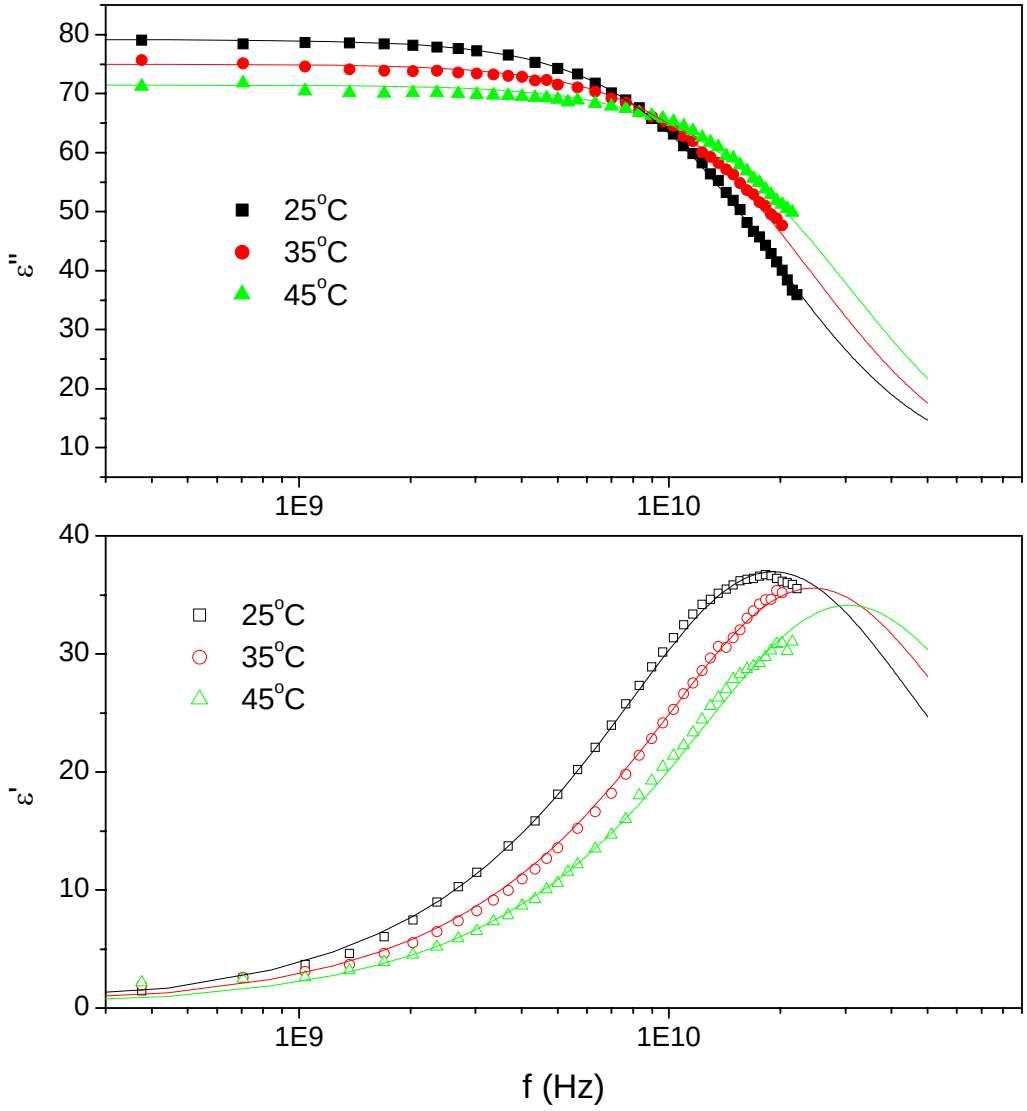

Fig. **2.6**: Frequency dependence of relative permittivity (ε′) and dielectric loss factor (ε″) for liquid water at higher temperatures. The solid lines in the figure represent the Debye relaxation fitting.

2.4.2 DRS of Teflon

PSA membranes are solid and are in sheet form. In order to assess the validity of this technique for the PSA samples, initial measurements were made on thin strips (0.003") of Teflon. The dielectric spectra of Teflon measured at 25^{o}C are shown in Fig. **2.7**. The relative permittivity of Teflon is constant at a value around 2.0 over the frequency range of 45 MHz to 26 GHz, as anticipated. The dielectric loss factor of Teflon was found to be small (of the order of 10^{-3}) but scattering. These results agree well with recent measurements carried out by Geyer and Krupka [**20**]. They reported a value of 2.055 for the dielectric constant of Teflon at 9.93 GHz and 300K.

The initial experiments on water and Teflon indicate that this technique is appropriate for the dielectric measurements of PSA membranes.

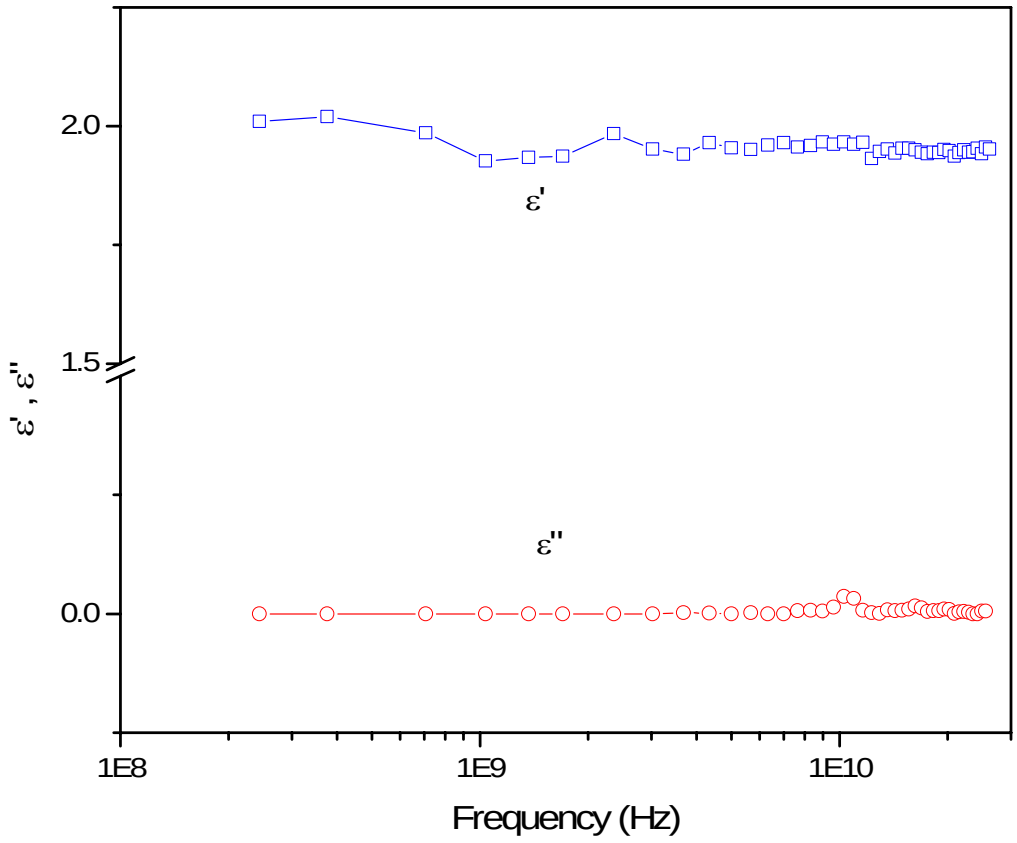

Fig. **2.7**: Complex permittivity spectra (ε′, ε″) of Teflon at 25^{o}C.

2.5 References

1. B.K.P. Scaife, *Principles of Dielectrics*, Clarendon Press, Oxford, 1998

2. C.J.F. Bottcher and P. Bordewijk, *Theory of Electric Polarization*, 2nd ed., Vol. 2, Elsevier, Amsterdam, 1978

3. A.R. Blythe, *Electrical Properties of Polymers*, Cambridge University Press, Cambridge, 1979

4. N.G. McCrum, B.E. Read, G. Williams, *Anelastic and Dielectric Effects in Polymers Solds*, Wiley, London, 1967 and Dover Publ., New York, 1991

5. S. Havriliak and S. Negami, *Polymer*, **8**, 161 (1967)

6. R.H. Cole, *J. Chem. Phys.*, **42**, 637 (1965)

7. A.R. von Hippel, *Dielectric Materials and Applications*, MIT Press, Cambridge, MA, 1966

8. M.T. Lanagan, *Microwave Dielectric Properties of Antiferroelectric Lead Zirconate*, Ph.D. dissertation, the Pennsylvania State University, 1987

9. A.R. Blythe, *Electrical Properties of Polymers*, Cambridge University Press, Cambridge, 1979

10. J.P. Runt and J.J. Fitzgerald, *Dielectric Spectroscopy of Polymeric Materials*, ACS Publications, Washington DC, 1997

11. W.C. Hasz, C.T. Moynihan, P.A. Tick, *J. Non Cryst. Solids*, **172-174**, 1363 (1994)

12. M.J.C. van Gemert, *Philips Res. Pep.*, **28**, 530 (1973)

13. Hewlett-Packard, Technical Data, 16, 1984

14. S.S. Stuchly and M. Matuszewski, *IEEE Trans. Instru. Meas.*, **IM-27**, 285 (1978)

15. T. Park, *Dielectric Relaxation Behavior of Poly(3-hydroxybutyrate)*, Ph.D. Dissertation at Virginia Polytechnic and State University, 1994

16. R. Buchner, J. Barthel, J. Stauber, *Chem. Phys. Letters*, **306**, 57 (1999)

17. U. Kaatze, *J. Chem. Eng. Data*, **34**, 371 (1989)

18. W.J. Ellison, K. Lamkaouchi, J.M. Moreau, *J. Mol. Liq.*, **68**, 171 (1996)

19. J. Barthel, K. Bachhuber, R. Buchner, H. Hetzenauer, *Chem. Phys. Lett.*, **165**, 369 (1990)

20. R.G. Geyer and J. Krupka, *IEEE Trans Instru. Meas.*, **44**, 329 (1995)

Chapter 3

Experimental

3.1 Materials

3.1.1 Perfluorosulfonic acid membranes

Nafion 117 and Flemion SH150 were utilized as perfluorosulfonic acid membrane sample. These two membranes have similar chemical structure, but have different equivalent weight. Nafion 117 membrane, a product of DuPont, was purchased from Ion Power, Inc. The Flemion membrane, manufactured by Asahi Glass, was kindly provided by a friend. The chemical structure and physical properties of Nafion and Flemion are collected in Table **3.1**.

The PSA membranes were treated in a conventional protocol [**1**]: boiling in 3% H_2O_2 for 1 hour, rinsing in boiling deionized water repeatedly, then boiling in 0.5M H_2SO_4 for 1 hour, and finally rinsing again in deionized water. After this treatment, the membrane was dried in room temperature under vacuum condtitions. The ion exchange capacity (IEC) measurements indicate that this treatment had no influence on IEC compared with that of as received membrane.

Table 3.1: Chemical structural, equivalent weight (EW), and thickness for Nafion 117 and Flemion SH 150.

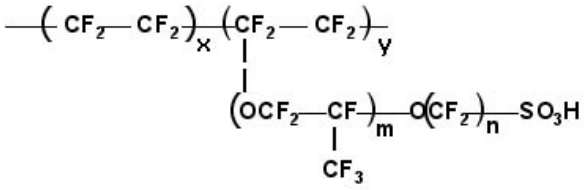

Membrane	Structural parameters	EW (mequiv.g^{-1})	Thickness (um)	IEC
Nafion 117	x= 6.5, y = 1, m = 1, n = 2	1100	178	0.91
Flemion SH 150	m = 0, n = 1-5	909	160	1.0

3.1.2 Reagents

Dimethyl sulfoxide (DMSO, $(CH_3)_2S=O$), tert-butanol (t-BuOH, $(CH_3)_3COH$), and dimethyl sulfone ($DMSO_2$, $(CH_3)_2SO_2$) were used as reagents in this work. The grade reagents of these materials were purchased from Sigma-Aldrich Corporation. Water was carefully purified by deionization and double distillation and was used for the measurements immediately after the purification.

3.2 Water sorption of PSA membranes

The sorption of water by perfluoronated sulfonic acid samples in the temperature range of 25-90^{o}C was determined by two methods:

1. By measuring the weight increases of a dry sample after isopiestic equilibrium [2] with a controlled water activity, which is expressed as the ratio of water pressure to the saturated vapor pressure at the temperature of experiment, 25^{o}C. The pre-treated Nafion 117 and Flemion SH150 membranes were suspended in a closed container where the relative humidity was controlled by various solutions. Five distinct water activities were selected to encompass the whole water content region. Table 3.2 shows the selected solutions and the activities.

2. By continuous measurement of the weight of a PSA sample in contact with a known water vapor pressure using the quartz spring sorption experiment. The membrane sample was hung on a very sensitive quartz spring inside an evacuated glass column. One end of the glass column was connected to a water reservoir and the other end connected to a vacuum system. The weight gained by the sample upon exposure to water vapor was measured by the deflection of the quartz spring. In the experiments, a pre-dried sample was transferred to the glass column, the system was evacuated, and the sample was then re-dried under vacuum conditions at 120^{o}C for 2 hours. This heating treatment kept all the samples in a same initial state. Next, the glass column was then adjusted to various experiment temperatures. The water vapor was admitted into the column from the water reservoir, and the vapor pressure was measured by a pressure gauge. The corresponding spring deflections were measured after waiting for sufficient time to establish

equilibrium. The vapor pressure was increased in suitable increments up to near the saturation vapor pressure. In avoidance of the condensation of water on the membrane surface, the sorption was stopped before the saturation vapor pressure was reached.

Table 3.2: The solutions selected to control the water sorption by PSA samples and corresponding relative humidity at 25^{o}C.

Solutions	Water activity
Saturated water vapor	1
1 mol/kg LiCl solution	0.96
Saturated NaCl solution	0.75
Saturated $MgCl_2$ solution	0.33
Dried at 120^{o}C under vacuum for 12 hours	0

3.3 DSC

Differential scanning calorimetry (DSC) measurements were carried out using a TA Q-100 DSC. The sample was scanned from 25 to –80^{o}C to observe the water crystallization peak. The cooling rate was 10^{o}C/min. Through the procedure, the sample was loaded quickly in contact with the ambient atmosphere; no water loss was observed.

3.4 Deuteron NMR of water in Nafion

^{2}H NMR is particularly advantageous for the study of the motion of the hydrogen nucleus because the ^{2}H quadrupolar interation is so large that other interactions can usually be neglected.

For NMR measurements, the deuterated Nafion films, equilibrated to different relative humidities at room temperature, were rolled into cylinders and placed into 10 mm o.d. Pyrex tubes of length 25 mm. The tubes were sealed with epoxy. The ^{2}H NMR measurements were performed on a Novex NMR spectrometer in conjunction with a Cryomagnet System 7-T magnet. The quadrupole echo pulse sequence was used to obtain ^{2}H spectra at 45.65 MHz. T_1 values of the central aqueous peaks were determined with the inversion recovery pulse sequence.

3.5 Microwave dielectric relaxation spectroscopy

3.5.1 Microwave DRS of PSA membrane

In DRS measurements, the PSA membranes were wrapped around the inner conductor of the coaxial airline. Different sample lengths were used to cover the whole frequency range. The complete filling of Nafion into the coaxial airline was critical for precise measurement. For this purpose, the Nafion 117 solution was used to enforce the connection and better filling. The DRS measurements were carried out at a temperature range of 25-45^{o}C at intervals of increasing 5^{o}C. The airline was heated using a heating

tape. Through the procedure, the temperature was controlled by a current controller to a precision of ±0.2^{o}C.

To enable the study of the effects of water content, the membrane samples were equilibrated in various controlled relative humidities, as listed in Table **3.2**. For membranes equilibrated in the lower relative humidity (RH<75%), the microwave DRS measurement was immediately started after the sample was filled into the airline. For the membrane equilibrated in higher relative humidity (RH ≥ 75%), the system was exposed to the same relative humidity for several days after the membrane was filled. The purpose of this process was to recover the water loss during the filling of membrane into the airline. The pre-experiment shows that the temperature scanning does not lead to significant water loss.

3.5.2 Microwave DRS of aqueous solutions

The dielectric relaxation process of aqueous solutions was also measured over frequency range of 45 MHz to 26 GHz by transmission technique using a coaxial line device. In order to achieve a good signal-to-noise ratio a set of length adapted to the desired permittivity and frequency range was used. The sample length was determined by accurate measurement of the sample volume.

3.6 References

1. T.A. Zawodzinski Jr., M. Neeman, L.D. Sillerud, S. Gottesfeld, *J. Phys. Chem.*, **95**, 6040 (1998)

2. ASTM Standard E 104

Chapter 4

Water vapor absorption of Nafion 117

In proton exchange membrane fuel cell (PEMFC) applications, the membranes are humidified by contact with humidified gases, and, therefore, the interactions of water vapor with the Nafion membrane are of interest and importance. The interactions between water and Nafion concern the hydration properties of Nafion, the physical state of water in the membrane, as well as the effects of the membrane on the state and molecular mobility of water. In this chapter, the hydration properties of Nafion 117 are studied by means of equilibrium and dynamic water sorption isotherm measurements. Then, the apparent diffusion coefficient of water and the distinction of sorbed water in different states or phases are investigated. Next, the thermodynamics of water-Nafion interactions are analyzed based on the equilibrium water sorption isotherms. The physical states of water are also studied by means of differential scanning calorimetry (DSC) in compensation with the water sorption.

4.1 Water sorption by Nafion 117

4.1.1 Sorption kinetics

An example of the sorption kinetics for Nafion 117 over the range of water activities, 0.087 to 0.93, measured by quartz spring sorption technique at 50^{o}C is shown in Fig. **4.1**. In this figure, the normalized water sorption, M_t/M_∞, defined as the water

uptake at time t divided by the corresponding limiting value at equilibrium, is plotted versus water activity, which is expressed as the ratio of water pressure to the saturated vapor pressure at the temperature of experiment. The data show good linearity to at least $M_t/M_\infty = 0.6$, which suggests that the sorption processes are controlled by a simple Fickian diffusion [**1**]. The values of the diffusion coefficient, D, were calculated from the initial linear part ($M_t/M_\infty \leq 0.6$) of the plots by using the following equation

$$\frac{M_t}{M_\infty} = \left(\frac{16D}{\pi}\right)^{1/2} \frac{t^{1/2}}{d} \qquad (4.1)$$

where *d* is the thickness of the sample and is presumed constant over the whole sorption process. For simplification, the value of the thickness of the dry membrane, 0.018cm, is taken for *d*.

From Fig. **4.1**, it is seen that the sorption rate increases rapidly with the water activity at low water activity, reaching a maximum at about a=0.41, and then decreases dramatically as water activity increases further. For Fickian diffusion, this implies that the diffusion coefficient increases initially and then decreases with water concentration. Such a trend for the water diffusion coefficient was also observed at two other temperatures, 30 and 90^{o}C in this work, see Fig. **4.2** and Fig. **4.3**, respectively.

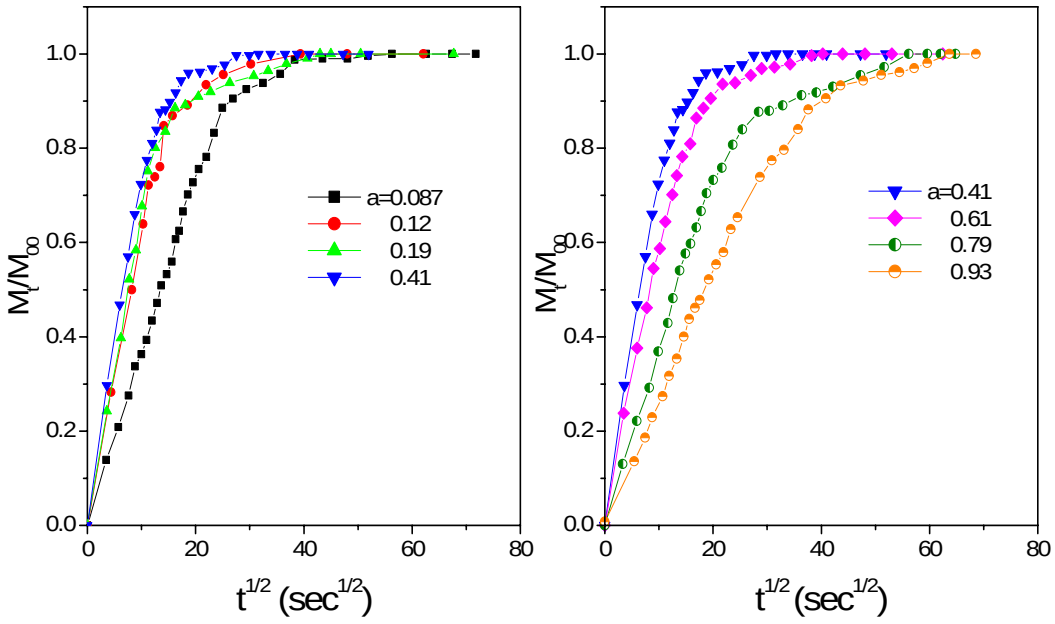

Fig. **4.1**: Incremental sorption curves for Nafion 117 from water vapor at 50°C. The numbers in the figure represent the water activities.

The apparent water diffusion coefficients at three temperatures are collected in Table **4.1** and plotted against the water activity in Fig. **4.4**. It is evident from Fig. **4.4** that the diffusion coefficient of water in Nafion is a strong function of the water activity (thus, of water content) and temperature. Furthermore, D reaches a maximum value at an activity of about 0.4 at the experimental temperature range of 30 - 90^{o}C. A value of around 1×10^{-8} cm^{2}/s was obtained for the diffusion coefficient of water at 30^{o}C, though the value varies with water content. From water-immersion experiments, Yeo and Eisenberg [**2**] reported a value of 1.7×10^{-6} cm^{2}/s for the diffusion coefficient of water in swollen Nafion at 25^{o}C, which is two orders of magnitude higher than the value of D obtained in this work. Lower diffusion coefficient for water obtained from experiments involving water vapor than that involving liquid water has also been observed by other researchers. Takematsu *et al*. [**3**] reported $D=2\times10^{-8}$ cm^{2}/s for water sorption by Nafion at 23^{o}C. Values in similar magnitude were also reported by Morris and Sun [**4**] for D of water at 25^{o}C. The self-diffusion coefficient of water in hydrated Nafion has been determined using NMR spectroscopic and imaging diffusion measurements [**5**], and a value of about 4×10^{-6} cm^{2}/s was reported, which is two orders of magnitude higher than the value of D obtained from vapor sorption experiments. It needs to be pointed out that the diffusion coefficient obtained from water sorption experiments is generally "chemical" diffusion coefficient, not self-diffusion coefficient.

Fig. **4.4** displays a concentration-dependent diffusion coefficient for water in the Nafion membrane. A similar trend for D has also been observed by Morris and Sun [**4**]. In their water sorption experiments, they found that the diffusion coefficient increases

rapidly at low concentrations, but reaches a maximum at $\lambda = 4$ H_2O per $-SO_3H$ site (corresponding to water activity of about 0.4), with a value of about 4×10^{-7} cm^2/s at 25^oC. The self-diffusion coefficients of water in Nafion, obtained by pulse field gradient NMR [**5**], also exhibited a maximum at $\lambda \sim 3$ $H_2O/-SO_3H$ when converted to "chemical" diffusion coefficients. Free volume concepts have been applied to describe the concentration dependence of D, both above and below the glass transition temperature [**6**].

The activation energy for water diffusion was estimated from the Arrhenius plots, as shown in Fig. **4.5**. For different water activity, the activation energy has almost same value and is estimated to be 18.3 kJ/mol. This value is close to that obtained by Morris and Sun [**4**] from the water sorption experiments. They reported a value of 23 kJ/mol for the activation energy for water diffusion in Nafion. The activation energy for water diffusion in a swollen Nafion membrane was reported to be 20.2 kJ/mol [**2**]. These values indicate that, in experiments involving both water vapor and liquid water, water diffuses via a similar molecular mechanism. The much higher diffusion coefficient for water in the swollen membrane is due to the larger pre-exponential factor in the Arrhenius equation, which is possibly due to the decrease of tortuosity of the diffusion path in the swollen sample as compared to the less hydrated sample.

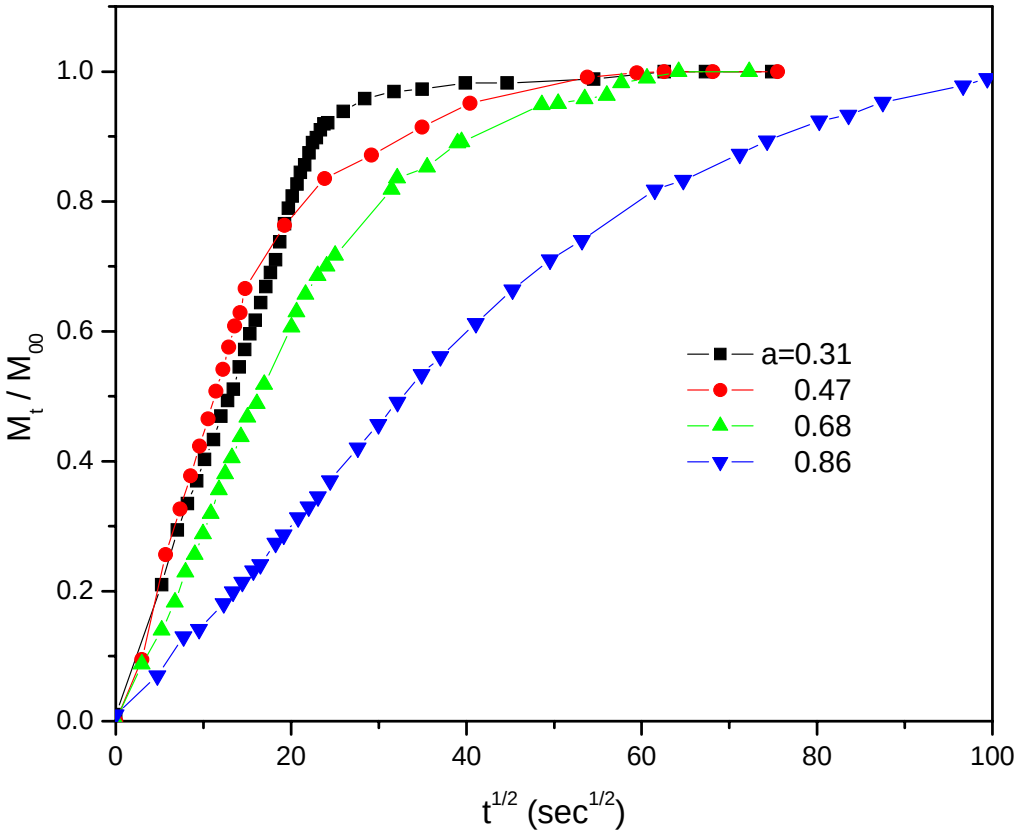

Fig. **4.2**: Incremental sorption curves for Nafion 117 from water vapor at 30^{o}C. The numbers in the figure represent the water activities.

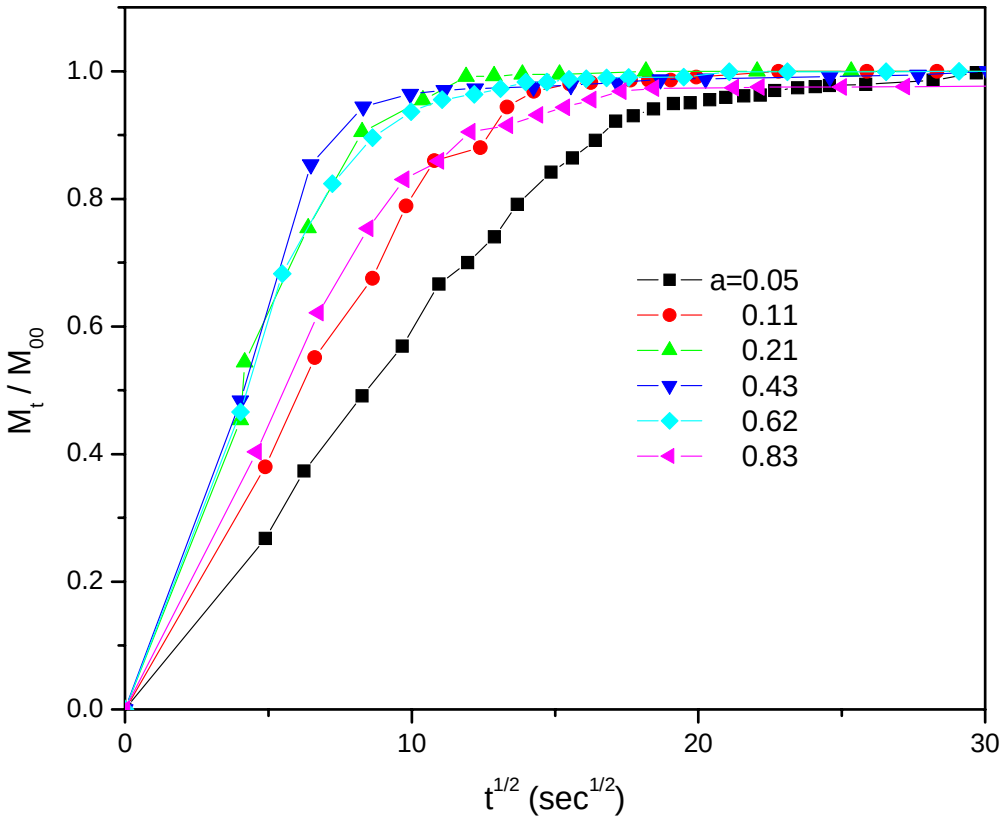

Fig. **4.3**: Incremental sorption curves for Nafion 117 from water vapor at 90°C. The numbers in the figure represent the water activities.

Table **4.1**: Diffusion coefficients for water in Nafion

Water activity	D ($\times 10^{-7}$ cm^2/s)	Water activity	D ($\times 10^{-7}$ cm^2/s)
T=30°C		T=90°C	
a=0.31	0.98	a=0.05	2.68
0.47	1.19	0.11	6.8
0.68	0.57	0.21	11.6
0.86	0.14	0.43	17.6
		0.62	14
T=50°C		0.83	6.25
a=0.09	0.88		
0.12	1.27		
0.2	2.75		
0.41	3.3		
0.61	1.88		
0.79	0.97		
0.93	0.48		

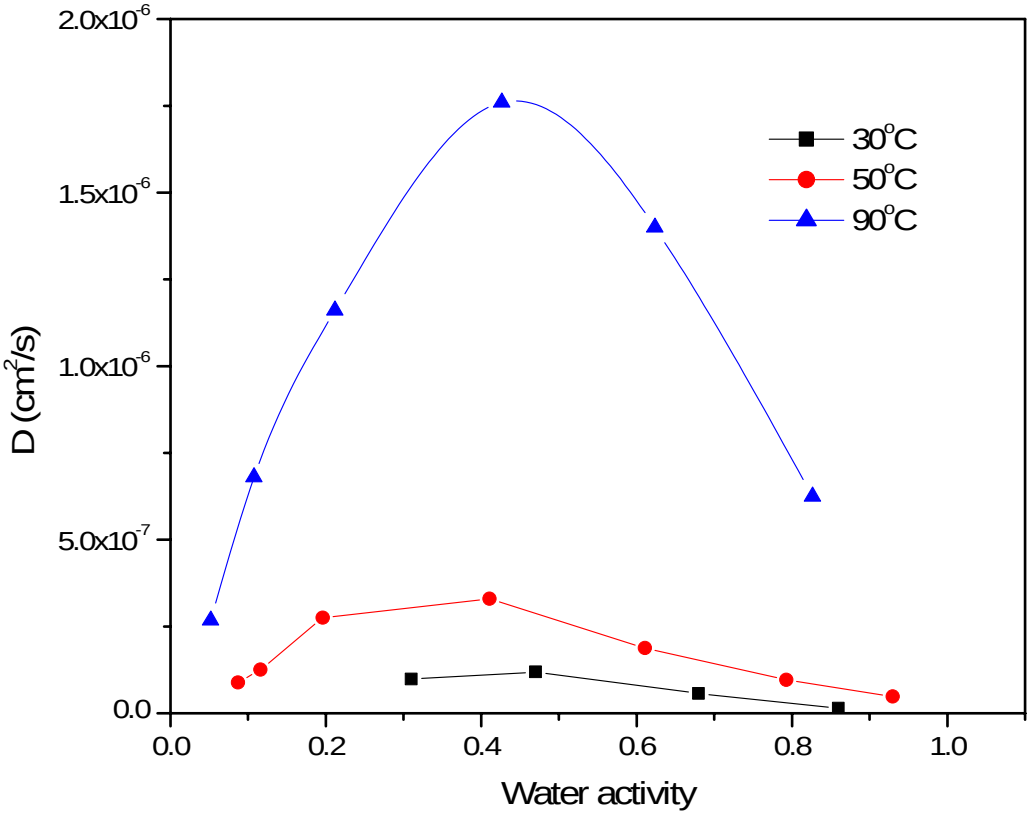

Fig. **4.4**: Diffusion coefficients for water in Nafion 117 membrane vs. water activity at 30, 50, and 90°C.

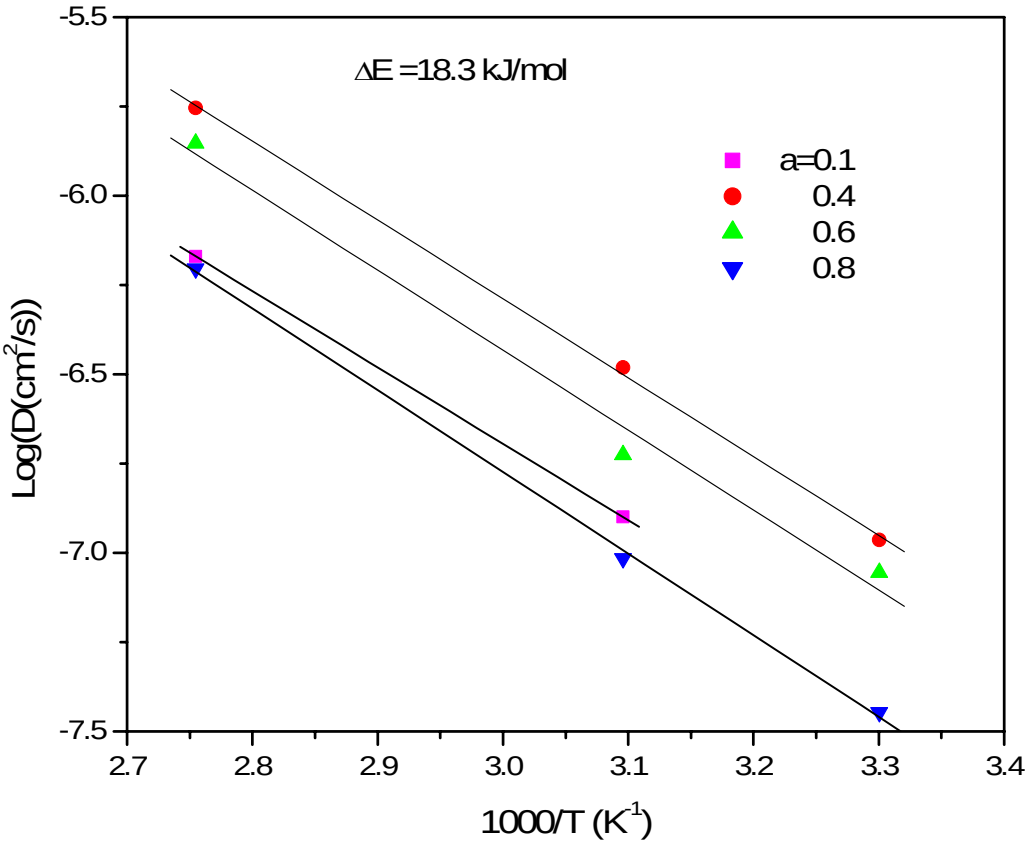

Fig. **4.5**: Arrhenius plot of water diffusion coefficient vs. T^{-1}. The numbers in the figure denote the water activity.

4.1.2 Equilibrium water sorption isotherms

Water uptake is often represented by the number of moles of water molecules per mole of ion exchange site, $\lambda = n_{H_2O} / n_{-SO_3H}$. λ is related to the mass ratio of water to Nafion, f_m, by the equation, $\lambda = \frac{n_{H2O}}{n_{H^+}} = \frac{m_{H2O}/18}{m_O/1100} = 61.0 \times f_m$, where m_o is the mass of dry Nafion with equivalent weight of 1100. The isotherms for water sorption by Nafion 117 membranes from water vapor at different temperatures are shown in Fig. **4.6**. For comparison, the water sorption isotherms measured at 80^{o}C [**7**] are also shown in the figure. It is interesting to note from Fig. **4.6** that the water uptakes of Nafion 117 at 30^{o}C are higher than those at 50 and 90^{o}C, but λ at 90^{o}C is higher than the values at corresponding water activity at 50^{o}C. The comparison of water uptake at room temperature to that at elevated temperatures has led to controversial conclusions in the literature. For instance, Morris and Sun [**4**] measured the water vapor sorption isotherms in the temperature range of 25-100^{o}C and found that the water uptake increases with increasing temperatures. On the other hand, several works showed that the water sorption from water vapor decreases with increasing temperature [**7**-**9**]. Moreover, the water uptake values at room temperature in the literature [**4**,**7**-**9**] are very scattered. These observations indicate that the water uptake is sensitive to the history of treatment of the membrane. Probably no real internal equilibrium has been achieved in the range of 18.5-30^{o}C owing to low temperatures.

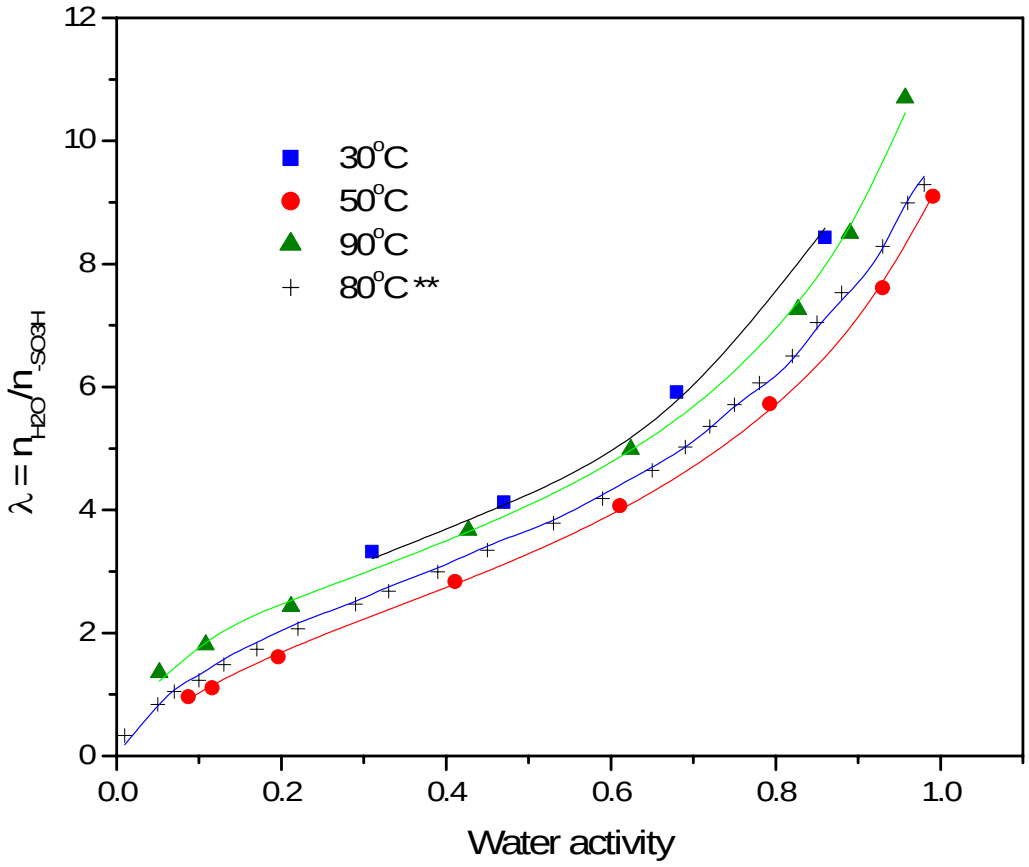

Fig. **4.6**: Sorption isotherms of Nafion 117 at 30, 50, and 90°C. For comparison, the sorption at 80°C [**7**] is also shown in this figure. The lines are the results calculated according to Eq. **4.2**.

The S-shape of the sorption isotherms allows us to analyze the data according to the famous Brunauer-Emmett-Teller (B.E.T.) equation. We have used Anderson's modification [**10**]:

$$\lambda = \lambda_m \frac{Cka}{(1-ka)(1+(C-1)ka)} \qquad (4.2)$$

where a is the activity of water (relative humidity), and λ_m is the number of sorption sites per (-SO_3H) group, which indicates the first monolayer sorption capacity. C is the ratio of the binding constants of a water molecule directly bound to the sorption site in the first layer and of one indirectly bound in the succeeding liquid-like layers. k is the ratio of the standard chemical potential of the indirectly bound water to that of the molecule in the bulk liquid state. The equation reduces to the B.E.T. equation when $k = 1$.

The values of the parameters have been derived from the sorption isotherm data by using the linear form of Eq. **4.2** [**11**,**12**], and the optimized parameters are listed in Table **3.2**. The fitted results according to Eq. **4.2** are also shown in Fig. **4.6** as the solid lines. The fitting parameters at 30^{o}C are in divergence with those obtained at higher temperatures, which indicates again that no real internal equilibrium has been achieved at low temperature. An important result is that the first monolayer capacity, λ_m, was found to remain constant at a value of about 2.7 in the temperature range of 30-90^{o}C. This means that the first layer of water, which is tightly bound to the sorption site, is composed of about three water molecules.

Table 4.2: Parameters used in BET modeling of equilibrium water sorption.

T (oC)	C	λ_m	k
30	23.09	2.73	0.8
50	7.41	2.55	0.74
90	18.14	2.70	0.78
80 *	10.28	2.70	0.74

As seen from Fig. 4.6, Eq. 4.2 fits the experimental data well up to at least a = 0.8. The large degree of upturn observed at higher activities may suggest clustering of water molecules [11]. Zimm and Lundberg [13] created a quantity called the cluster integral, G_{11}, to determine the tendency of penetrant molecules to form clusters in a polymer. G_{11} can be calculated from the equilibrium sorption isotherm data by the following equation:

$$\frac{G_{11}}{V_1} = -(1-\varphi_1)\left[\frac{\partial(a/\varphi_1)}{\partial a}\right]_{P,T} - 1 \qquad (4.3)$$

where V_1 represents the partial molar volume of water, and *a* represents water activity. φ_1 is the volume fraction of water in the polymer and can be calculated by $\varphi_1 = \frac{V_{H_2O}}{V_{H_2O} + V_O} = \frac{\rho_o f_m}{\rho_{H_2O} + \rho_o f_m}$, where ρ_o and ρ_{H2O} are the density of dry polymer and pure water, respectively, and f_m is the mass ratio of sorbed water to dry Nafion.

$\frac{\varphi_1 G_{11}}{V_1}$ indicates the quantity by which the average number of water molecules is excess of the mean concentration of water molecules in the neighborhood of a given water molecules. Thus, clustering of water molecules is indicated when $\frac{\varphi_1 G_{11}}{V_1}$ is greater than 0. Fig. **4.7** shows $\frac{\varphi_1 G_{11}}{V_1}$ as a function of water activity at different temperatures. The values of $\frac{\varphi_1 G_{11}}{V_1}$ are calculated from the equilibrium sorption data (Fig. **4.6**) by using a 6^{th} order polynomial fitting to the a/φ_1 vs a plot and taking the derivative at the corresponding values of a. The values of $\frac{\varphi_1 G_{11}}{V_1} > 0$ for $a > 0.8$ suggest clustering of water molecules, as shown in Fig. **4.7**. The clustering of water leads to the filling of the pores with water and the swelling of the polymer at water activity beyond 0.8. This result is in accordance with the dimensional and density change measured by Morris and Sun [**4**]. These authors observed a dramatic decrease in density at water content higher than 6 water molecules per SO_3H site, which corresponds to a water activity of 0.8.

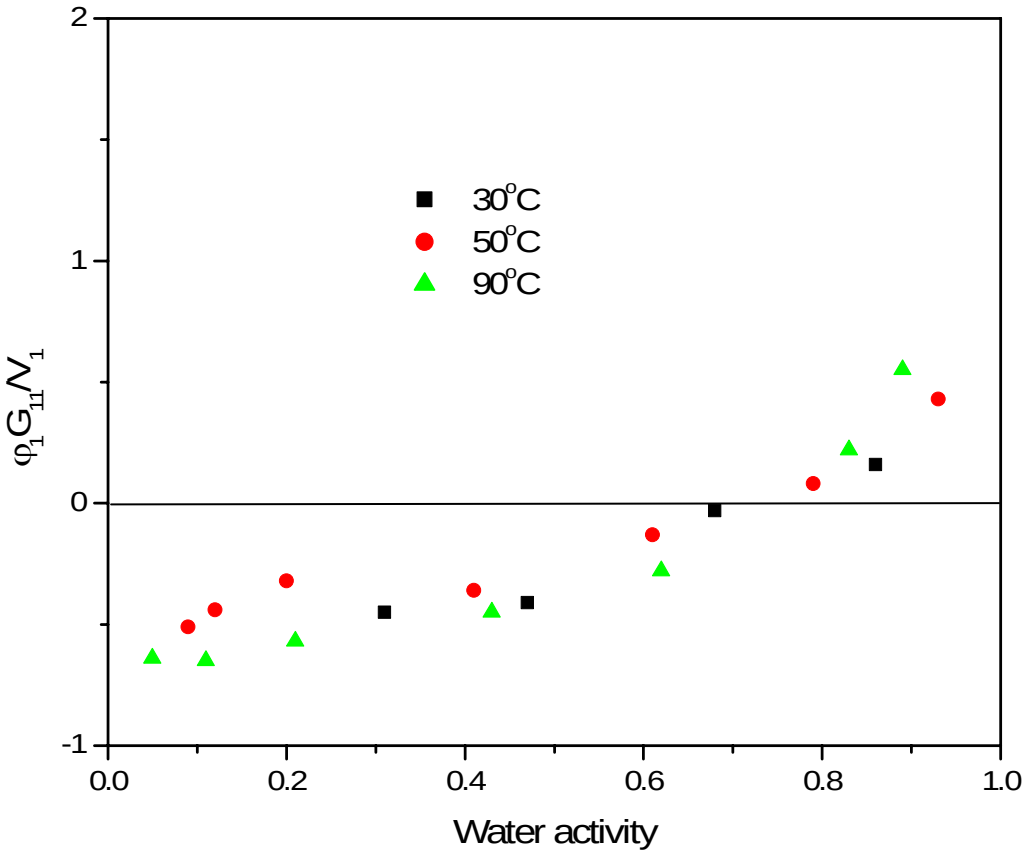

Fig. **4.7**: $\varphi_1 G_{11}/V_1$ as a function of the activity at 30, 50, and 90°C.

4.2 State of water studied by DSC

The DSC cooling curves of Nafion 117 with various water contents are shown in Fig. **4.8**. An exothermic peak, beginning at ca. –20^{o}C, was observed for the two higher water contents, namely λ=21 (which was soaked in liquid water) and λ = 15 (which was dried in ambient temperature for 10 minutes after soaking in liquid water). The exothermic peak was due to the freezing of water in membranes. In contrast to the soaked samples, no exothermic peak was observed for samples conditioned at various level of relative humidity, which contains lower water content. The lack of exothermic peak indicates that the water in these samples remained unfrozen upon lowering the temperature.

Yoshida and Miura [**14**] studied the DSC cooling of Nafion in alkali ion forms with various water contents. Water molecules in the membranes were classified into three types: non-freezing water, freezing-bound water, and free water. The free water was found to freeze at higher temperature than does the freezing-bound water. Both the non-freezing and freezing-bound water strongly interacted with ions. The non-freezing water was considered to exist in hydration shells of the cations and $-SO_3^-$ groups, while the freezing-bound water was assumed to be connected with the hydration of the counter ions. Both the non-freezing and freezing bound water increase with water content, but approach constant values above certain water content.

In this work, for acid Nafion membrane, only two types of water, freezing and non-freezing, were observed from the DSC cooling curves. The amount of unfrozen water is up to around 10 water molecules per sulfonic acid group. A similar value was

also reported for non-freezing water in Nafion 117 [15]. Above this water content, the freezing water starts to appear. No freezing-bound water can be detected from the DSC experiment.

4.3 Solid state NMR measurements

^2H NMR experiments were carried out at the magnetic field of 6.98 Tesla at room temperature. The quadrupole echo pulse sequence was used to obtain ^2H spectra at 45.65 MHz. A single sharp peak has always been observed for water contents between 1 and 9 water per SO_3^- site. It is well-known that water molecules exist in different states in Nafion membrane, this behavior thus may indicate an exchange rate larger than 10^{-3} to 10^{-4} sec between different kinds of water moleucles.

^2H T_1 relaxation times were determined for the single sharp water peak with the inversion recovery technique. Fig. 4.9 plots T_1 values as a function of water content. The relaxation time increases as the water content increases, which is in accord with the literature [16]. This indicates increased hindrance to rotational motion of water at lower water contents. Two regions are discriminated in this figure: (1) a region of relatively little increase of T_1 with increasing water content ($\lambda < 3 - 4$) and (2) a region of significantly greater increase of T_1 with water content ($\lambda > 4$). Region (1) corresponds to the first hydration layer of water, determined from the water sorption isotherm. This result is important because it means that the first few water molecules have almost same binding energy. They are all tightly bound to the sulfonate ions and form the first hydration layer. In region (2), water moleucles are more mobile.

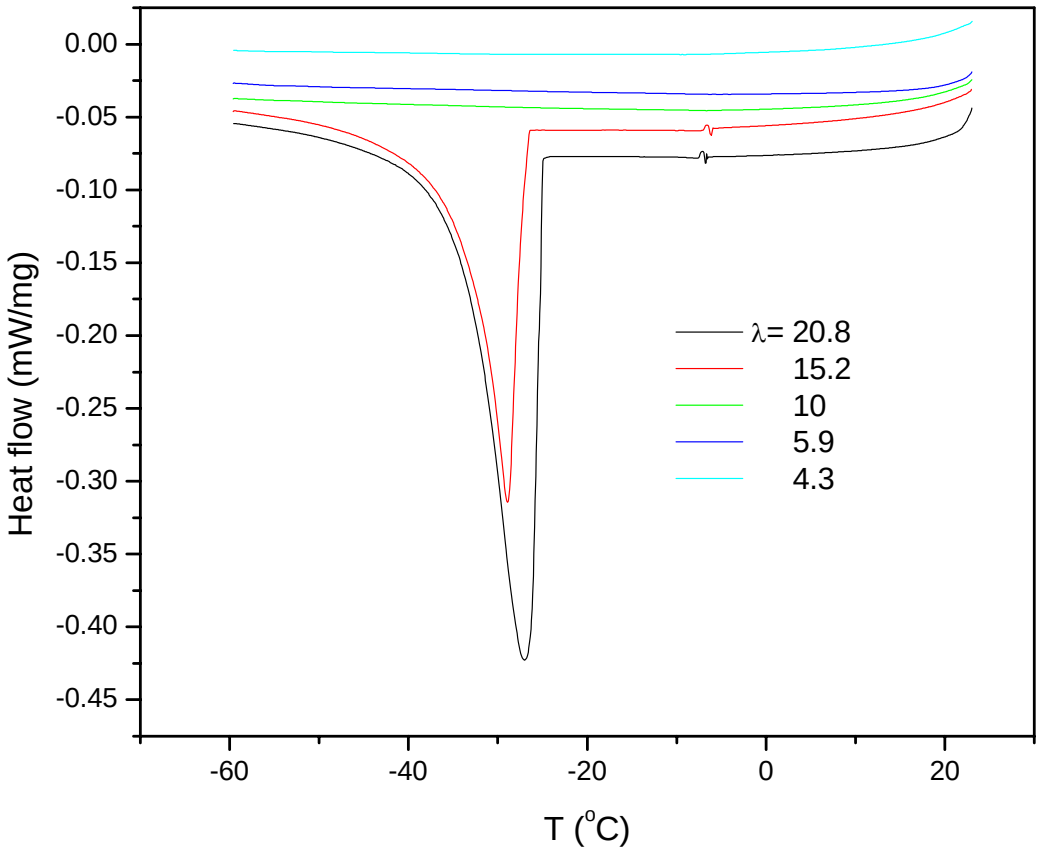

Fig. **4.8**: DSC cooling curves of Nafion 117 with various water contents. The numbers in the figure show water content in numbers of water per $–SO_3H$.

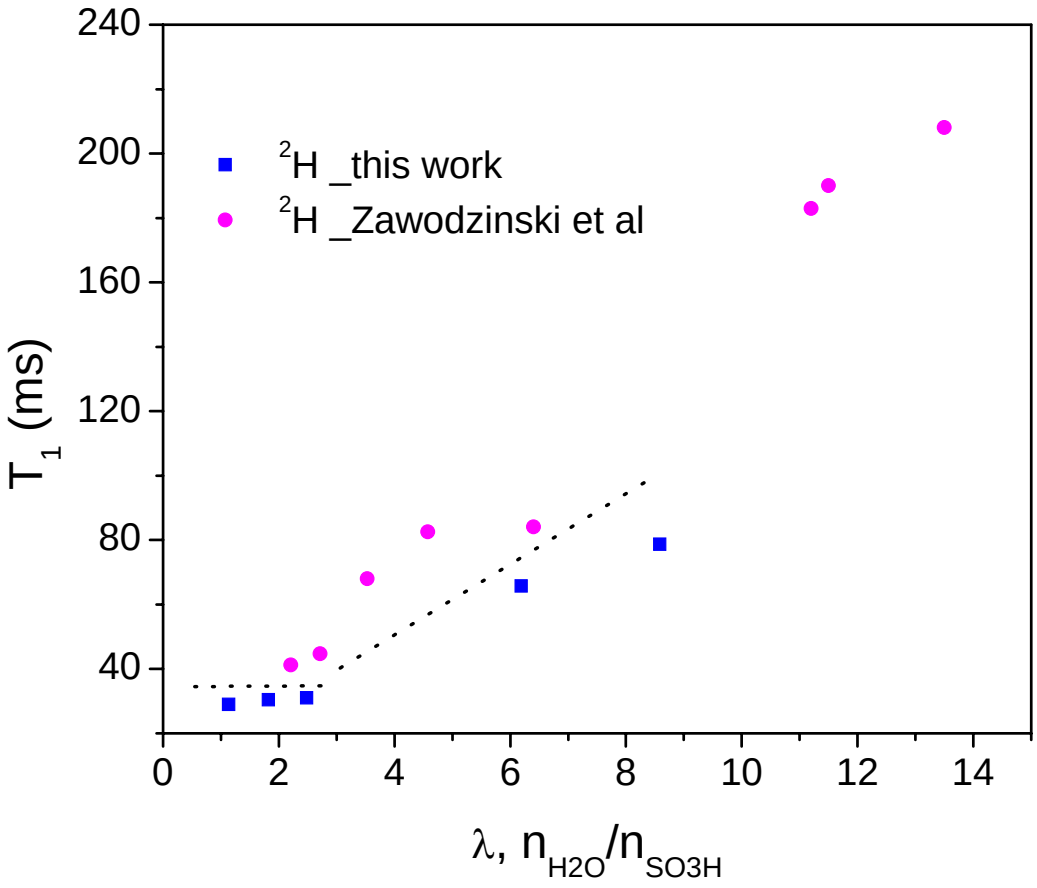

Fig. **4.9**: ^{2}H spin-lattice relaxation time of deuterated water in Nafion 117 as a function of the water content. Also plotted in this figure is the data from reference [**16**] at 30oC.

4.4 Summary

The dynamic and equilibrium sorption isotherms of Nafion 117 membrane from water vapor over the temperature range 30 to 90^{o}C were determined. The equilibrium sorption isotherms may be quantitatively analyzed according to the modified BET equation for multilayer sorption processes up to water activity of 0.8. The first monolayer capacity, i.e., the first hydration layer of Nafion membrane, was found to be about three water molecules per sulfonic acid group. The analysis of the equilibrium sorption isotherm, using the method of Zimm and Lundberg, suggests clustering of the water molecules at high water activities above 0.9.

DSC cooling scans of the hydrated Nafion membranes indicated two types of water in terms of freezing and non-freezing fractions. The amount of non-freezing water is up to about 10. The ^{2}H spin lattice relaxation time (T1) of $^{2}H_2O$ in Nafion was measured as a function of state of membrane hydration. The first hydration layer of sulfonic acid group was estimated to be about 3 water molecules per sulfonic acid group, which is in agreement with the water sorption isotherms.

Either DSC or solid state NMR is sensitive to the state of water in Nafion membrane for all water contents. DSC is relatively sensitive at higher water contents, while NMR is sensitive at lower water contents. New technique is required to study the water state in Naifon membrane.

4.5 References

1. J. Crank, *The Mathematics of Diffusion*, 2nd ed. Clarendon Press, Oxford, 1975, Chapter 9

2. S.C. Yeo and A. Eisenberg, *J. Appl. Polym. Sci.*, **21**, 875 (1977)

3. T. Takematsu, M. Hashiyama, A. Eisenberg, *J. Appl. Polym. Sci.*, **24**, 2199 (1979)

4. D.R. Morris and X. Sun, *J. Appl. Polym. Sci.*, **50**, 1445 (1993)

5. T.A. Zawodzinski Jr., M. Neemand, L.O. Silerud, S. Gottesfeld, *J. Phys. Chem.*, **95**, 6040 (1991)

6. J.L. Duda, I.H. Romdhane, R.P. Danner, *J. Non-Cryst. Solids*, **172-174**, 715 (1994)

7. J.T. Hinatsu, M. Mizuhata, H. Takenaka, *J. Electrochem. Soc.*, **141**, 1493 (1994)

8. T.A. Zawodzinski Jr., T.E. Springer, F. Uribe, S. Gottesfeld, *Solid State Ionics*, **60**, 199 (1993)

9. K.K. Pushpa, D. Nandan, R.M. Iyer, *J. Chem. Soc., Faraday Trans. I*, **84**, 2047 (1988)

10. R.B. Anderson, *J. Am. Chem. Soc.*, **68**, 686 (1946)

11. E.O. Timmermann, *J. Chem. Soc. Faraday Trans. I*, **85**, 1631 (1989)

12. C. Tsonos, L. Apekis, P. Pissis, *J. Mater. Sci.*, **35**, 5957 (2000)

13. B.H. Zimm and J.L. Lundberg, *J. Phys. Chem.*, **60**, 425 (1956)

14. H. Yoshida and Yuka Miura, *J. Membr. Sci.*, **68**, 1 (1992)

15. N. Walsby, S Hietala, S.L. Maunu, F. Sundholm, T. Kallio, G. Sundholm, *J. Appl. Polym. Sci.*, **86**, 33 (2002)

16. T.A. Zawodzinski Jr., T.E. Springer, F. Uribe, S. Gottesfeld, Solid State Ionics, 60, 199 (1993)

Chapter 5

Microwave Dielectric Relaxation Spectroscopy of Nafion 117

Much information about the state of water in Nafion membrane has been obtained from the water sorption isotherms, DSC, and NMR measurements. The first few water molecules ($\lambda \sim 3$) are tightly bound to the polymer, primarily forming the first hydration layer of the sulfonic acid group. No freezable water can be detected by DSC experiments until λ increases to above 10 water molecules per sulfonic acid group. Above this water content, water clustering occurs, and the freezable water starts to appear. However, the specific interaction between water and perfluorosulfonic acid membranes, the distribution of water, and the dynamics of water in PSA membranes are still unclear. These aspects are closely related to the mechanism of water and proton transport in these materials.

Dielectric spectroscopy is one of the most extensively used techniques to understand water-polymer interaction. This method essentially probes molecular orientational relaxation. The dielectric relaxation mechanisms of water molecules and the influence of the membrane environments on water behavior are the main concerns. The DRS provides additional information on the physical nature of water in PEM membrane as well. In this work, the dielectric relaxation spectra of dry and hydrated Nafion samples were measured over the frequency range of 45 MHz to 26 GHz and at temperatures of 25-45^{o}C.

5.1 Results and data analysis

5.1.1 Dry Nafion membrane

The membrane was dried under vacuum conditions at 120^{o}C for 12 hours before the dielectric measurement. Fig. **5.1** shows the dielectric spectra of a dry sample. As anticipated, the dielectric response is quite similar to that of Teflon (see Fig. **2.7**). The relative permittivity of the dry membrane remains constant at a value of about 3.5, which is higher than the value of 2.0 for Telfon, in the frequency range of 0.1-26 GHz. The imaginary part of the permittivity is also somewhat higher than that observed in Tefolon, which is due to the presence of sulfonic acid groups tethered at the end of the side chains. No relaxation process can be distinguished from the dielectric loss spectrum within the experimental accuracy. These results are in accordance with the dielectric measurements of Paddison *et al*. [**1**]. These authors measured the dielectric spectra of Nafion samples dried over P_2O_5, which contains a water content of $\lambda \sim 1$, over 0.045-30 GHz using reflection technique. They concluded that no relaxation exists in this frequency range for dry membranes. The relative permittivity of their dried membrane was obtained to be ca. 4.0 from the measurements.

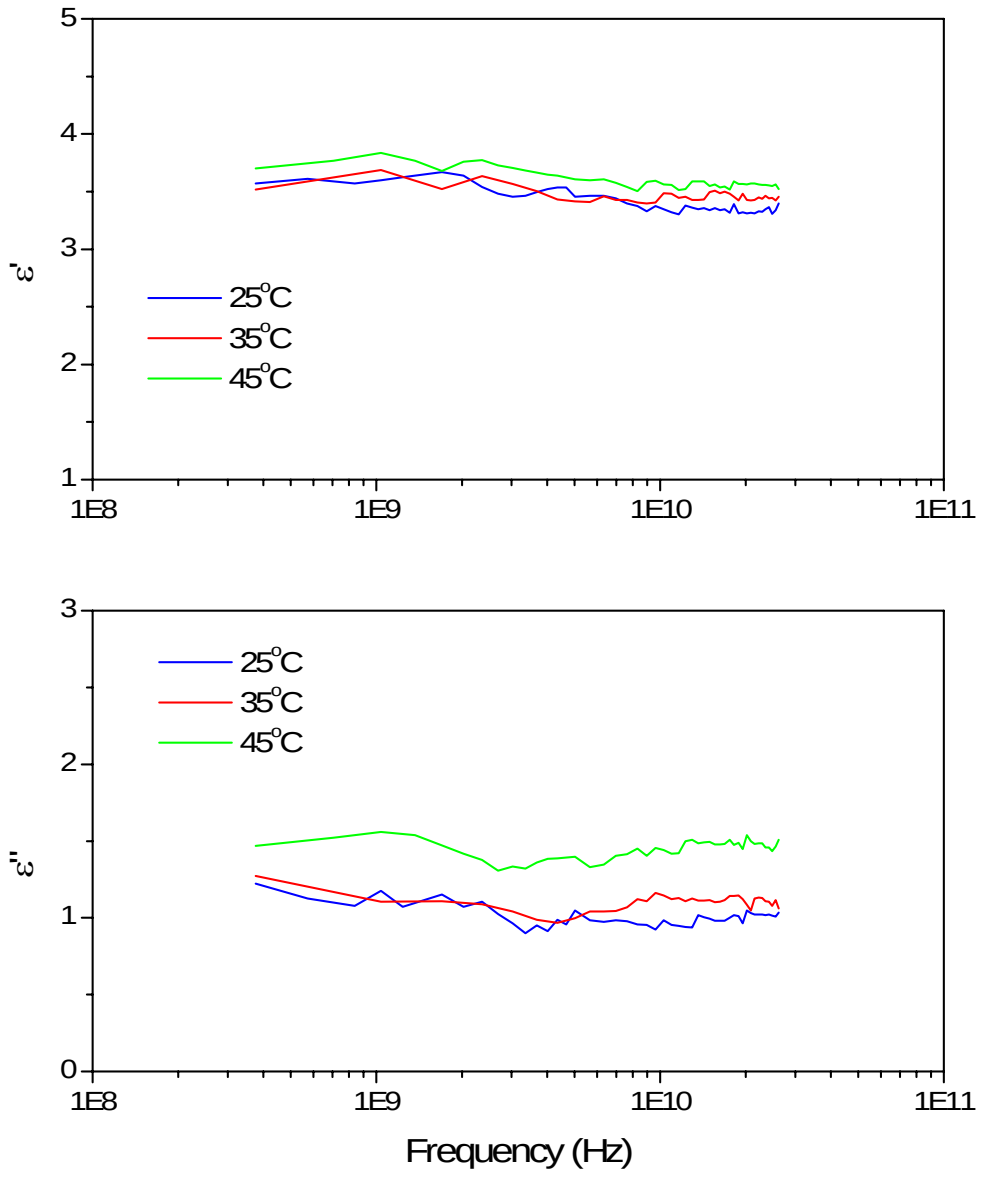

Fig. **5.1**: Dielectric dispersion, ε′(ω), and loss spectrum, ε″(ω), of dry Nafion at 25, 35, and 45°C.

5.1.2 Hydrated Naifon membranes – equilibrated in water vapor

To enable the study of the effects of water content on the DRS of Nafion 117, four distinct hydration states were obtained by using the isopiestic equilibrium scheme. Table 5.1 shows the water content, λ, defined as the number of absorbed water molecules per SO_3H site.

Table 5.1: Parameters for selected water contents of Nafion 117 at 25°C.

Solution	Relative Humidity, %	Water content, λ
Saturated water vapor	100	12
1mol/kg LiCl solution	96	9
Saturated NaCl solution	75	6
Saturated $MgCl_2$ solution	33	3

The dielectric spectra, permittivity, ε′(ω), and absorption, ε″(ω), of various hydrated Nafion 117 (λ = 12, 9, 6, and 3) are plotted in Figs. **5.2**-**5.5**. Several points can be drawn from these figures: 1) the shape of the dielectric spectra of hydrated Nafion is in marked difference from that of dry Nafion. The well-defined dielectric dispersions (Δε′) are apparently presented in permittivity spectra. These dispersions indicate that there are dielectric relaxations in hydrated Nafion membrane, in contrast to the case of dry Nafion, where no relaxation can be distinguished; 2) the absorption spectrum, ε″(ω), displays a f^{-1} relation at low frequencies. This behavior can be attributed to the contribution of the conductivity, resulting from the long-range motion of H_3O^+. The high conductivity of Nafion leads to the high value of ε″, which dominates the absorption of the sample at lower frequencies; 3) these figures show that the water content has a significant influence on the DRS of Nafion membrane. The permittivity decreases dramatically as water content decreases. At the same time, the absorption of the sample decreases as well; and 4) the temperature also shows an important effect on the dielectric response. For each water content, the permittivity and absorption increase with temperature. This phenomenon may be attributed to the increased ionic conductivity at higher temperatures and is common for ionic conducting materials [**2**].

Due to the specific conductivity, σ, of hydrated Nafion, the measured absorption of hydrated membranes comprises the contribution of the conductivity, which is given by $\frac{\sigma}{\omega\varepsilon_0}$, and the true absorption of the sample. The relation is shown as Eq. **5.1**.

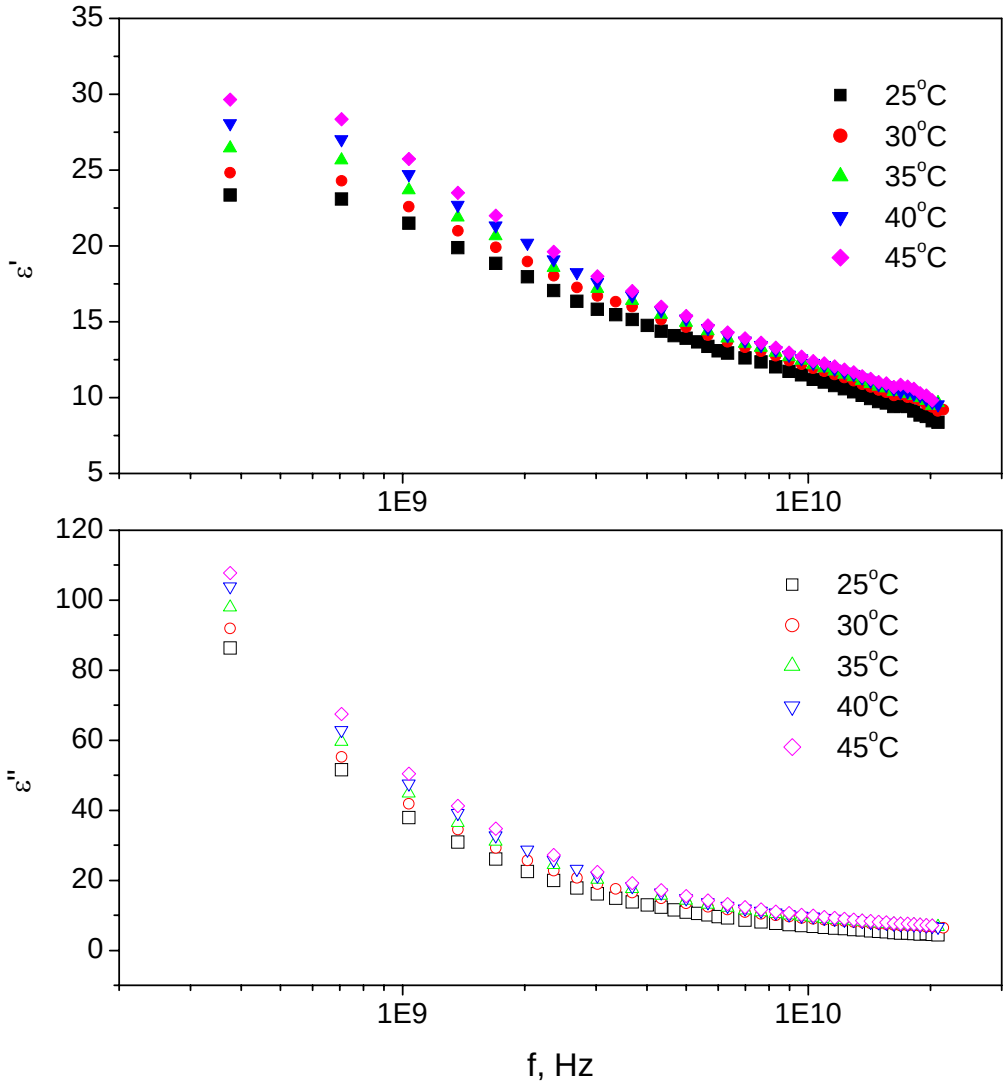

Fig. **5.2**: Measured permittivity, ε′(ω), and absorption, ε″(ω), for Nafion 117 membrane equilibrated in saturated water vapor (RH=100%, λ=12) at 25-45°C in steps of 5°C.

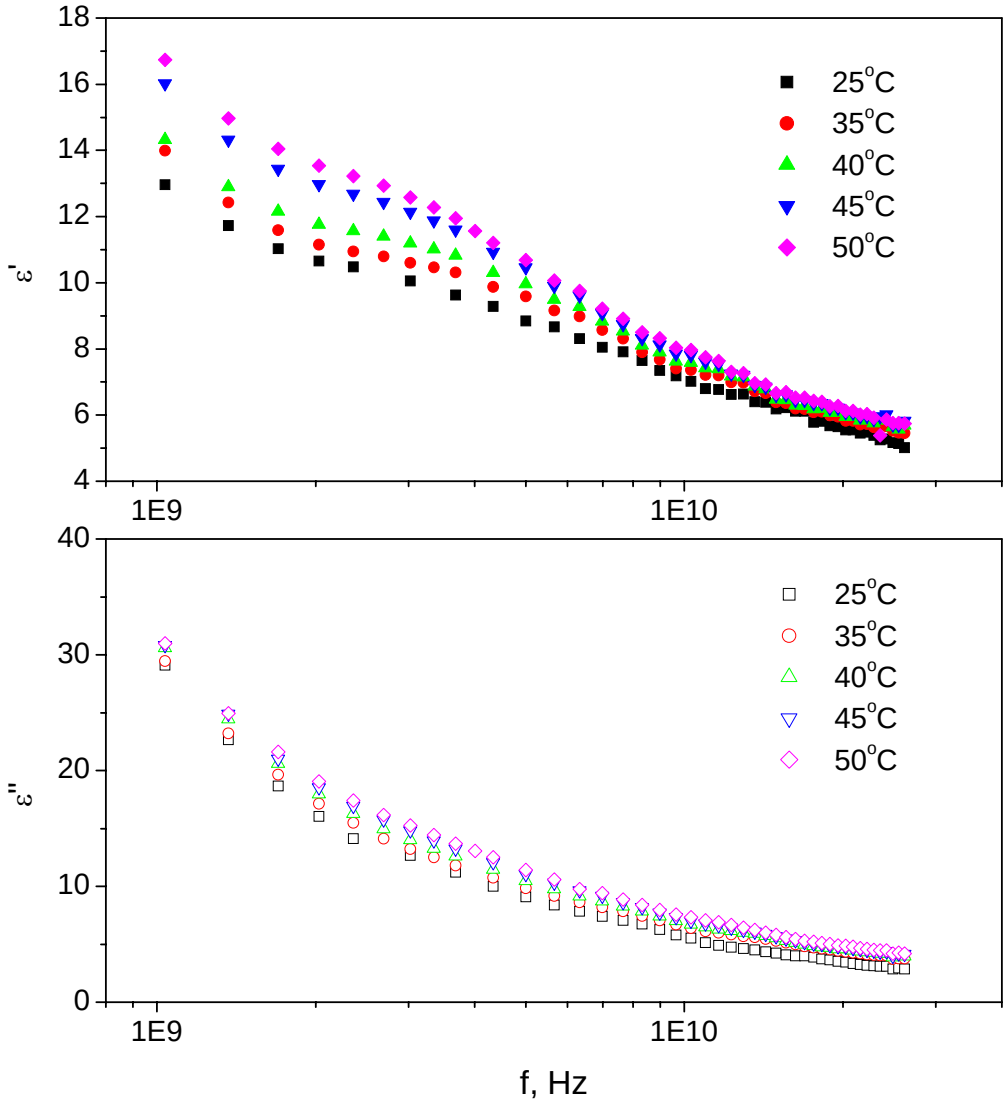

Fig. **5.3**: Measured permittivity, ε′(ω), and absorption, ε″(ω), for Nafion 117 membrane equilibrated in 1mol/kg LiCl solution (RH=96%, λ=9) at 25-50°C.

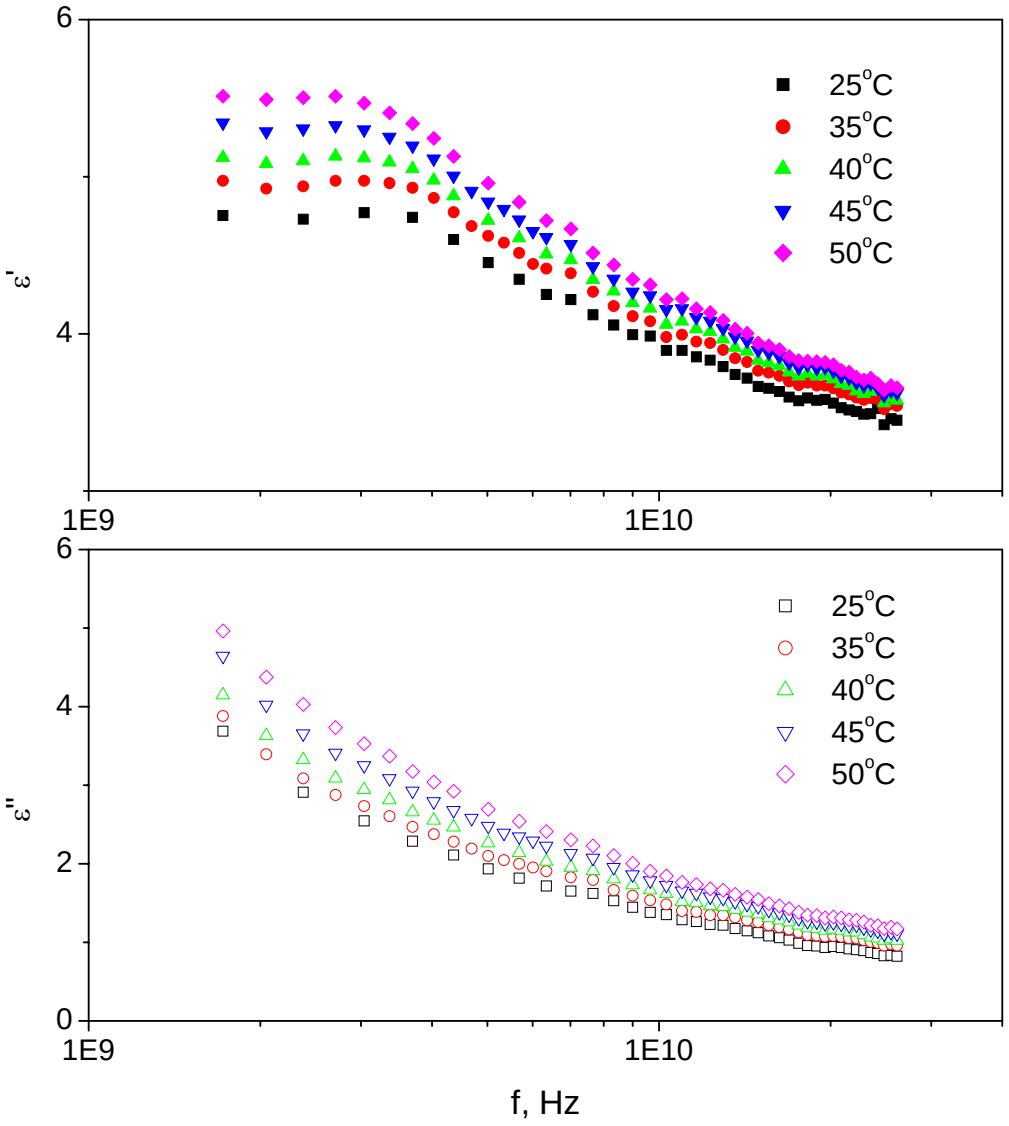

Fig. **5.4**: Measured permittivity, ε′(ω), and absorption, ε″(ω), for Nafion 117 membrane equilibrated in saturated NaCl solution (RH=75%, λ=6) at 25-50°C.

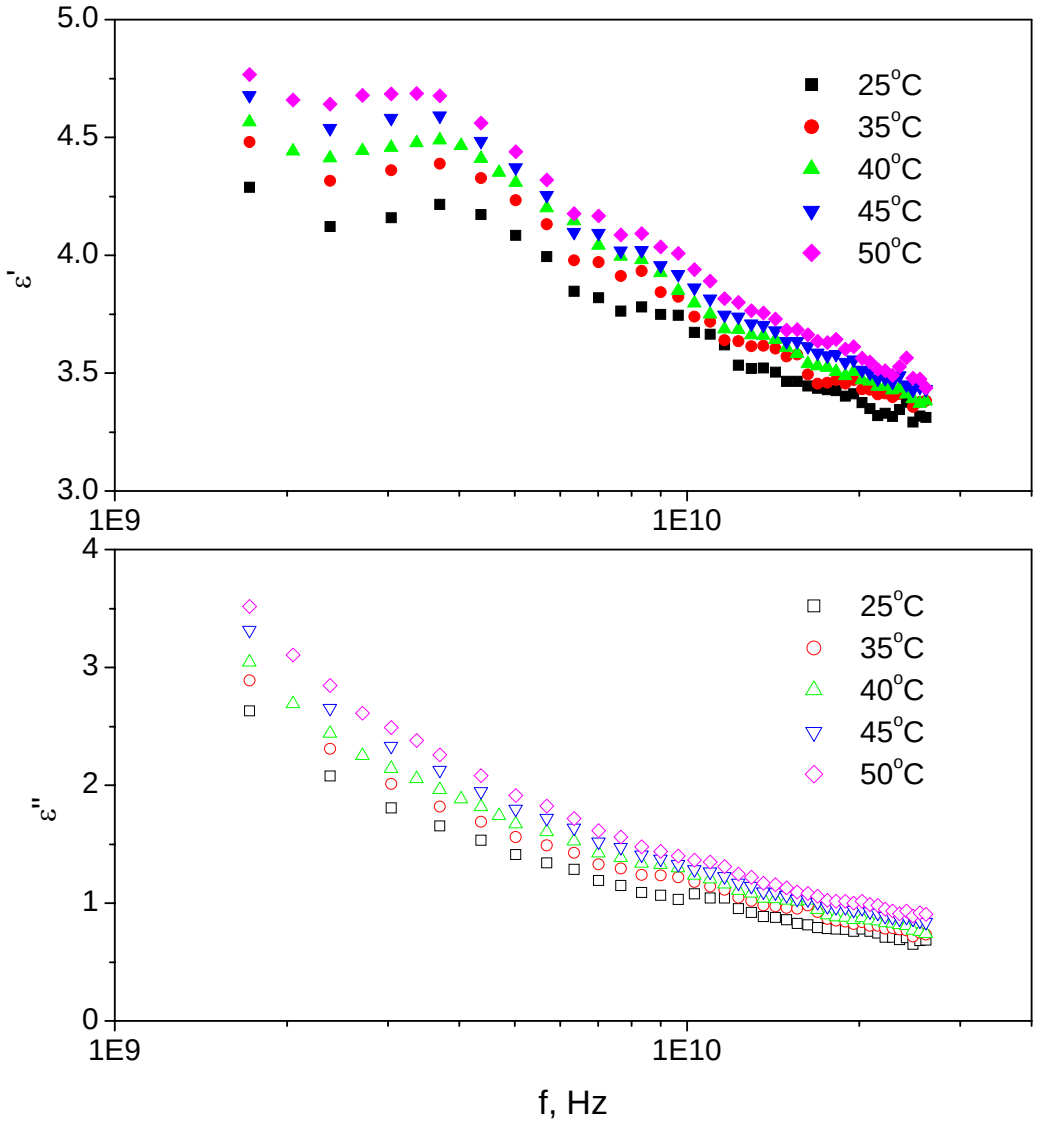

Fig. **5.5**: Measured permittivity, ε′(ω), and absorption, ε″(ω), for Nafion 117 membrane equilibrated in saturated $MgCl_2$ solution (RH=33%, λ=3) at 25-50°C.

$$\varepsilon''_{total}(\omega) = \varepsilon''(\omega) + \frac{\sigma}{\omega\varepsilon_0} \qquad (5.1)$$

where ε''_{total} and ε″ represent the total absorption and the true absorption by the sample, respectively. ω is the angular frequency, $\omega = 2\pi f$.

The complex permittivity spectra shown in Figs. 5.2-5.5 were analyzed by simultaneously fitting ε′(ω) and ε″(ω) with a least-square procedure described in Chapter 2. The program allows to model ε*(ω) as the sum of multiple dispersion steps, where for each relaxation process a band shape defined by the Debye ($\alpha = 0, \beta = 1$), the Cole-Cole ($0 \le \alpha < 1$, $\beta = 1$), the Davidson-Cole ($\alpha = 0$, $0 < \beta \le 1$), and the Havriliak-Negami equation ($0 \le \alpha < 1, 0 < \beta \le 1$) can be selected. Various relaxation models have been tested. A summary of the results of the fitting procedure using various models is listed in Table 5.2 in order to provide statistical information for choosing appropriate models. For most samples, the best results (i.e., the minimum variance, χ^2, of the fit) and a consistent set of relaxation parameters as a function of water content or temperature were obtained with a sum of one to three Debye relaxation process (D1, D2, and D3 models). The general form of the superposition of multiple Debye relaxations is presented by:

$$\varepsilon^*(\omega) = \varepsilon_\infty + \sum_{j=1}^{n} \frac{\Delta\varepsilon_i}{1 + i\omega\tau_j} + \frac{\sigma}{i\omega\varepsilon_0} \qquad (5.2)$$

with n denoting the number of assumed relaxation processes. According to Table **5.2** , for λ = 9 and 12, the D3 model provides good fitting of the dielectric data. Comparatively, the D2 model is the best fitting for λ = 6. For λ = 3, a single Debye relaxation (D1) provides a very good fit.

Generally, it is not possible to merge two or more of the Debye terms into one process by assuming a distribution of relaxation times. As shown in Table 5.2, the fitting by a Havriliak-Negami process (HN1) either reduces to a Debye process or leads to unacceptable variance. It can not be excluded that some of the resolved Debye terms should be better represented by relaxation time distributions rather than by a single relaxation time. However, the accuracy and the frequency range of the present data are not sufficient to pursue more complicated relaxation models.

The true dielectric spectra of the hydrated membranes were obtained by subtracting the contribution of the dc conductance from the total dielectric loss, $\varepsilon''_{total}(\omega)$, according to Eq. **5.1**. Figs. **5.6**-**5.9** plot the fitted ε′(ω) and ε″(ω) and the contribution of individual relaxation processes to the absorption as a function of frequency at 25°C. The dielectric parameters obtained by fitting the dielectric spectra according to Eq. **5.2** are collected in Table **5.3**.

The temperature dependence of dielectric spectra for Nafion 117 membrane equilibrated in 100% RH (λ= 12) are shown in Fig. **5.10**, as an example. The dielectric data were fitted according to Eq. **5.2** for n = 3, and the parameters are collected in Table **5.3**. All three assumed relaxation processes move to higher frequency as temperature increases, as expected.

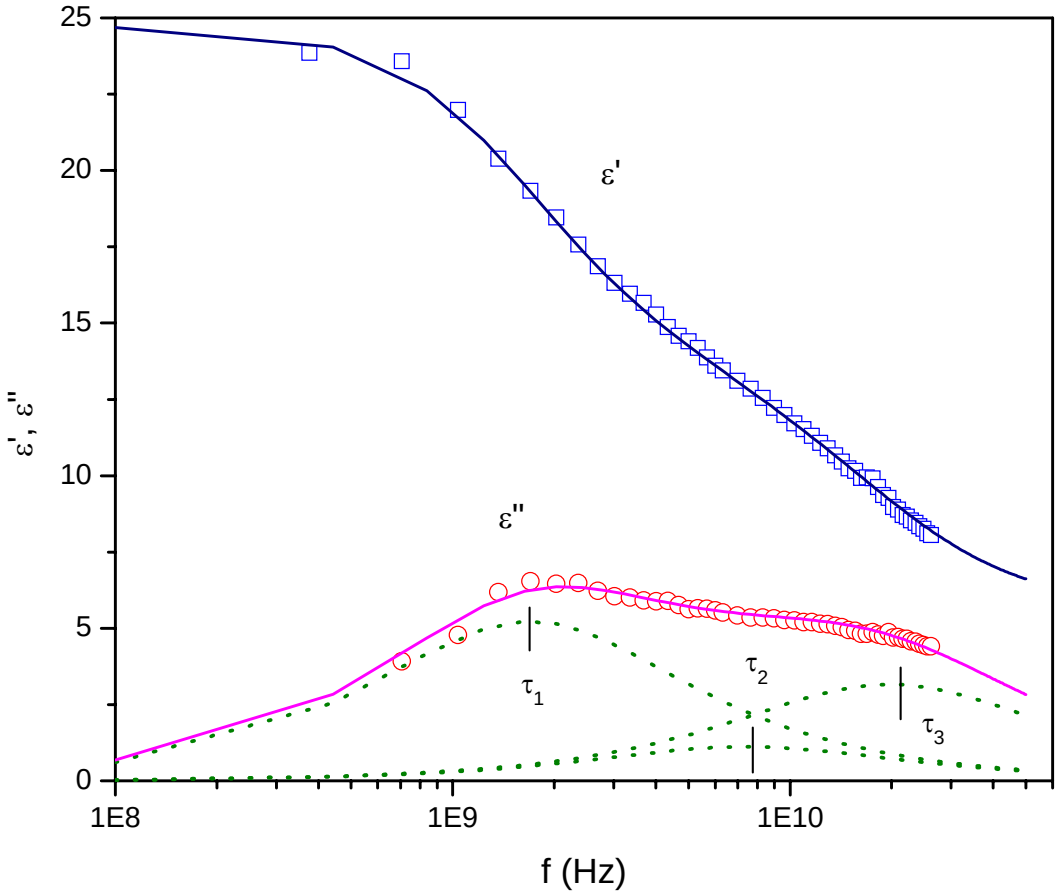

Fig. **5.6**: Permittivity, ε′(ω), and absorption, ε″(ω), for a Nafion 117 membrane equilibrated with saturated water vapor (λ=12) at 25°C. The contribution from conductivity has been subtracted. The solid lines are the best fitted results according to Eq. **5.1**. The dash lines represent the three components.

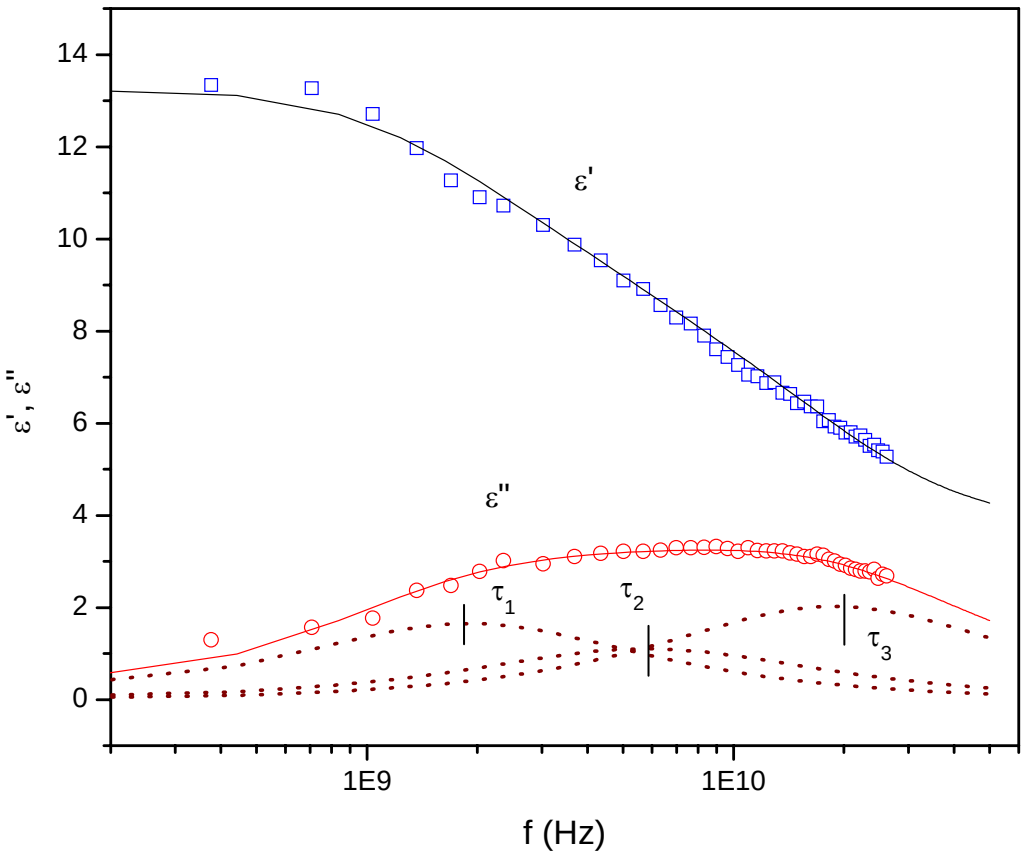

Fig. **5.7**: Permittivity, ε′(ω), and absorption, ε″(ω), for a Nafion 117 membrane equilibrated in 1mol/kg LiCl solution (RH=96%, λ=9) at 25°C. The contribution from conductivity has been subtracted. The solid lines are the best fitted results according to Eq. **5.1**. The dash lines represent the two components.

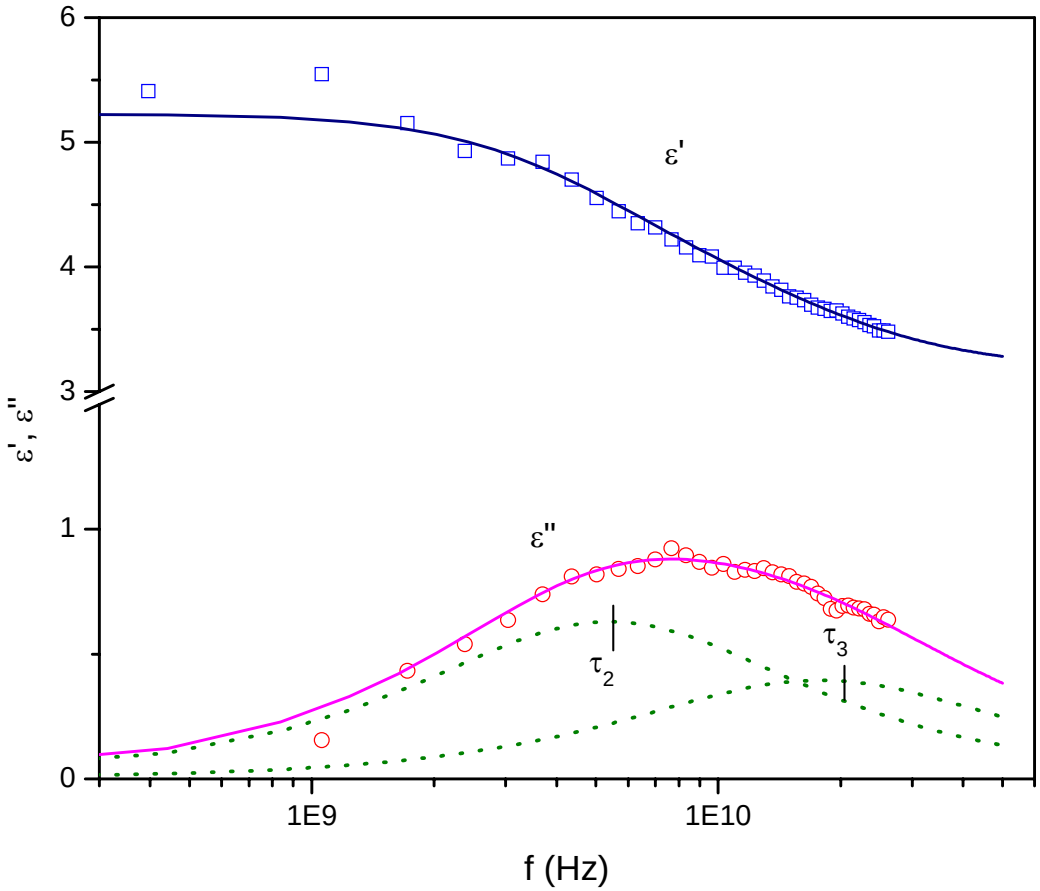

Fig. **5.8**: Permittivity, ε′(ω), and absorption, ε″(ω), for a Nafion 117 membrane equilibrated in saturated NaCl solution (RH=75%, λ=6) at 25°C. The contribution from conductivity has been subtracted. The solid lines are the best fitted results according to Eq. **5.1**. The dash lines represent the two components.

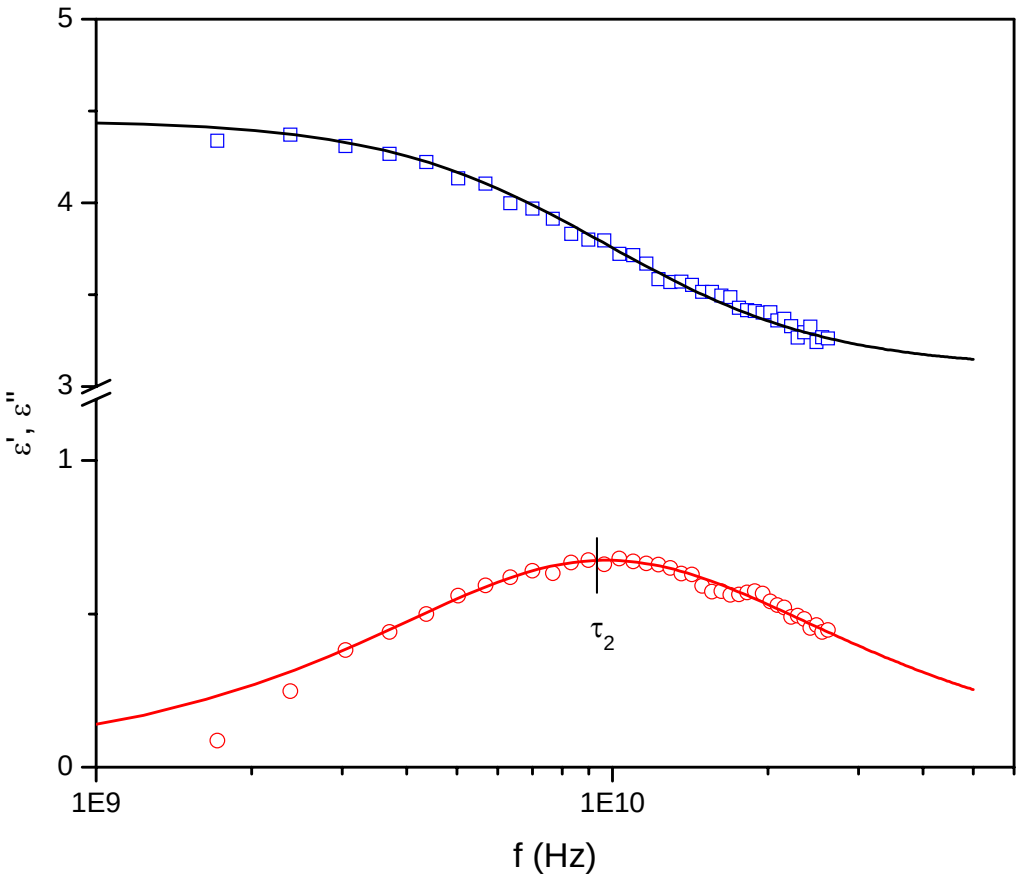

Fig. **5.9**: Permittivity, ε′(ω), and absorption, ε″(ω), for a Nafion 117 membrane equilibrated in saturated $MgCl_2$ solution (RH=33%, λ=3) at 25°C. The contribution from conductivity has been subtracted. The solid lines are the best fitted results according to Eq. **5.1**.

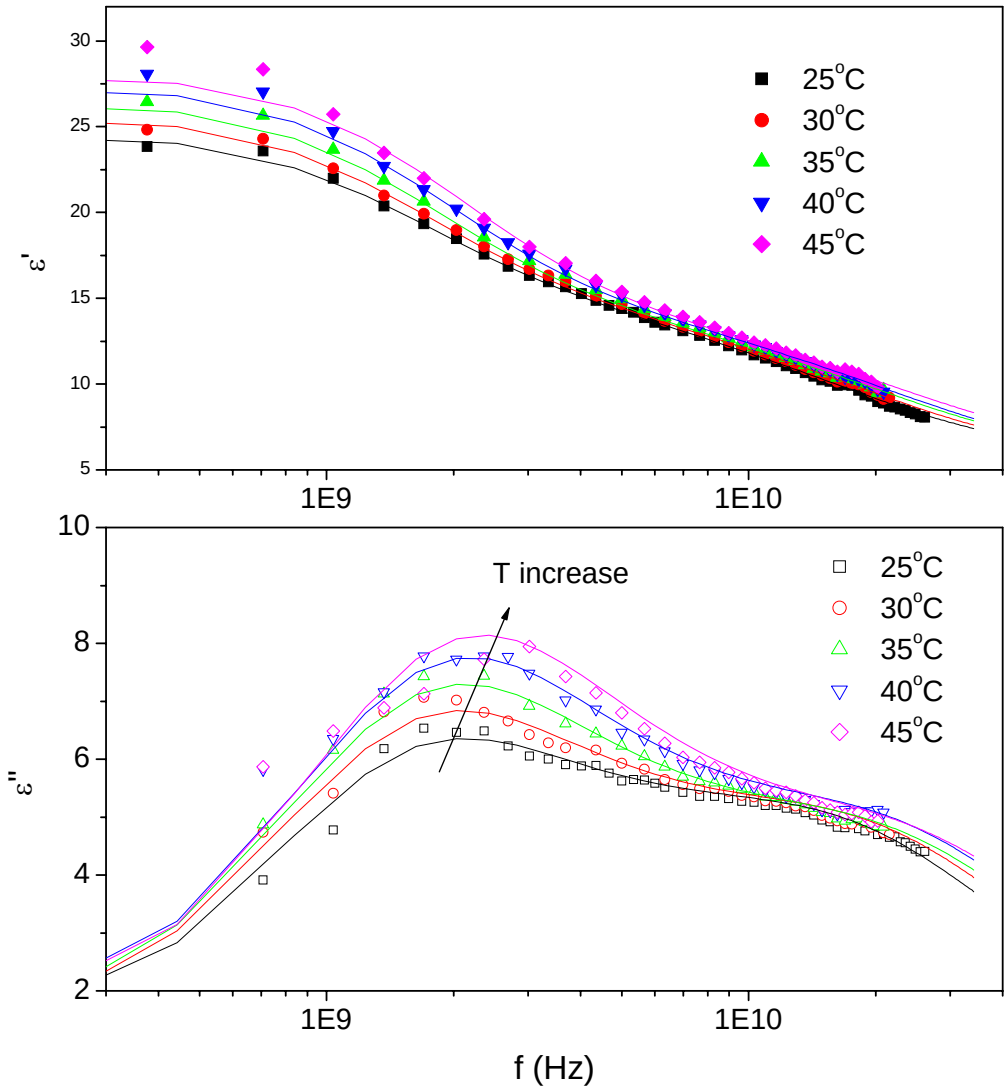

Fig. **5.10**: The effect of temperature on the dielectric response of Nafion membrane equilibrated with water vapor (λ~12). The contribution from dc conductivity has already been subtracted. The solid lines are the best fitted results according to Eq. **5.2** (n=3).

Table 5.2: Summary of the results of the fitting procedure using various models. Dielectric relaxation parameters in Eq. 5.2 for hydrated Nafion 117 at various water contents with the variance, χ^2, are listed.

Model	$\Delta\varepsilon_1$	τ_1, ps	α_1	β_1	$\Delta\varepsilon_2$	τ_2, ps	$\Delta\varepsilon_3$	τ_3, ps	ε_∞	σ, S/cm	$\chi^2 \times 10^2$
(1) λ = 12 at 25°C											
D3	10.46	94.19			2.23	21.46	6.32	8.09	5.7	2.03	0.109
D2	10.16	71.35					7.33	8.32	5.6	2.08	0.152
HN1	16.82	23.83	0.27	1					5.4	2.22	12.9
(2) λ = 9 at 25°C											
D3	3.31	88.04			2.21	27.57	4.05	8.42	3.73	1.72	0.13
D2	5.21	38.19					3.55	8.4	3.9	1.78	0.42
HN1	8.86	19.55	0.17	0.999					4.0	1.79	7.88
(2) λ = 6 at 25°C											
D2	1.26	29.5					0.79	8.97	3.2	0.34	0.023
HN1	2.36	19.67	0.183	1					3.1	0.331	0.283
(2) λ = 3 at 25°C											
D1	1.35	16.37							3.1	0.246	0.102
HN1	1.35	16.37	0	1					3.1	0.246	0.102
D2	1.01	24.32					0.57	13.92	3.1	0.225	0.16

5.1.3 Fully hydrated Nafion membrane - soaked in water

The microwave dielectric spectrum of Nafion membrane with the highest water content (soaked in liquid water, λ = 22) has also been measured. Fig. **5.11** shows the dielectric response at 25^{o}C. In contrast to the DRS of the membranes conditioned in various levels of relative humidity, the dielectric spectra of the fully-hydrated membrane are difficult to be well fitted by a superposition of multiple Debye relaxation processes. From this figure, at least three relaxation processes are present. The fitted results by the D3 model are also shown in Fig. **5.11**. However, large errors are obvious for the low frequency relaxation (i.e., τ_1, $\Delta\varepsilon_1$, and σ_{dc}). The reason for these large errors may be due to the high conductivity of the fully hydrated membrane because the conductivity has the greatest influence on the low-frequency process but less influence on the high-frequency ones.

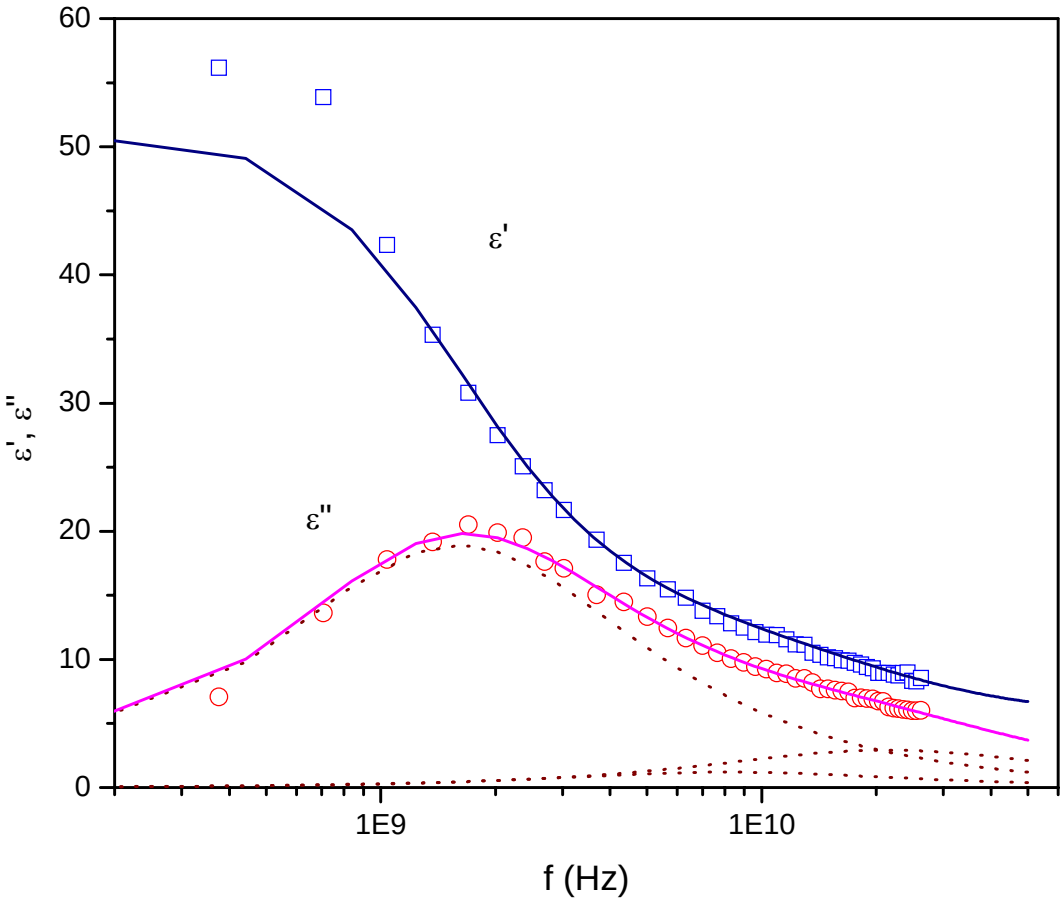

Fig. **5.11**: Permittivity, ε′(ω), and absorption, ε″(ω), for a Nafion 117 membrane soaked in liquid water (λ=22) at 25°C. The contribution from conductivity has been subtracted. The solid lines are the best fitted results according to Eq. **5.1**. The dash lines represent the three components.

Table 5.3: Fitted parameters of Eq. 5.2 for various hydrated Nafion membranes.

T, ^{o}C	$\Delta\varepsilon_1$	τ_1, ps	$\Delta\varepsilon_2$	τ_2, ps	$\Delta\varepsilon_3$	τ_3, ps	ε_∞	σ,S/cm
RH100%, λ = 12, D3 model								
25	10.06	94.19	2.23	21.46	6.52	8.09	5.7	2.03
30	11.62	92.08	2.15	20.37	6.37	7.21	5.6	2.10
35	12.67	87.78	2.11	19.34	6.2	6.50	5.6	2.23
40	13.67	83.02	1.79	18.49	6.24	6.37	5.6	2.31
45	14.45	77.11	1.89	18.09	6.12	5.69	5.7	2.42
RH96%, λ = 9, D3 model								
25	3.71	88.04	2.21	27.57	3.66	8.42	3.73	1.52
35	4.41	82.69	2.97	25.46	3.55	6.75	3.64	1.56
40	4.86	79.02	3.53	24.23	3.32	6.29	3.62	1.63
45	5.63	75.48	4.56	22.87	2.94	5.43	3.64	1.67
RH75%, λ = 6, D2 model								
25			1.62	34.5	0.69	8.97	3.18	0.32
35			1.59	33.12	0.86	6.84	3.05	0.34
40			1.67	30.23	0.86	6.28	3.05	0.36
45			1.89	29.72	0.93	5.0	2.95	0.4
RH33%, λ = 3, D1 model								
25			1.26	18.37			3.11	0.24
35			1.30	17.33			3.13	0.30
40			1.37	16.45			3.14	0.32
45			1.47	16.15			3.13	0.36
Soaked sample, λ = 22, D3 model								
25	37.87	100.3	2.42	19.48	6.85	8.44	5.7	4.20

5.2 Discussion

5.2.1 Static permittivity and dielectric dispersions

From Table 5.3 and Figs. 5.6- 5.9, one to three dispersion steps are assumed to fit the dielectric data of hydrated Nafion samples. The dielectric dispersions ($\Delta\varepsilon$) for individual relaxation steps are plotted as a function of water content in Fig. 5.12. The corresponding values for the fully-hydrated Nafion are also plotted in this figure, in spite of the large error in the dispersion of the low-frequency process. From this figure, the medium-frequency (τ_2) dispersion step is presented in all hydrated samples. However, the high frequency (τ_3) dispersion step appears only in samples with water content $\lambda \geq 6$, and the low-frequency (τ_1) dispersion only appears for $\lambda \geq 9$.

It is observed from Fig. 5.12 that $\Delta\varepsilon$ for the high- and medium-frequency step increases with λ and approaches a constant value at λ above 12, while $\Delta\varepsilon$ for the low-frequency process increases rapidly with increasing water content. The dielectric dispersion is generally a measure of the number of the relaxing units. These relaxation processes have very short relaxation times (in magnitude of picoseconds) indicating that they are not likely due to the motion of the polymer chains, which have a much longer relaxation time. It is already known that water in the Nafion membrane exists in different states from the water sorption isorthems, DSC, and NMR, as studied in Chapter 4. Thus, these dispersions may be reasonably interpreted in terms of different types of water within the membrane. Detailed assignments are given in the later section based on the combined analysis of the relaxation times and the dielectric dispersions.

The static permittivity (ε_s) is an important dielectric parameter from which the structure of the matter can be assessed. ε_s of hydrated Nafion membranes can be calculated from the individual dispersion by the equation, $\varepsilon_s = \sum_{i=1}^{n} \Delta\varepsilon_i + \varepsilon_\infty$, where n = 1, 2, or 3, depending on the dielectric model. The static permittivity, for example, for a sample with $\lambda = 12$ is calculated to be about 25. This value is in good agreement with the measurement of Paddison *et al* [**1**]. They reported a dielectric constant of 20 for Nafion 117 with $\lambda = 13$ at 30^{o}C and at 5 GHz. Fig. **5.13** shows the change of the static permittivity of Nafion 117 with water content at 25^{o}C. Two regions are discriminated from this figure: (1) a region of relatively little increase of static permittivity with increasing water content and (2) a region of significantly greater increase of static permittivity with increasing water content. The upturn point occurs between $\lambda = 6$ and 9. From the water sorption isotherms and DSC studies, the clustering of water molecules starts to occur at these water contents. This water clustering leads to the appearance of the freezing water in Nafion and the swelling of the membrane. Thus, the rapid increase of static permittivity and the presence of the freezable water in Nafion membrane at high water activities (thus, high water contents) may result from the same origin, i.e., from the water clustering. However, the DRS provide much more information not only on the state of water, but also on the dynamics of water in PSA membranes, compared to water sorption isotherms and DSC. A detailed analysis is given in the following.

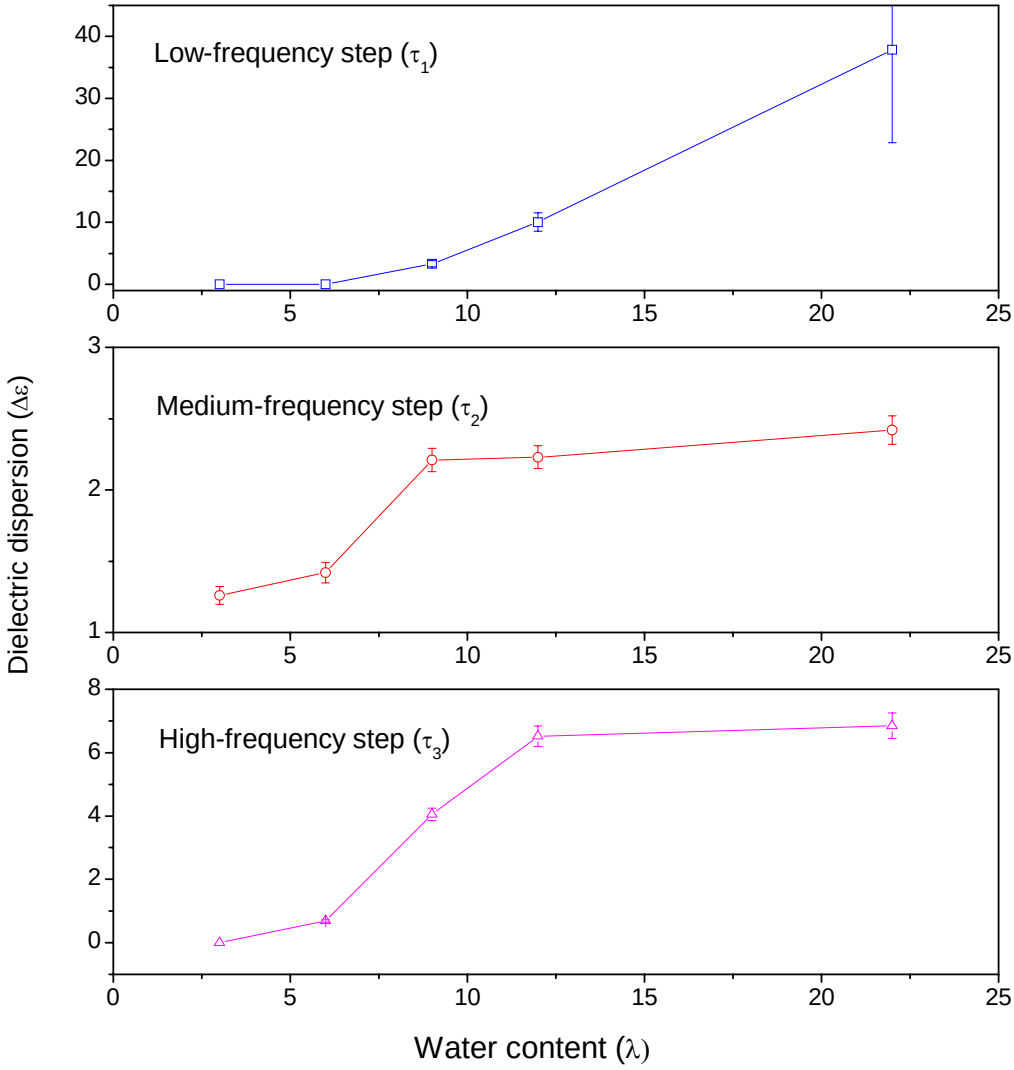

Fig. **5.12**: The individual (high-, medium-, and low-frequency) dielectric dispersion for hydrated Nafion at 25^{o}C plotted as a function of water content.

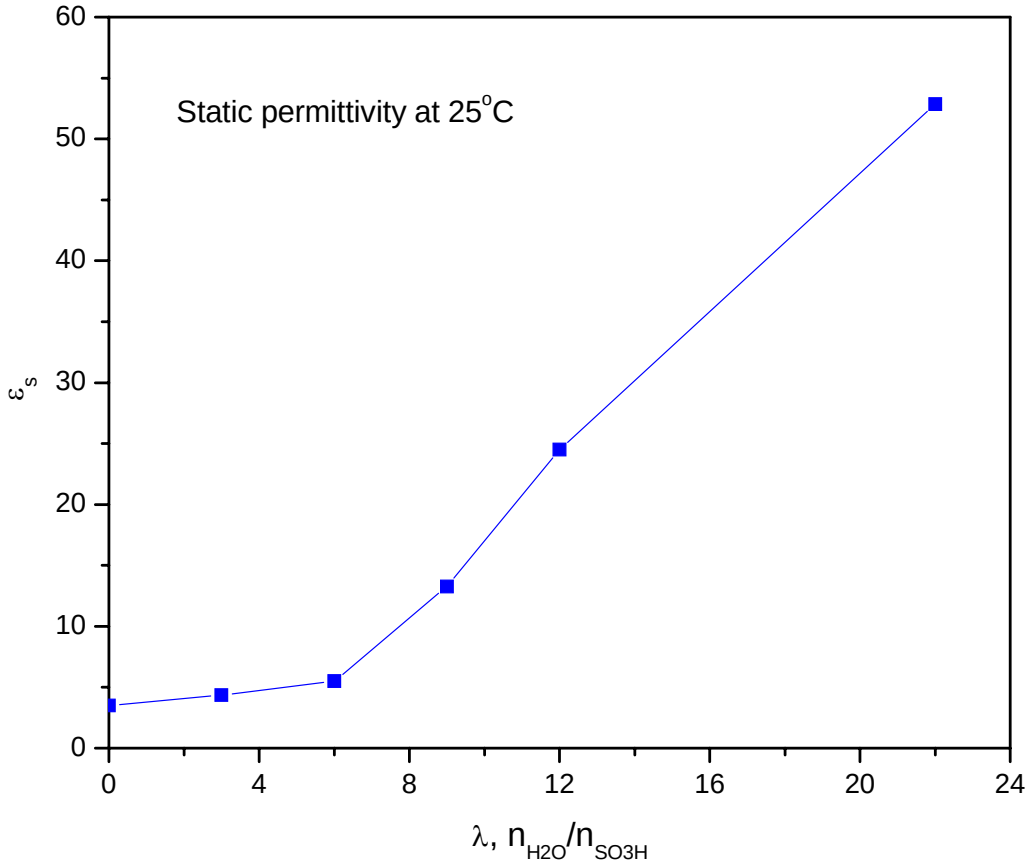

Fig. **5.13**: Static permittivity of Nafion 117 samples at 25°C plotted versus the water content.

5.2.2 Relaxation times

Fig. 5.14 shows the relaxation times for each process versus the temperature. The high-frequency dispersion step (τ_3) has a relaxation time of about 8 ps at 25^{o}C. This value is approximately equal to that of bulk water (8.31 ps) measured using the same technique (see Chapter 2). Therefore, the high-frequency process is readily attributed to the cooperative relaxation of the hydrogen bond network of "free" water molecules. The free water disappears at water content below 6 and approaches a constant amount at higher water contents, as reflected in Fig. 5.12.

The medium-frequency dispersion step (τ_2) has a relaxation time of 18-40 ps at 25^{o}C. This dielectric process is presented in all hydrated samples and approaches a constant value at high water contents (Fig. 5.12). Comparable relaxation times, τ = 16 – 30 ps, were reported for aqueous micelles [3] and protein solutions [4]. These relaxations have been attributed to water molecules surrounding the surface of micelles and proteins. It is also known from ^{17}O NMR that the rotational correlation time of water molecules at the surface of micelles exceeds the value of the pure solvent by a factor of 2 to 3 [5]. Due to the presence of large number of sulfonic acid groups in Nafion membranes [6-8], part of water molecules is inevitably associated with the polymer, mainly with sulfonic acid groups. Thus, it may be assumed that the medium-frequency relaxation process results from the water molecules surrounding SO_3H. However, it should be noted that not all the water molecules bound to the sulfonic acid groups can move at this short time scale. The first few water molecules, about 3 per sulfonic acid group measured from the water sorption isotherms and NMR ^{2}H relaxation time T_1 (see Chapter 4), are very tightly

bound to the ions, forming the first hydration layer of the sulfonic acid group. Due to the strong ion-dipole and dipole-dipole interactions between water and sulfonic acid groups, the directly bound water in the first hydration shell is expected to relax at very low frequencies. Pissis *et al*. [**9**] reported a dielectric relaxation occurring at 50 kHz at 25^{o}C in Nafion-K membrane (-SO_3K) for the first hydration water molecules, which is far below the microwave range. Beyond the first hydration shell, the interactions between water and the sulfonic acid ions significantly decrease, thus forming the second hydration layer. Water molecules in the second hydration layer are subject to two types of interactions simultaneously, namely the attractive interaction imposed by the sulfonic acid ions and the hydrogen bonding imposed by other outer water molecules. The balance between these two interactions leads to a longer relaxation time than that of water in bulk state. Thus, it is reasonable to assign the medium-frequency process to the water molecules located in the second hydration layer of the sulfonic acid groups. In general, the water molecules in the second hydration layer can exist only up to several molecular layers [**10**,**11**]. The amount of water in the second hydration layer in Nafion membrane is expected to reach a constant value as increasing water content, as reflected from the amplitude of the corresponding dielectric dispersion in Fig. **5.12**.

A third relaxation process with much longer relaxation times (τ_1), around 100 ps at 25^{o}C, is presented in samples with water content $\lambda \geq 9$. The assignment of this relaxation process is less straightforward. This low-frequency process, occurring at about 2 GHz at 25^{o}C, is obviously too fast to be the motion of the sulfonate tether head and/or vinyl either side chain, which occurs at frequencies lower than 1 kHz [**12**].We may, thus, assume the low-frequency dispersion to reflect the relaxation of some “slow” water

species. These long relaxation times for the low-frequency process are typical of the reorientation of the hydration water of particles with predominant hydrophobic hydration [**13**]. In Nafion membranes, the hydrophobic fluorocarbon backbone and the perfluorinated side chains may function as the hydrophobic hydration sites. FTIR [**14**] and DSC [**15**] measurements indeed showed that a significant amount of water in the Nafion membranes is associated with the fluorocarbon phase. This may lead to the conclusion that part of water in Nafion membrane is practically associated with the polymer side chain and/or backbone. This type of water is confined in a hydrophobic environment, thus, called "hydrophobically confined" water in this work.

The dielectric relaxation can be treated as a rate process involving a path over a potential barrier [**16**]. The relaxation times can thus be modeled by the Eyring equation:

$$\tau = \frac{h}{k_B T}\exp\left(\frac{\Delta G^{\neq}}{RT}\right) \text{ with } \Delta G^{\neq} = \Delta H^{\neq} - T\Delta S^{\neq} \qquad (5.3)$$

In this equation, $\Delta G^{\neq}$, $\Delta H^{\neq}$, and $\Delta S^{\neq}$ denote the free energy, enthalpy, and entropy of activation, respectively. h denotes the Plank constant, k_B the Boltzmann constant, and R the gas constant. Plotting relaxation time, τ, as a function of T yields the enthalpy, $\Delta H^{\neq}$, and entropy, $\Delta S^{\neq}$, of activation for the dielectric relaxation process. These thermodynamic parameters characterize the molecular interactions and dynamics of the relaxation process. Table **5.4** summarizes the activation parameters ($\Delta H^{\neq}$ and $\Delta S^{\neq}$) for each process. For comparison, the $\Delta H^{\neq}$ and $\Delta S^{\neq}$ for bulk water are also listed in this table.

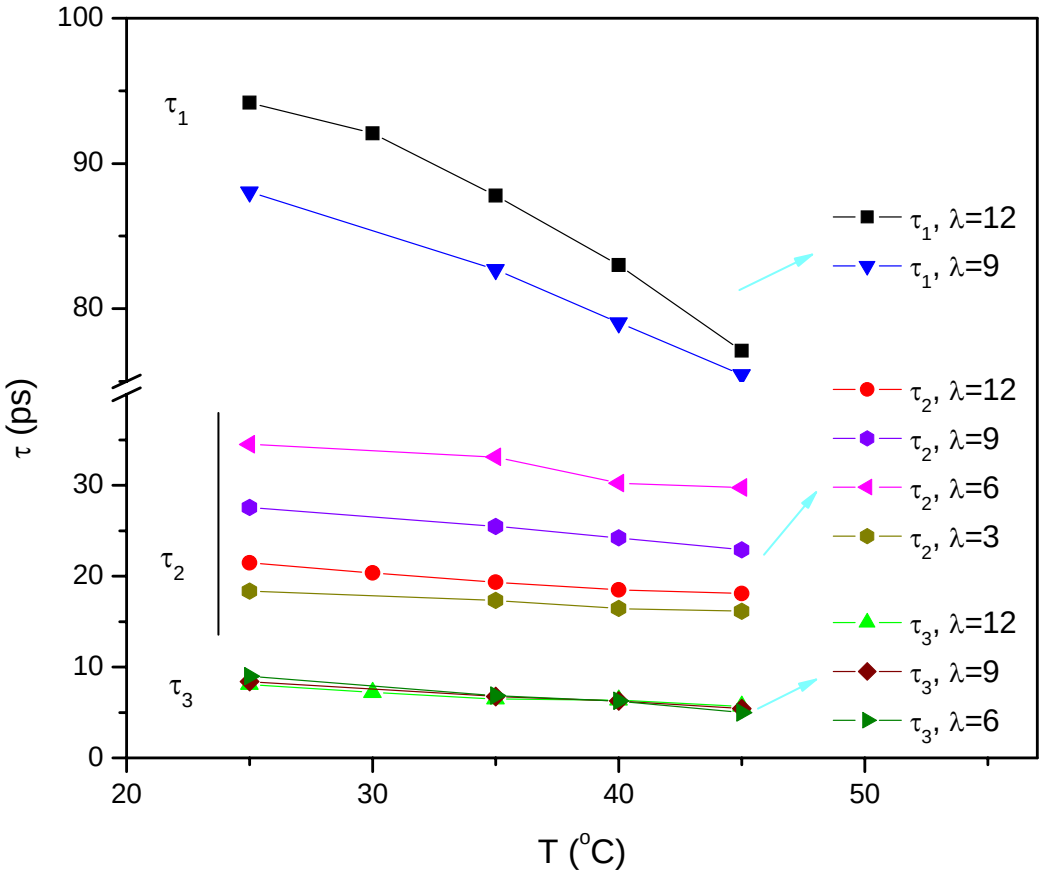

Fig. **5.14**: The relaxation times for the low- (τ_1), medium- (τ_2) and high-frequency (τ_3) dielectric processes plotted as functions of temperature and water content.

$\Delta H^{\neq}$ and $\Delta S^{\neq}$ for the high-frequency process showed almost the same values for all water contents. Their magnitudes are close to the characteristic values of bulk water [**17**], i.e., 15.9 kJ/mol for $\Delta H^{\neq}$ and 20.7 J/mol.K for $\Delta S^{\neq}$. This agreement further supports our previous attribution of the high-frequency process to the "free" water molecules. The large positive activation enthalpy for the high-frequency relaxation reflects the fact that the relaxation in free water involves the breaking and reforming of hydrogen bonds. Due to the reorganization of the hydrogen bond network, the transition state for water molecule relaxation is in a more random configuration, reflected by the positive activation entropy. These results point to a significant degree of water binding in the Nafion membranes.

In contrast to the "free" water, the low-frequency relaxation displays small activation enthalpies and negative activation entropies (see Table **5.4**). The activation enthalpies for this relaxation process are negligible compared to the strength of hydrogen bonding, which is about 10 kJ/mol [**18**]. This suggests both that the reorientation process occurs readily without involving breaking or forming of chemical bonds and also that the state of bonding in the transition state is similar to that in the initial state. A noticeable feature for the dynamics of the low-frequency process is the large negative activation entropies, which imply that the transition state for those water molecules is a much more ordered configuration than is the initial state. These dynamic characteristics reveal a distinct reorientation process from the free water.

For comparison, the activation energies for proton conduction [**19**], which vary with the water content, are also listed in Table **5.4**. It can be seen that the activation energies of conductivity is in the similar magnitude as the activation enthalpies of the free

water. This implies that the proton transport is correlated with the rotation of the “free” water molecules. A similar conclusion has also been reported by Fontanella *et al*. [**20**]. They studied the effect of high-pressure variation on the conductivity as well as the ^{1}H and ^{2}H NMR spectra of Nafion 117. They found that the activation volumes for the ^{1}H and ^{2}H NMR experiments were close to each other as well as to the activation volumes derived from the conductivity. These results indicate that the presence of a hydrogen bond network is an essential condition for enhanced proton mobility and, thus, high proton conductivity. The difference between the dependence of the activation energies of the proton conduction and the free water dielectric relaxation on water contents (Table **5.4**) may suggest that the sulfonate group and side chains participate in the proton conduction process, especially at low water content. Obviously, however, information from other experimental techniques and from molecular dynamics simulations is required to substantiate this hypothesis.

Table **5.4**: Activation parameters, $\Delta H^{\neq}$ and $\Delta S^{\neq}$, for the high-, medium-, and low-frequency relaxation in Nafion membrane with different contents.

Relaxations	$\Delta H^{\neq}$ (kJ/mol)	$\Delta S^{\neq}$ (J/mol.K)
Bulk water:	15.91	20.68
High-frequency ("free" water):		
	14.02	16.56
Low-frequency:		
λ~12	5.35	-35.17
λ~9	3.44	-40.89
Activation energy for proton conduction [38]:		
λ~22	10.56	
λ~12	12.48	
λ~3	21.12	

5.2.3 Thermodynamics of water-Nafion interaction

Three types of water and their dynamics have been determined by the microwave dielectric relaxation studies: 1) the second hydration water, which gives rise to the medium-frequency process (τ_2), is present at all water contents higher than 3 water molecules per sulfonic acid; 2) the "free" water appears when $\lambda \geq 6$, and first increases with increasing λ, but approaches a constant value at high water contents. It is commonly assumed that the "free" water locates in the center of the ion cluster regions where the ion-water interaction is negligible; and 3) the hydrophobically defined water is present only when $\lambda \geq 9$. This part of water is assumed associated with the perfluorinated side chain and maybe even with the backbone. In addition, when the water content is lower than about 3 water molecules per SO_3H, the water locate in the first hydration layer of SO_3H, which cannot be detected by the microwave DRS but is observed by the water sorption isotherms and ^2H NMR spectrum. Table **5.5** summarizes the types of water in Nafion, the corresponding water content, and the techniques that can be used to study them.

Table 5.5: Summary of the water states in Nafion membranes

Water content, λ	Water states	Technique
0-3	First hydration water	Water sorption isotherm ^2H NMR T_1 Broadband DRS [9]
3-6	Second hydration water	Microwave DRS
λ>6	Free water	Microwave DRS
λ>9	Hydrophobically confined water	Microwave DRS FTIR [14]

From the thermodynamics view, water molecules interact not only with the hydrophilic groups (e.g., SO3H), but also with the hydrophobic phases (e.g., perfluorinated side chains and polymer backbone). Due to the strong ion-dipole and dipole-dipole interaction between H_2O and SO_3H, water molecules are preferably bound to these sites at low water content. As a result, the first hydration layer is formed around the sulfonic acid groups. These water molecules are tightly bound to SO_3H, and can not move at microwave frequency but give a dielectric relaxation at kHz which has been observed by the broadband DRS [9]. The dielectric strength ($\Delta\varepsilon$) for the first hydration layer is expected to be very small. Due to the dielectric saturation, the amount of the first hydration water is limited to about 3 water molecules per SO_3H. Beyond this water content, the second hydration layer of sulfonate ions is formed. This layer of water practically forms a transition region between the tightly-bound first hydration water and far away free water. A distribution of dielectric relaxation time is expected for this part of water, as indicated by the variation of τ_2 in Fig. 5.14. With further absorption of water,

the ion clusters in Nafion swell to hold pools of free water surrounded by ionic groups. The interaction between free water and sulfonate ions is negligible and the water-water interaction (by hydrogen bonding) is expected to be dominant, as shown from $\Delta H^{\neq}$ and $\Delta S^{\neq}$ values in Table **5.4**. The fact that the amount of free water approaches constant value at high water contents (see Fig. **5.12**) may imply that the size of ion cluster regions will reach a maximum value, rather than increase constantly with increasing water content. As the water content is further increased (by conditioned in saturated water vapor or soaked in liquid water), the sorbed water can not be held by the ion cluster regions any more and starts to associate with the side chains and even the polymer backbone. In these regions, the number of sulfonic groups is low and water molecules contact directly with the hydrophobic polymer. A hydrophobic hydration is thus possible. At the same time, the polymer backbone and side chain may reorganize to decrease the contact between the hydrophobic phases and water. Consequently, the rodlike structure may be obtained. This may correspond to the structural inversion proposed by Gebel in his conceptual model [**22**].

The dielectric strength for the first and second hydration water is small because of the strong interaction between water molecules and sulfonic acid groups. For free water and hydrophobically confined water, the dielectric strengths for water molecules is expected to be equivalent to that of bulk water, but weighed by the concentration of each type. The concentration of each type of water is schematically shown in Fig. **5.15**, based on above arguments. Due to their higher concentrations and larger dielectric strengths, the large dielectric dispersions (see Fig. **5.12**) for the free water and hydrophobically confined water can be qualitatively explained.

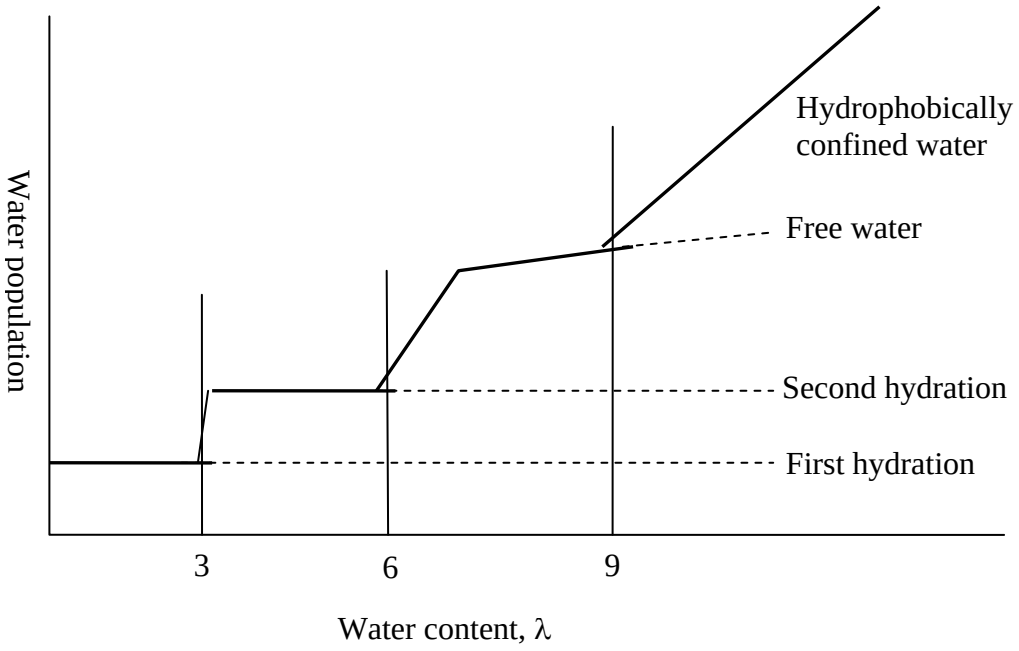

Fig. **5.15**: Schematic plot of water states and their population in Nafion membrane as a function of water content.

5.2.4 The fraction of "free water"

For a multi-step relaxation model, the Cavell equation shows that the dielectric dispersion, $\Delta\varepsilon_i$, of process i is proportional to the concentration, c_i, of the relaxation species [21]:

$$c_i = K(\Delta\varepsilon_i) \qquad (5.4)$$

where K is the proportionality constant, which contains information about the species (polarizability and gas-phase dipole moment) and other factors including the reaction field factor, the geometry factor, as well as the Kirkwood correlation factor. For a single species (e.g., water molecules in Nafion membrane) it is reasonable to assume K remains constant for different relaxation processes. Accordingly, the fraction of each relaxing unit can be evaluated from their dielectric dispersions.

Fig. 5.16 shows the fraction of free water in Nafion as a function of water content. From the discussion above, it is clear that the presence of free water is essential to the high proton conductivity. The fraction of free water increases with water content. This explains high proton conductivity of Nafion at high water uptake. However, a noticeable result from this figure is that the fraction of free water is less than 0.5, even in the sample conditioned in saturated water vapor. In other words, most of water in Nafion is located in the hydration shell of sulfonic acid groups and/or confined in a hydrophobic environment, rather than to help the proton conduction. Accordingly, optimization of the proton conductivity requires maximization of the amount of free water in the membrane.

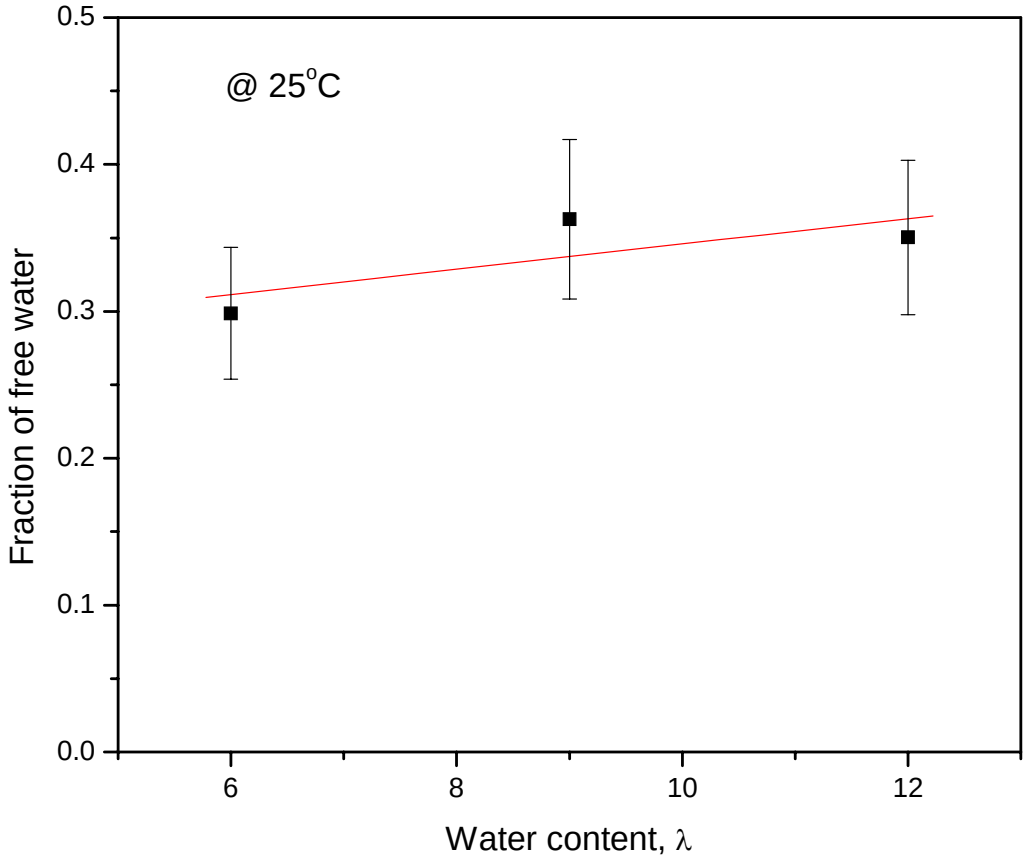

Fig. **5.16**: Fraction of free water calculated from the dielectric data at 25°C plotted versus water content.

5.3 Summary

Dielectric relaxation spectra of Nafion 117 and Flemion SH150 membranes have been measured using the transmission line method over the frequency range of 45 MHz to 26 GHz and over the temperature range of 25-45^{o}C. The spectra were well-fitted by a superposition of one to three Debye relaxation processes, depending on the nature of membrane and water content. The first high-frequency dispersion step, with relaxation time $\tau \approx 8$ ps at 25^{o}C, shows the characteristic dynamics of bulk water and is attributed to the cooperative relaxation of hydrogen bonded networks of "free" water. Free water is assumed to comprise the water molecules at the center of the ion cluster regions or pores. The second step, having a relaxation time of $\tau \approx 30$ ps at 25^{o}C, is attributed to the water molecules in the second hydration shell of sulfonic acid groups. The water molecules in the first hydration shell of SO_3H has a dielectric relaxation at kHz, and can not be detected by the microwave DRS. The remaining relaxation process occurs at low-frequency, having a relaxation time of $\tau \approx 90$ ps, and is postulated to result from the motion of the water molecules associated with the perfluorinated side chains and polymer backbone. The low-frequency relaxation showed negligible activation enthalpies and large negative activation entropies, which may indicate the feature of hydrophobic hydration. The presence of the low-frequency process is found to correspond to the clustering of water and the appearance of the freezing water.

5.4 References

1. S.J. Paddison, D.W. Reagor, T.A. Zawodzinski Jr., *J. Electroana. Chem.*, **459**, 91 (1998)

2. O. Bohnke and J.C. Badot, *J. Phys. Cond. Matter*, **15**, 7571 (2001)

3. C. Baar, R. Buchner, W. Kunz, *J. Phys. Chem. B*, **105**, 2906 (2001)

4. N. Nandi and B. Bagchi, *J. Phys. Chem. B*, **101**, 10954 (1997)

5. B. Halle and G. Carlstrom, *J. Phys. Chem.*, **85**, 2142 (1981)

6. T.D. Gierke, G.E. Munn, F.C.J. Wilson, *J. Poly. Sci., Polym. Phys.*, **19**, 1687 (1981)

7. M.H. Litt, *Polym. Prepr.*, **38**, 80 (1997)

8. L. Rubatat, A.L. Rollet, G. Gebel, O. Diat, *Macromolecules*, **35**, 4050 (2002)

9. C. Tsonos, L. Apekis, P. Pissis, *J. Mater. Sci.*, **35**, 5957 (2000)

10. C.Y. Lee and J.A. McCammon, P.J. Rossky, *J. Chem. Phys.*, **80**, 4448 (1984)

11. S.H. Lee, P.J. Rossky, *J. Chem. Phys.*, **100**, 3334 (1994)

12. S.A. Perusich, P. Avakian, M.Y. Keating, *Macromolecules*, **26**, 4756 (1993)

13. A.K. Lyashchenko, A.S. Lileev, T.A. Novskova, V.S. Kharkin, *J. Mol. Liquids*, **93**, 29 (2001)

14. M. Falk, *Can. J. Chem.*, **58**, 1495 (1980)

15. H. Yoshida and Y. Miura, *J. Membr. Sci.*, **68**, 1 (1992)

16. S. Glasstone, L.J. Laidle, H. Eyring, *The Theory of Rate Processes*, McGraw-Hill, New York, 1941

17. R. Buchner, J. Barthel, J. Stauber, *Chem. Phys. Letters*, **306**, 57 (1999)

18. G.E. Walrafen, M.R. Fisher, M.S. Hokmabadi, W.H. Yang, *J. Chem. Phys.*, **85**, 6970 (1985)

19. M. Cappadonia, J.W. Erning, U. Stimming, *J. Electroanal. Chem.*, **376**, 189 (1994)

20. R.S. Chen, P.E. Stallworth, S.G. Greenbaum, J.J. Fontanella, M.C. Wintersgill, *Electrochim Acta*, **40**, 309 (1995)

21. E.A.S. Cavell, P.C. Knight, M.A. Sheikh, *J. Chem. Soc. Faraday Trans.*, **67**, 2225 (1971)

22. G. Gebel, *Polymer*, **41**, 5829 (2000)

Chapter 6

Microwave Dielectric Relaxation Spectroscopy of Flemion SH150

The prior microwave dielectric relaxation spectroscopy studies indicate that the dielectric properties of Nafion are closely related to its specific structure, and an important factor that determines the structure of the perfluorosulfonic acid membranes is the equivalent weight. Therefore, the investigation of membranes having different EW values is quite important for further understanding of the mutual relationships between the structure of the membranes, the water state in membrane, and the transport behaviors of proton and water molecules in the membranes. In this study, the dielectric properties of Flemion SH150, which has an EW of 909, are studied. The investigation is especially focused on the changes in the membrane properties due to the difference of the EW value.

6.1 Results and data analysis

6.1.1 Dry membrane

The microwave dielectric spectra of a vacuum-dried Flemion SH150 sample (at 120^{o}C for 12 hours) are shown in Fig. **6.1**. The dielectric responses of the dry Flemion SH150 are similar to those of the dry Nafion 117 samples (see Chapter 5). No relaxation process is displayed in the absorption spectra. The dry Flemion SH150 has the same

relative permittivities as the dry Nafion 117 (3.5), which indicates that the equivalent weight has no effect on the dielectric properties of dry PSA membranes.

6.1.2 Hydrated Flemion membranes

6.1.2.1 Equilibrium water sorption

The sorption by Flemion SH150 of water vapor in a controlled water activity is measured using isopiestic sorption method and is shown in Fig. **6.2**. The water content was calculated as the number of water molecules per sulfonic acid group, λ, from the weight measurements using the relation:

$$\lambda = \frac{(W_{wet} - W_{dry}) \times EW}{18 \times W_{dry}} \qquad (6.1)$$

where W_{wet} and W_{dry} represent the weight of the membrane in dry and hydrated states, respectively. EW is the equivalent weight for the membrane, 1100 and 909 for Nafion 117 and Flemion SH150, respectively.

From Fig. **6.2** , the Flemion membrane sorbs more water than Nafion from water vapor at same water activity. Since Flemion SH150 has a lower EW value than Nafion 117, it may be concluded that the water content, expressed in units of λ, increases with decreasing EW value. The same conclusion has also been reported by Saito *et al.* [**1**]. Considering the contribution of the ion-exchange group to form the ion cluster regions, it

suggests that the Flemion SH150 membrane is likely to form larger and/or more numerous ionic cluster regions. Therefore, it is expected that the dielectric properties of Flemion SH150 are somewhat different from Nafion 117.

6.1.2.2 Microwave dielectric relaxation spectroscopy of hydrated Flemion samples

The dielectric spectra, permittivity, $\varepsilon'(\omega)$, and absorption, $\varepsilon''(\omega)$, of various hydrated Flemion SH150 ($\lambda \approx 13.5$, 7.1, and 4.5, corresponding to a = 1, 0.75, and 0.33, respectively) are plotted in Figs. **6.3**-**6.5** . These spectra have similar shapes when compared to Nafion 117. The dielectric data were fitted by Eq. **5.2**, i.e., by a superposition of multiple Debye relaxations. The best fitting models and the corresponding dielectric parameters are listed in Table **6.1**.

For $\lambda = 13.5$, the dielectric spectra were fitted by the sum of three Debye relaxation process, as shown by the top figure in Fig. **6.6**, where the contribution from the dc conductivity has been subtracted from the measured $\varepsilon''(\omega)$. These relaxation processes are essentially identical to those of Nafion 117 with high water content ($\lambda \geq 9$) and reflected by the same magnitude of the dielectric relaxation times. Therefore, the high-frequency process is attributed to the “free” water, the medium-frequency one is attributed to the water molecules located in the second hydration layer of the sulfonic acid groups, and the low-frequency process is due to the water molecules associated with the perfluorinated side chains and fluorocarbon backbone.

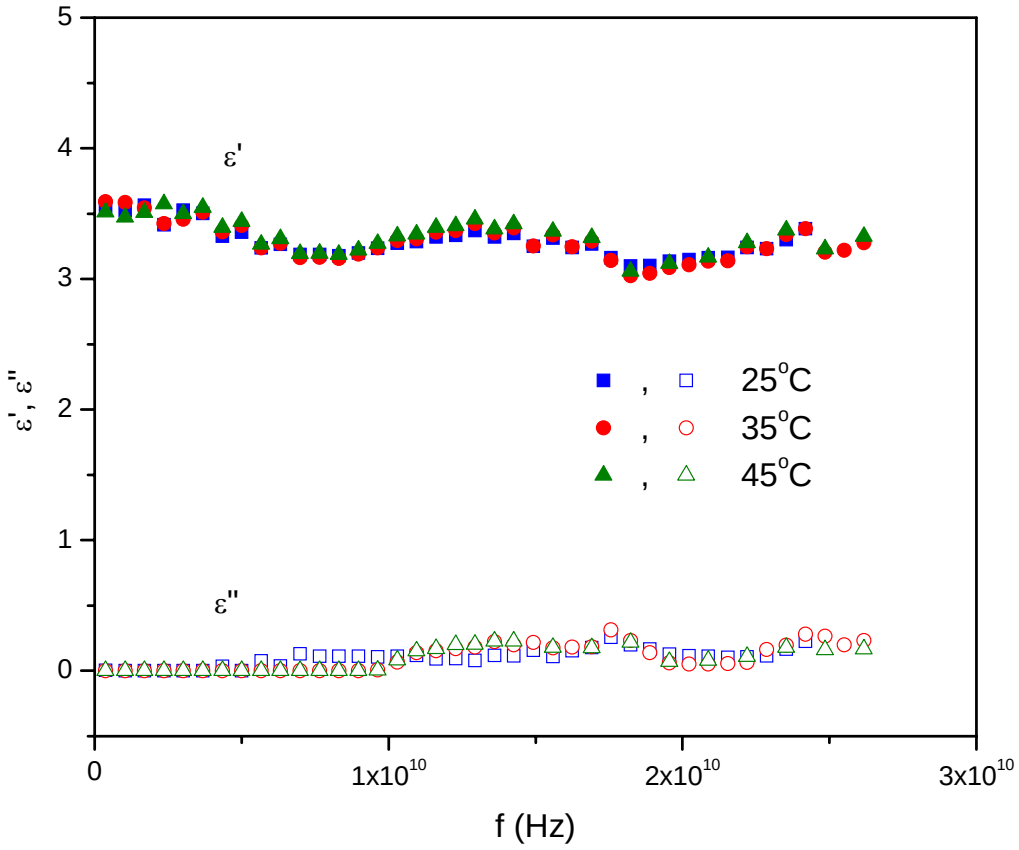

Fig. **6.1**: Relative permittivity, ε′(ω), and absorption, ε″(ω), of dry Flemion SH150 at 25, 35, and 45°C.

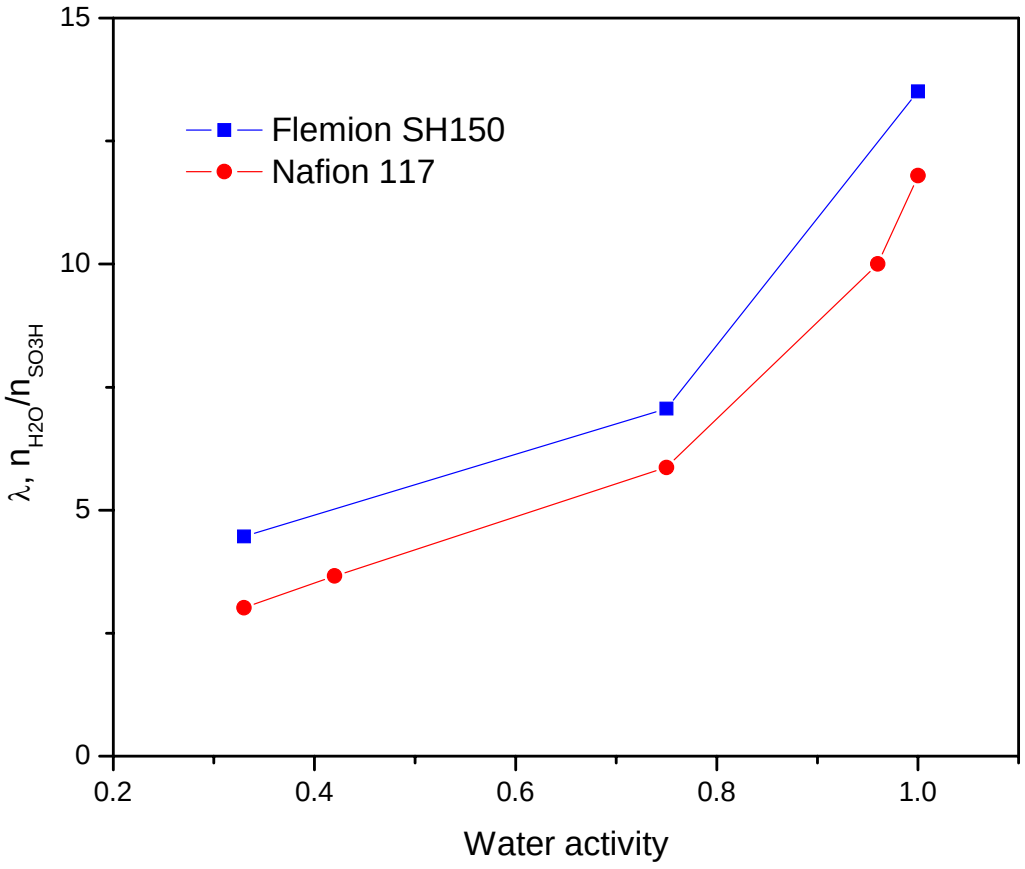

Fig. **6.2**: Isopiestic sorption of water vapor in Flemion SH150 and Nafion 117 membranes at 25^{o}C.

However, the dielectric spectra for Flemion samples with lower water contents have different assignments from Nafion 117. For the Flemion sample equilibrated in water activity of 0.75 and having a water content of $\lambda = 7.1$, the spectra were best fitted by the sum of three Debye processes (Table **6.1**), which is in contrast to Nafion where the spectra for the corresponding water content were fitted by two Debye processes. The spectra for $\lambda = 4.5$ (equilibrated in water activity of 0.33) were better fitted with the sum of two Debye processes rather than with a single Debye process. Fig. **6.6** shows both the comparison of the fitted $\varepsilon''(\omega)$ as a function of frequency at 25^{o}C and the contribution of individual relaxation processes to the absorption. These dielectric processes can be readily assigned to the same sources as those in the Nafion 117 membrane, based on their magnitude of relaxation times.

These different dielectric responses must be structural in origin. The significant difference between Nafion 117 and Flemion SH150 is the equivalent weight. In the following section, a detailed analysis will be given with the focus on the influence of the EW.

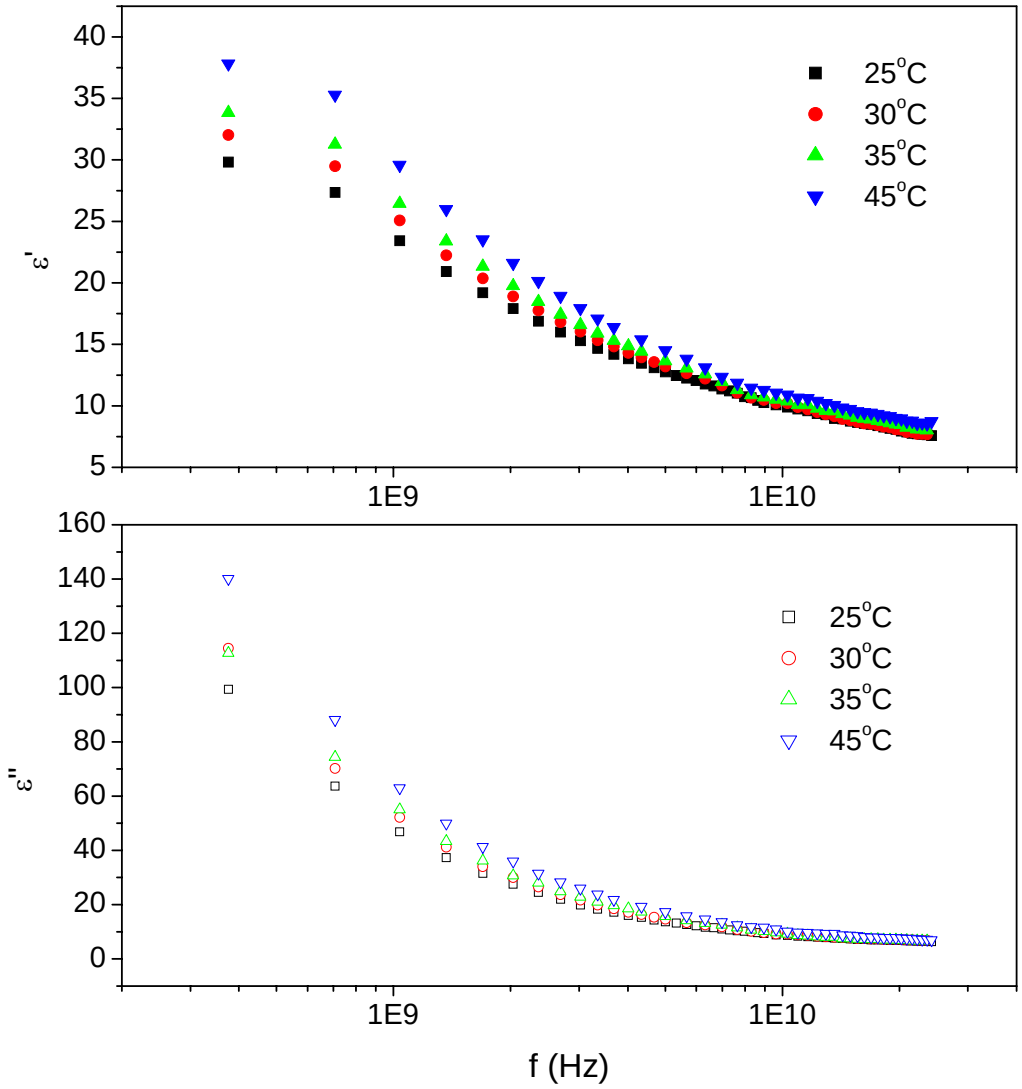

Fig. **6.3**: Measured permittivity, ε′(ω), and absorption, ε″(ω), for Flemion SH150 membrane equilibrated in saturated water vapor (RH=100%, λ=13.5) at 25-45°C in steps of 5°C.

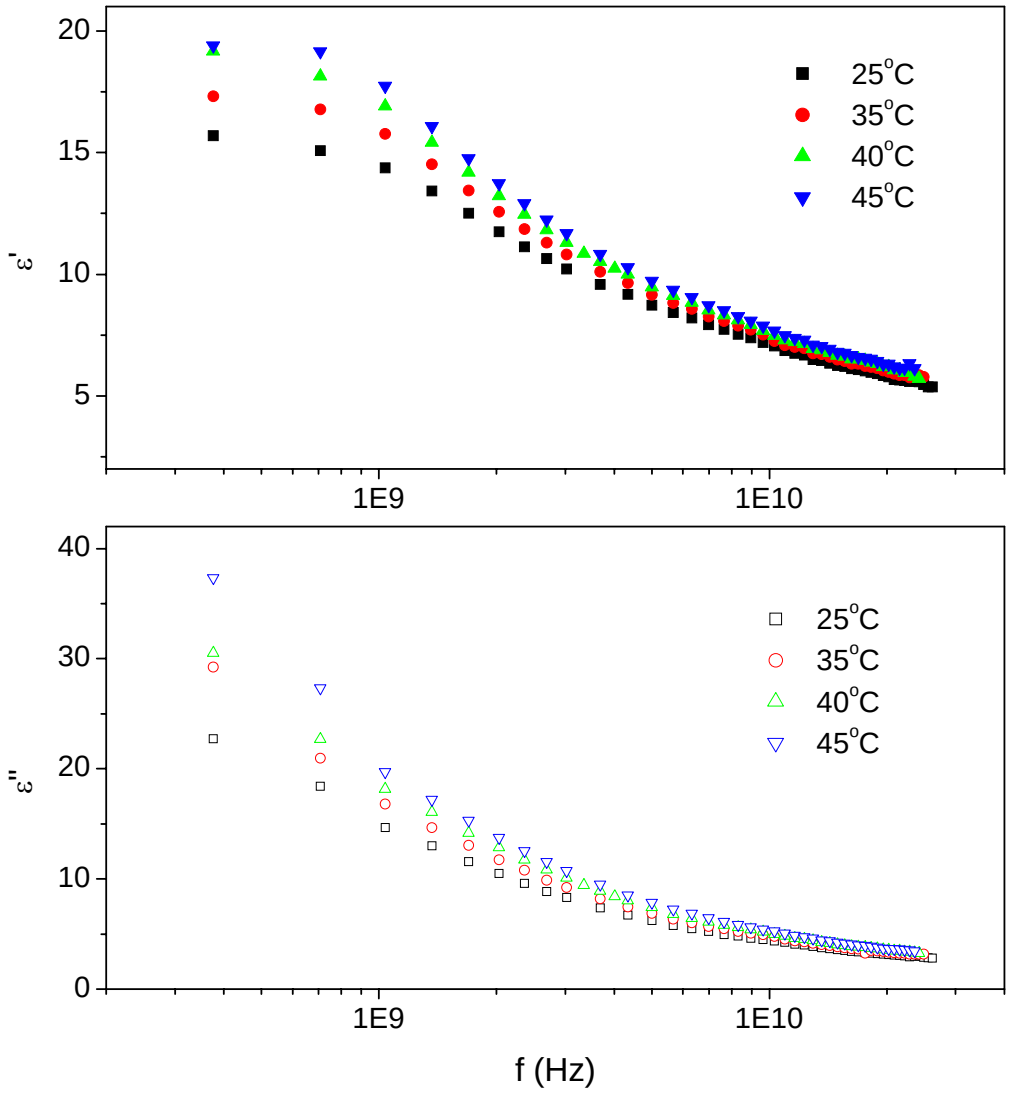

Fig. **6.4**: Measured permittivity, ε′(ω), and absorption, ε″(ω), for Flemion SH150 membrane equilibrated in saturated NaCl solution (RH=75%, λ= 7.1) at 25-45°C in steps of 5°C.

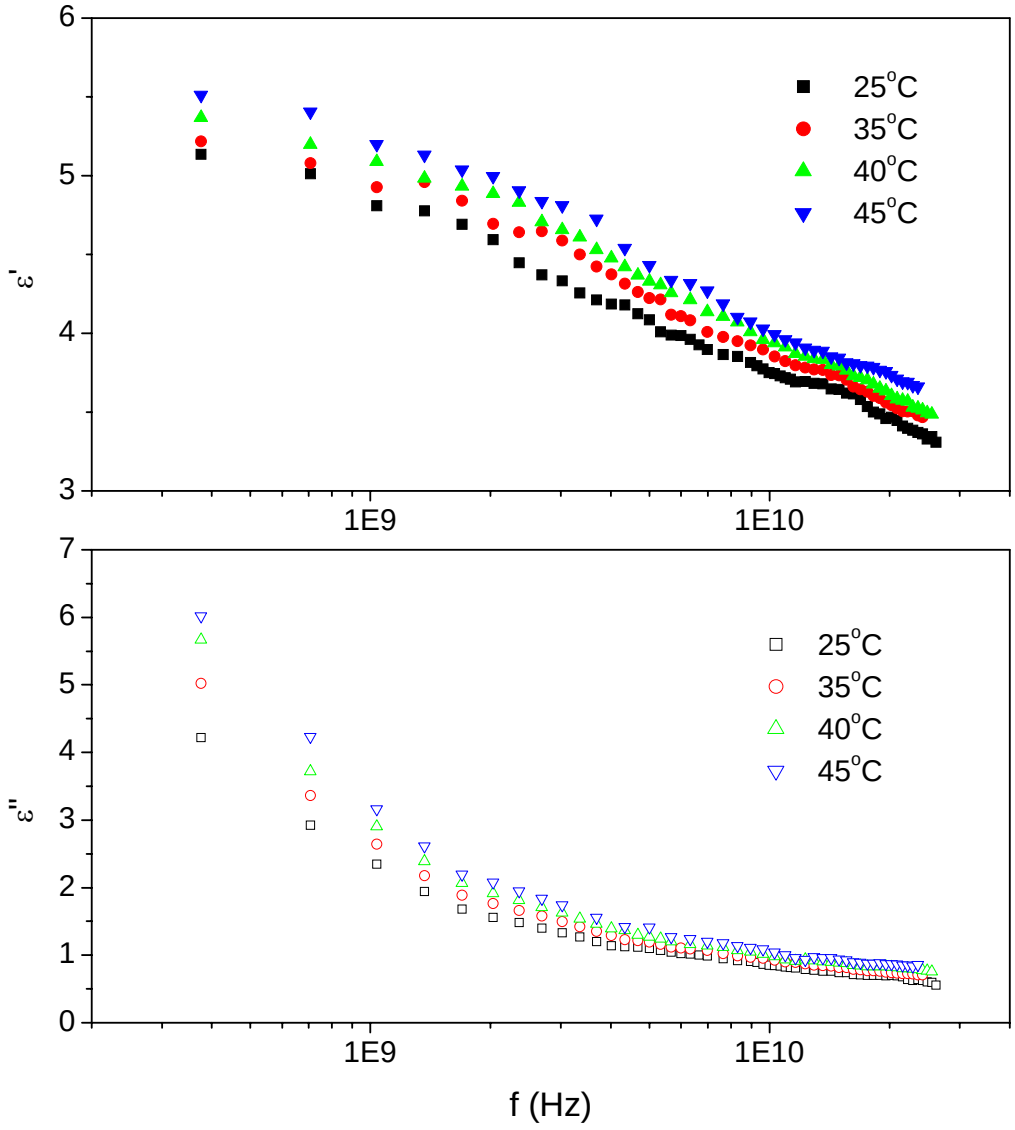

Fig. **6.5**: Measured permittivity, ε′(ω), and absorption, ε″(ω), for Flemion SH150 membrane equilibrated in saturated $MgCl_2$ solution (RH=33%, λ= 4.5) at 25-45°C in steps of 5°C.

Table **6.1**: Summary of the results of the fitting procedure using various models. Dielectric relaxation parameters obtained by fitting the DRS data of hydrated Flemion SH150 at various water contents are listed.

T, ^{o}C	Model	$\Delta\varepsilon_1$	τ_1, ps	$\Delta\varepsilon_2$	τ_2, ps	$\Delta\varepsilon_3$	τ_3, ps	ε_∞	σ, S/cm
(1) RH = 100%, λ = 13.5									
25	D3	17.7	95.57	0.79	43.27	6.32	7.82	4.52	2.11
30	D3	18.06	93.35	0.85	39.4	6.11	6.58	4.32	2.25
35	D3	18.85	91.35	0.86	36.4	6.61	5.78	3.97	2.32
45	D3	20.81	87.91	1.4	35.2	6.83	4.91	3.97	2.56
(2) RH = 75%, λ = 7.1									
25	D3	8.19	84.98	0.68	31.14	3.36	9.1	4.19	0.63
35	D3	9.27	78.33	0.69	27.42	3.21	7.07	4.21	0.75
40	D3	9.87	74.32	0.67	25.42	3.56	6.39	3.95	0.82
45	D3	10.11	72.98	0.97	24.63	3.67	5.5	3.8	0.9
(3) RH = 33%, λ = 4.5									
25	D2			0.96	48.29	0.84	8.65	3.05	0.117
35	D2			1.08	46.44	0.9	7.62	3.05	0.134
40	D2			1.18	43.45	0.96	6.51	3	0.148
45	D2			1.26	42.07	1.06	5.49	2.94	0.164

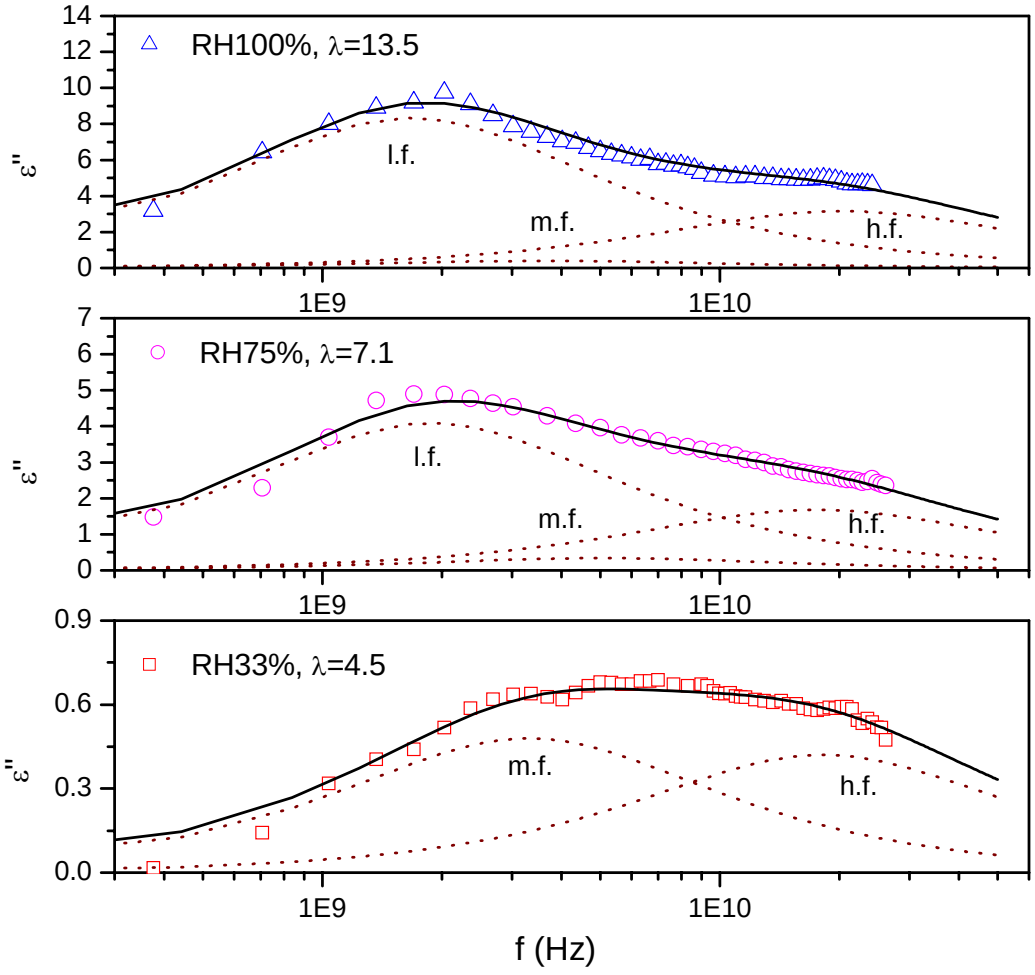

Fig. **6.6**: Permittivity, ε′(ω), and absorption, ε″(ω), for Flemion SH150 membranes having various water contents at 25°C. The contribution from conductivity has been subtracted. The solid lines are the best fitted results and the dash lines represent the three components. The notation l.f., m.f., and h.f. represent low-frequency, medium-frequency, and high-frequency processes, respectively.

6.2 Discussion

6.2.1 Dielectric dispersions, static permittivity, and equivalent weight of membrane

Generally, the dielectric data of the perfluorosulfonic acid membranes have been proposed to reflect mainly the properties of the ionic cluster regions in the membrane [2,3]. Therefore, the size and/or number of the ionic cluster regions would have an important effect on the dielectric responses of the membrane. In addition, these structural properties (size and number of the ionic clusters) depend on the water content [4,5] and the equivalent weight [6] of the membrane. The general conclusion is that those properties of the ionic cluster regions both increase with increasing water content in the membrane and also increase with decreasing equivalent weight of the membrane.

Fig. 6.7 shows the dielectric dispersion for (a) a low-frequency process, (b) a medium-frequency one, and (c) a high-frequency one measured for Flemion SH150 and Nafion 117 membranes at 25^{o}C, as an example, versus the water content λ. The largest contribution to the total dispersion results from the low-frequency process, which is attributed to the water molecules associated with the perfluorinated side chains and polymer backbone. The high-frequency process (due to the “free” water molecules) contributes less, and the medium-frequency one (due to water molecules in the second hydration layer of sulfonic acid groups) contributes least. From Fig. 6.7 , Flemion SH150 has higher values for both the high-frequency and the low-frequency dispersions than Nafion 117. This means that the contribution to the total dispersion from these processes increases with decreasing equivalent weight. Comparatively, for the medium-frequency

process, the reversed trend was observed. However, the contribution from the medium-frequency to the total dielectric dispersion is small compared to other processes.

The dispersion for individual processes reflects the number of relaxing unit for each relaxation. Therefore, the larger dispersions in Flemion membrane than in Nafion membrane suggest the larger amount of water. This may reflect in the larger size and/or larger number of the ionic cluster regions. This conclusion is consistent with the water sorption.

Fig. **6.8** shows the comparison of the static permittivity for Nafion 117 and Flemion SH150 membranes. The static permittivity is calculated as the sum of the individual dispersion plus ε_∞. εs increases with increasing water content. At low water content ($\lambda < 6$), these two membranes have approximately the same permittivity, which suggests that the two membranes have similar structure in their respective ionic cluster regions. As water content increases, εs of Flemion SH150 increases faster than that of Nafion 117. This may again suggest that the larger size and/or larger number of the ionic cluster regions in Flemion SH150 than Nafion 117.

6.2.2 Kinetics of the dielectric relaxation

Fig. **6.9** shows the relaxation times for the low-, medium-, and high-frequency process for Flemion SH150 membrane. These relaxation times have approximately the same magnitudes as those of Nafion 117 at corresponding water content.

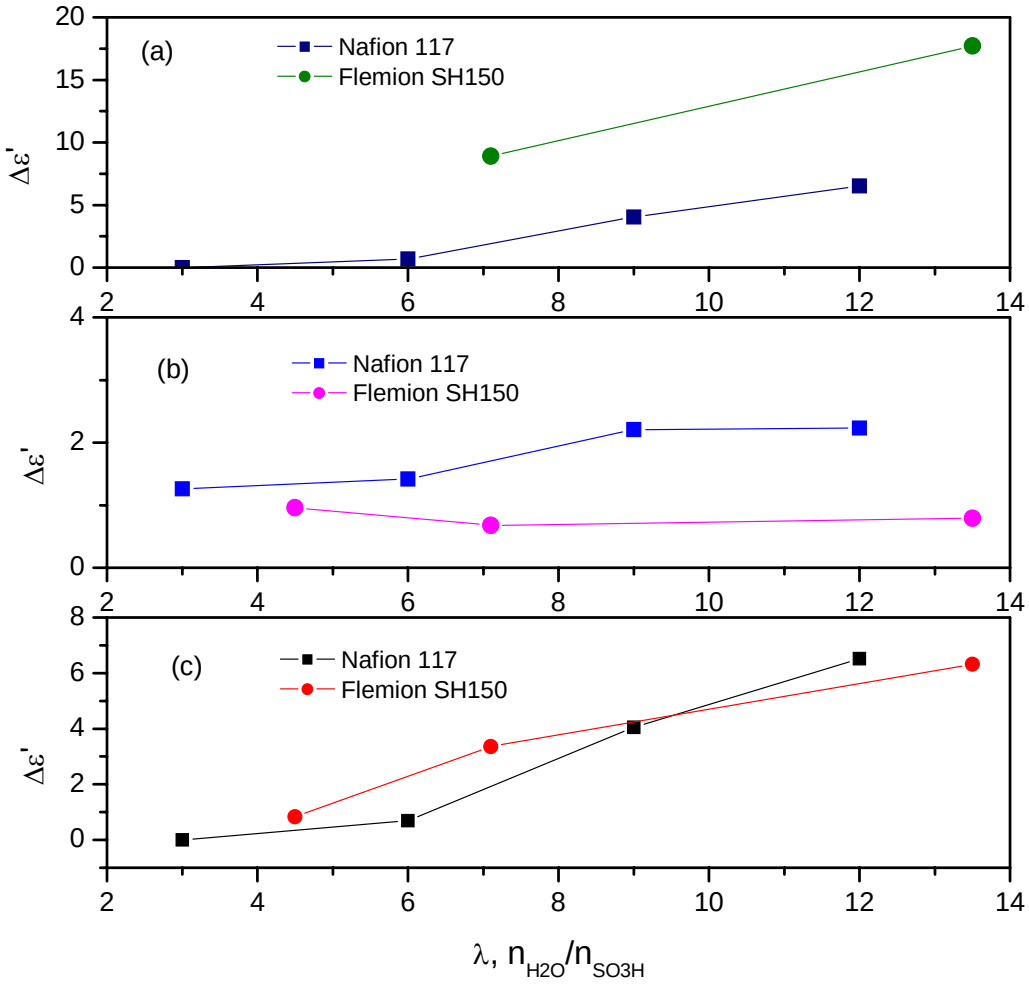

Fig. **6.7**: The (a) low-frequency, (b) medium-frequency, and (c) high-frequency dielectric dispersion for Nafion 117 and Flemion SH150 measured at 25°C and plotted as a function of water content.

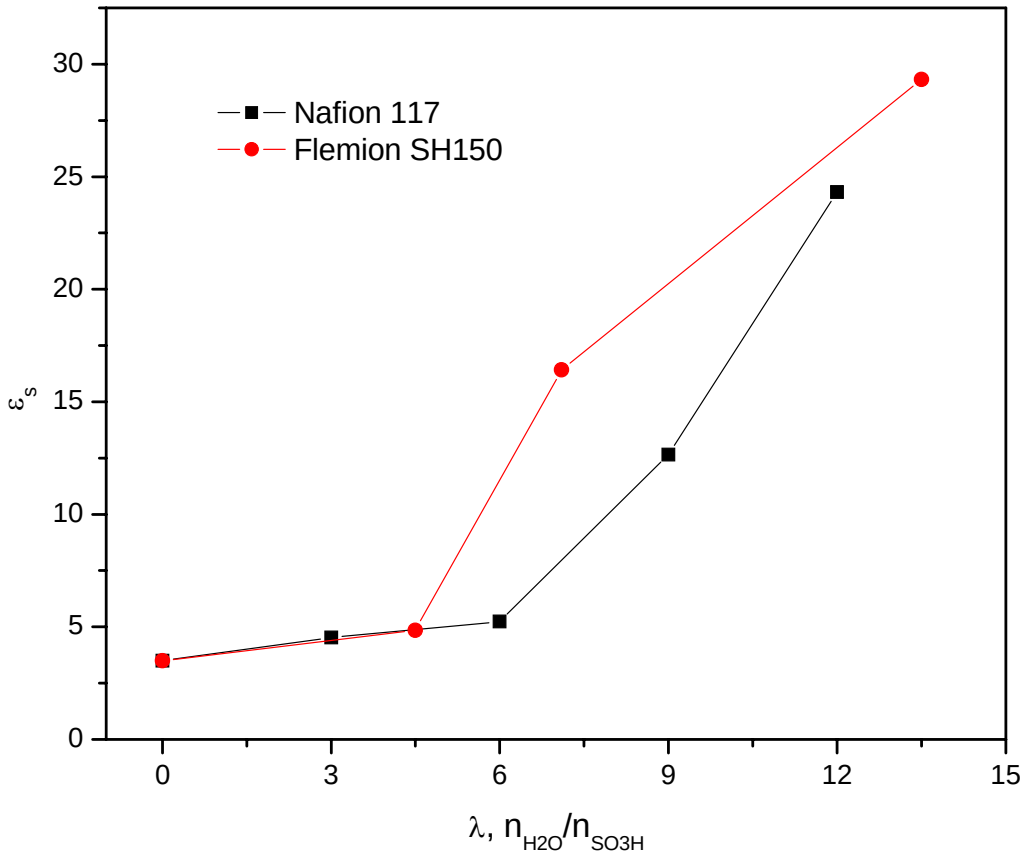

Fig. **6.8**: The static permittivity of Nafion 117 and Flemion SH150 samples measured at 25^{o}C plotted versus the water content.

The enthalpy ($\Delta H^{\neq}$) and entropy ($\Delta S^{\neq}$) of activation for individual dielectric processes have been calculated by the same procedure as in Chapter 5 and are shown in Table **6.2** for Flemion SH150 membrane. The dynamics of these relaxations are essentially identical to those of Nafion 117. This means that the EW values have no effect on the dynamics of each type of water. The changes due to the different EW values are reflected in the amount of each type of water. Lower EW values result in larger size and/or larger numbers of the ionic cluster regions, and, accordingly, the higher permittivity.

The structure and the hydration process of the Flemion SH150 are expected to be similar to that of Naifon 117. The difference is the presence of the “free” water at lower water content, due to the lower EW values.

6.3 Summary

The dielectric spectra of hydrated Flemion SH150, which has an equivalent weight of 909, were also determined to study the effect of equivalent weight on the water state in PSA membrane. Flemion SH150 sorbs more water from water vapor and shows higher static permittivity compared to Nafion 117. Three relaxation processes were found for Flemion SH150 equilibrated in water activity higher than 0.75, while two relaxation processes were found for samples equilibrated in water activity of 0.33. These relaxation processes are essentially identical to those of Nafion membrane, reflected from the similar relation times and dynamics. These results suggest that Flemion SH150 membrane is likely to form larger and/or more numerous ionic cluster regions.

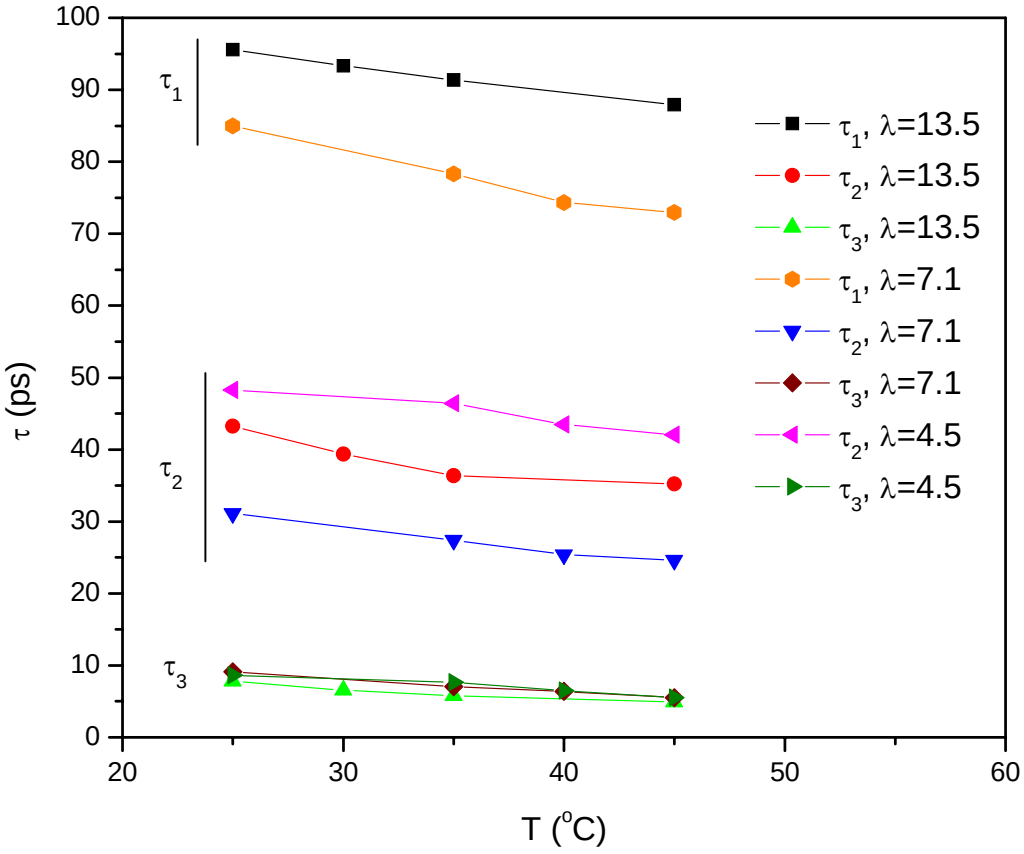

Fig. **6.9**: The relaxation times for the low- (τ_1), medium- (τ_2), and high-frequency (τ_3) dielectric process of Flemion SH150 plotted as a function of temperature and water content.

Table **6.2**: Activation parameters, $\Delta H^{\neq}$ and $\Delta S^{\neq}$, for the high-, medium-, and low-frequency relaxation in Nafion membrane with different contents.

Relaxations	$\Delta H^{\neq}$ (kJ/mol)	$\Delta S^{\neq}$ (J/mol.K)
Bulk water:	15.91	20.68
High-frequency ("free" water):		
Nafion 117	14.02	16.56
Flemion SH150	15.90	19.86
Low-frequency:		
Nafion 117		
λ~12	5.35	-35.17
Flemion SH150		
λ~13.5	0.72	-50.71
λ~7.1	3.96	-38.83

6.4 References

1. M. Saito, N. Arimura, K Hayamizu, T. Okada, *J Phys. Chem. B*, **108**, 16064 (2004)

2. S.J. Paddison, D.W. Reagor, T.A. Zawodzinski Jr., *J. Electroana. Chem.*, **459**, 91 (1998)

3. K.D. Kreuer, *J. Membr. Sci.*, **185**, 29 (2001); P.R. Paul and S.J. Paddison, *J. Chem. Phys.*, **115**, 7762 (2001)

4. T.D. Gierke, G.E. Munn, F.C. Wilson, *J. Polymer Sci., Polym. Phys.*, **19**, 1687 (1981)

5. G. Gebel, *Polymer*, **41**, 5829 (2000)

6. M. Saito, N. Arimura, K. Hayamizu, T. Okada, *J. Phys. Chem. B*, **108**, 16064 (2004)

Chapter 7

The study of DMSO/H_2O and Nafion 117/DMSO/H_2O system

The physical state and dynamics of water in perfluorosulfonic acid membranes have been studied by using microwave dielectric relaxation spectroscopy, water sorption isotherms, and DSC measurements. The primary conclusion was that the optimization of the proton conductivity of the membrane requires maximization of the free water content, which is responsible for proton conduction. Thus, the goal of this work is to try to increase the fraction of free water in membranes. The method is to use the dimethyl sulfoxide molecule to extract the water from being associated with the side chains and polymer backbone and thereby change them to free water.

7.1 Introduction

Diemthyl sulfoxide (DMSO) is a remarkable chemical compound and is widely used as a solvent and reaction media. Many observations [1-3] suggest that DMSO makes hydrogen bonds with water molecules. Studies of the thermodynamic properties [4,5] , transport properties [6,7] , and chemical shift behavior [3] of the DMSO/water system resulted in the generally accepted conclusion that DMSO and water molecules have a tendency to form hydrogen bonds in the relation 1:2 (molar DMSO fraction X_{DMSO} = 0.33). The structure of the dimethyl sulfoxide/water mixture has been studied on the molecular level by neutron diffraction [8,9]. The water structure is not strongly affected

by the presence of DMSO, but the percentage of water molecules that are hydrogen bonded to each other are substantially reduced compared to that in pure water. Furthermore, no evidence for hydrophobic association of DMSO molecules has been observed in DMSO/water mixtures. These results point to a “breaking” of the water structure caused by the presence of DMSO molecules. The same conclusion was also made based on measurements of temperature of maximum density of DMSO/water dilute solutions [**10**].

DMSO molecules have been found to lead to the dehydration of intermembrane space of 1,2-dipalmitoyl-sn-glycero-3-phosphatidylcholine (DPPC) [**11**-**13**]. As a result of the decreasing of intermembrane solvent space with increasing DMSO concentration, it has been deemed possible to divide water molecules in DPPC into two fractions based on the IR absorption spectroscopy and X-ray scattering measurements [**11**]: (a) bound water – where water molecules are bound to the polar head groups of the phospholipid molecules; and (b) free water molecules, which exist between lipid bilayers without any interactions with the membrane surface. The bound water can be further divided into the fraction of water molecules embedded in the spatial region of the polar head groups and the fraction located in the intermembrane space near the head groups. The number of bound water molecules located in the region of polar head groups and in the intermembrane space was measured to be equal to 2.2 and 8.6 per DPPC molecule, respectively. The DMSO-induced dehydration of the intermembrane space was explained as a result of strong interaction between DMSO and water molecules, which is stronger compared with interaction between water and the polar head group of the phospholipid membrane.

These studies shed a light on the idea of reducing the water molecules associated with the side chains and/or backbone in the Nafion membrane and, thus, increasing the fraction of free water. In this study, the influence of DMSO upon the dielectric spectra of binary DMSO/water and ternary Naifon 117/DMSO/water system are presented together with the proton conductivity measurements.

7.2 DRS of DMSO/water mixtures

The microwave DRS were measured over a wide frequency range of 45 MHz to 26.5 GHz and at temperatures ranging from 25 to 45^{o}C in steps of 5^{o}C. Fig. **7.1** shows the dielectric spectra, permittivity, $\varepsilon'(\omega)$, and absorption, $\varepsilon''(\omega)$, of the DMSO-water mixtures at 25^{o}C at various concentrations.

The dielectric spectra of DMSO-water mixtures were fitted by the general Havrilliak-Negami function, which is expressed as Eq. **2.12**, according to the complex nonlinear least-square (CNLS) routine described in Chapter 2.

$$\varepsilon^{*}(\omega) = \varepsilon_{\infty} + \frac{\varepsilon_{s} - \varepsilon_{\infty}}{[1 + (i\omega\tau)^{1-\alpha}]^{\beta}}, \qquad 0 \le \alpha < 1: \;\; 0 < \beta \le 1 \tag{2.8}$$

According to other studies [**14**,**15**], the dielectric spectra for DMSO-water mixtures are well described by the Davidson-Cole model or sometimes by a single Debye model. The best results of fitting of our data by the more complicated Havriliak-Negami model result

in very small α value at thorough concentrations. In order to increase the significance of other parameters, the spectra were fitted by the Davidson-Cole model ($\alpha = 0$).

The parameters that are required to describe the dielectric relaxation spectra of mixtures through the Davidson-Cole equation are collected in Table **7.1**. The DMSO/water mixtures show an unsymmetrical relaxation time distribution, as reflected by the large β values. Furthermore, the static permittivity decreases monotonically from the value for pure water to that of pure DMSO (Fig. **7.1**).

Fig. **7.2** shows the dielectric relaxation time, τ, of DMSO/water mixtures as a function of X_{DMSO} and temperature. For each temperature, τ first increases with X_{DMSO}, then reaches a maximum when X_{DMSO} is in the range of 0.3-0.4, and finally decreases to the value of pure DMSO.

The dielectric relaxation times were analyzed by the absolute rate theory [**16**]. The energy of activation for the dielectric relaxation process, $\Delta G^{\neq}$, can be calculated from the dielectric relaxation time by using the Eyring equation:

$$\Delta G^{\neq} = RT \ln(\frac{k_B T \tau}{h}) \qquad (7.1)$$

A plot of $\Delta G^{\neq}$ versus T ($\Delta G^{\neq} = \Delta H^{\neq} - T\Delta S^{\neq}$) can yield the enthalpy $\Delta H^{\neq}$ and entropy $\Delta S^{\neq}$ of activation for the dielectric relaxation process. These parameters characterize the molecular interactions and dynamics of the components and their mixtures.

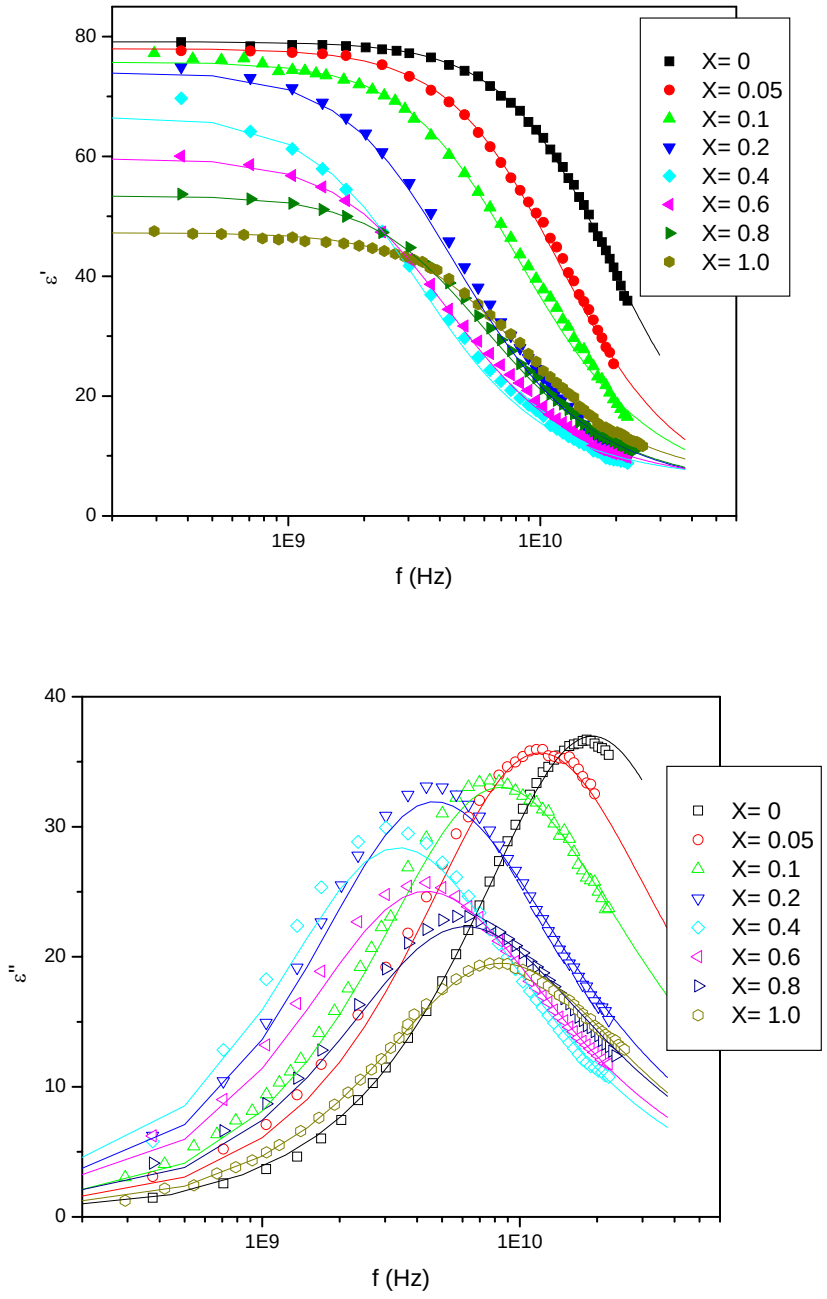

Fig. **7.1**: Frequency dependence of dispersion (ε′) and absorption (ε″) for the DMSO/water mixtures at 25°C at various concentrations. The solid curves are the fitting results.

Table 7.1: Parameters of the Davidson-Cole relaxation spectral function for DMSO/water mixtures

Mixture	ε_s	τ(ps)	β	ε_∞	Mixture	ε_s	τ(ps)	β	ε_∞
x_{DMSO}=0					x=0.4				
298K	78.89	8.25	1	5.20	298K	66.98	53.94	0.865	4.55
303K	76.67	7.29	1	4.71	303K	65.31	47.24	0.869	4.53
308K	74.65	6.48	1	4.21	308K	63.63	40.12	0.867	4.51
313K	72.84	5.75	1	3.73	313K	62.49	35.61	0.870	4.02
318K	70.64	5.17	1	3.25	318K	61.34	31.26	0.870	3.52
x=0.01					x=0.6				
298K	78.11	9.37	0.970	4.65	298K	59.83	42.88	0.815	5.0
303K	75.94	8.28	0.981	4.24	303K	58.52	38.13	0.818	4.68
308K	73.78	7.14	0.991	3.83	308K	57.21	34.66	0.820	4.35
313K	71.69	6.46	0.991	3.40	313K	56.25	31.37	0.824	4.01
318K	69.60	5.98	0.990	2.96	318K	55.30	28.88	0.822	3.66
x=0.05					x=0.8				
298K	78.02	14.65	0.882	4.26	298K	53.51	30.95	0.798	3.80
303K	75.22	12.82	0.882	3.95	303K	52.56	28.23	0.804	3.98
308K	72.43	11.44	0.884	3.65	308K	51.62	25.48	0.809	4.14
313K	71.17	10.46	0.885	3.29	313K	50.88	23.47	0.811	4.03
318K	69.92	9.50	0.886	2.94	318K	50.13	22.08	0.813	3.90
x=0.1					x=0.9				
298K	76.79	22.53	0.816	4.27	298K	50.4	25.93	0.822	4.24
303K	74.52	19.97	0.814	3.77	303K	49.77	23.43	0.824	4.16
308K	72.24	17.94	0.811	3.28	308K	49.13	21.65	0.823	4.07
313K	70.52	16.42	0.819	3.06	313K	48.48	20.12	0.826	3.90
318K	68.80	14.97	0.827	2.84	318K	47.83	18.86	0.827	3.72
x=0.15					x=1				
298K	75.16	31.98	0.810	3.91	298K	47.29	20.92	0.895	4.45
303K	72.54	27.51	0.808	3.48	303K	46.97	18.96	0.896	4.16
308K	69.93	24.53	0.805	3.05	308K	46.64	17.81	0.896	3.86
313K	68.46	21.76	0.809	3.10	313K	46.08	16.64	0.903	3.55
318K	66.98	19.18	0.813	3.15	318K	45.53	15.63	0.910	3.23
x=0.2									
298K	74.64	40.13	0.845	3.74					
303K	72.26	34.64	0.848	3.76					
308K	69.88	29.87	0.847	3.78					
313K	68.05	26.13	0.851	3.63					
318K	66.23	23.48	0.854	3.49					
x=0.33									
298K	68.97	52.78	0.860	3.97					
303K	67.30	46.53	0.860	3.73					
308K	65.62	39.25	0.859	3.51					
313K	64.71	34.52	0.865	3.53					
318K	63.80	30.31	0.870	3.56					

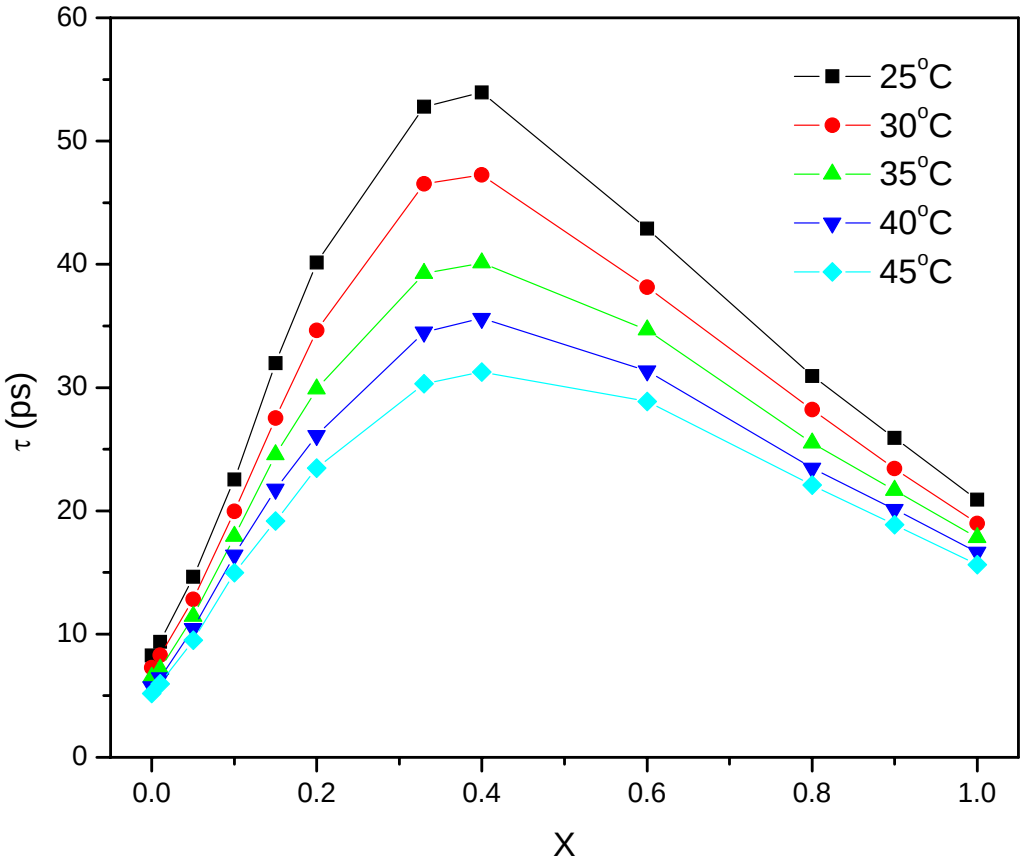

Fig. **7.2**: Plots of relaxation times, τ, of the Davidson-Cole function displayed as a function of mole fraction of the DMSO for DMSO/water mixtures at various temperatures.

Fig. **7.3** displays the free energy of activation as a function of temperature. $\Delta G^{\neq}$ of DMSO/water mixtures is a linear function of temperature for all compositions. The values of $\Delta H^{\neq}$ and $\Delta S^{\neq}$ are obtained from the slopes and intercepts, respectively, of the lines for different solution compositions. Fig. **7.4** displays the $\Delta H^{\neq}$ and $\Delta S^{\neq}$ as functions of system composition. For all mixtures, $\left|\Delta H^{\neq}\right| > \left|T\Delta S^{\neq}\right|$, indicating that the reorientation processes in pure liquids and mixtures are controlled by enthalpic rather than by entropic factors. Three regions, separated by boundaries at x ~ 0.1 and 0.6, can be classified based on the different dependencies of $\Delta H^{\neq}$ and $\Delta S^{\neq}$ on composition, as shown in Fig. **7.4**. In this work, we are interested in the DMSO/water mixtures in the dilute region. Thus, only the feature in this region will be analysis here.

The activation enthalpy ($\Delta H^{\neq}$) and entropy ($\Delta S^{\neq}$) for water are calculated to be 15.9kJ/mol and 20.7 J/mol.K, respectively. These values are in good agreement with the data in the literature [**17**]. According to [**17**], the cooperative relaxation time of water monitors both (1) the dwelling time required for the release of mobile H_2O (less than 2 hydrogen bonds) molecules from the hydrogen bond network and (2) the waiting time experienced before it is trapped into a new configuration of minimum energy. In pure water, Step (1) dominates, thereby permitting the determination of the average number of hydrogen bonds per water, n_{HB}, according to:

$$n_{HB} = \frac{\Delta H^{\neq}}{\Delta H_{HB}} + 1 \qquad (7.2)$$

where ΔH_{HB} is the strength of the hydrogen bond. ΔH_{HB} is taken as 10.9 kJ/mol, as determined by Walrafen *et al*. [**18**]. Adding 1 in this equation is based on the fact that these "mobile" molecules usually have one intact hydrogen bond. Thus, a value of 2.5 is obtained for the average number of hydrogen bonds per water molecule in the liquid state, which is close to the value obtained from Raman spectroscopy [**19**].

Compared to pure water, $\Delta H^{\neq}$ and $\Delta S^{\neq}$ for the DMSO/water mixtures are reduced by adding DMSO molecules, reaching minimum values at $X_{DMSO} = 0.1$ (Fig. **7.4**). The reduction of $\Delta H^{\neq}$ and $\Delta S^{\neq}$ in the mixtures can be attributed to a change in hydrogen bond strength and/or a decrease in the average number of hydrogen bonds. IR spectra measurements [**20**] showed that the addition of DMSO did not change the distribution of hydrogen bond energies of water. It is thus concluded that the reduction of $\Delta H^{\neq}$ and $\Delta S^{\neq}$ is due to the decrease of average number of hydrogen bonds. It is assumed that the value of $\Delta H_{HB} = 10.9$ kJ/mol for pure water can also be applied to dilute DMSO solutions. The average numbers of H-bonds were also calculated for the mixtures by using Eq. **7.2** and shown in Fig. **7.5**. The reduction of n_{HB} in the mixtures means that the cooperative relaxation of the hydrogen bond network is facilitated by the presence of DMSO. In other words, the DMSO molecules decrease the potential barrier for reorientation of the system dipole.

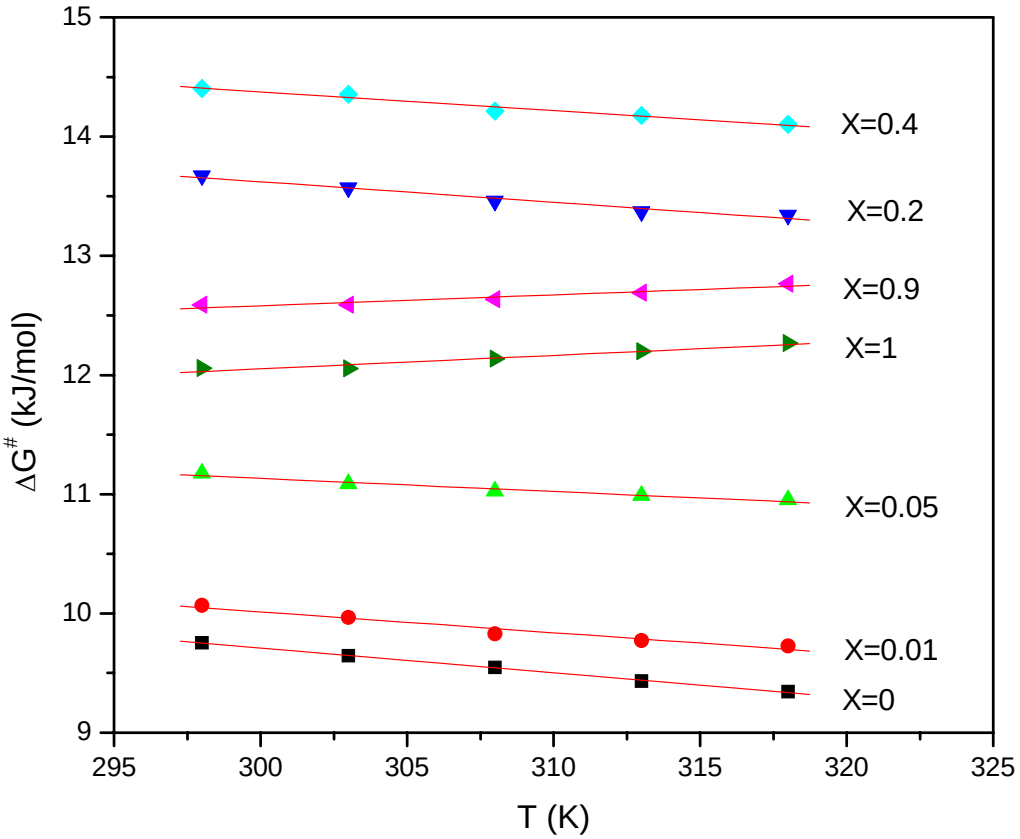

Fig. **7.3**: The free energy of activation for the dielectric relaxation process, $\Delta G^{\neq}$, for the DMSO/water mixtures as a function of temperature and solution composition. The numbers in the figure denote the mole fraction of DMSO.

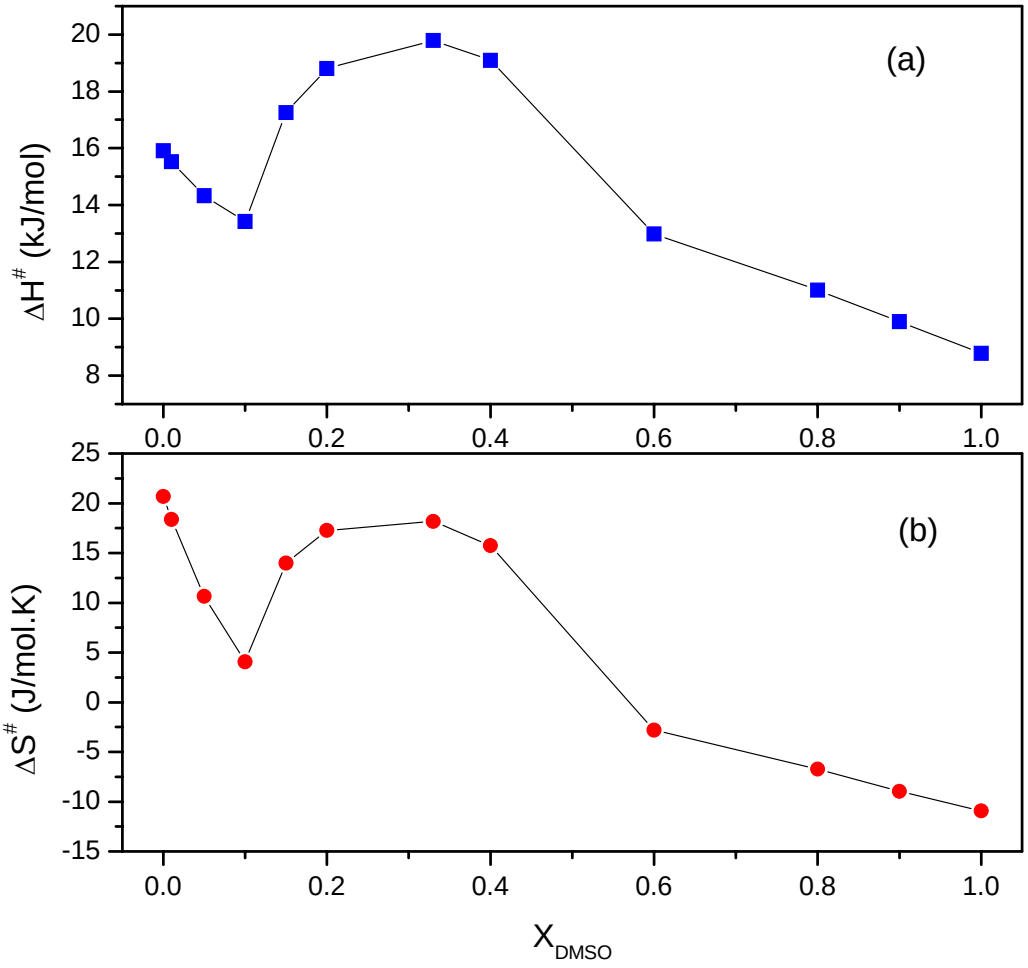

Fig. **7.4**: Composition dependence of (a) enthalpy of activation, and (b) entropy of activation for DMSO/water mixtures.

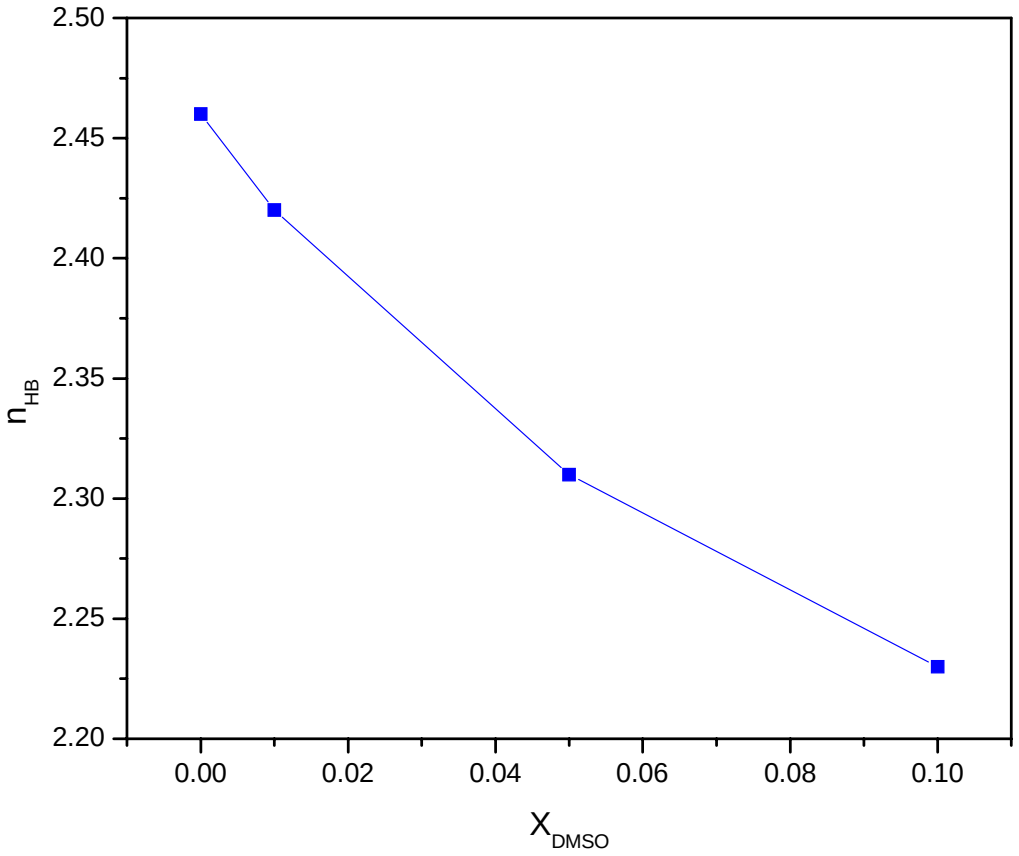

Fig. **7.5**: The average number of hydrogen bonds in DMSO/water mixtures calculated from the enthalpy of activation by Eq. **7.2** plotted versus the molar fraction of DMSO.

A hydrogen bonding configuration has been proposed by Luzar *et al*. [**8**] to account for the neutron diffraction results. The configuration is redrawn in Fig. **7.6**, where a water molecule is replaced by a DMSO molecule. Due to the ability for DMSO to accept two hydrogen bonds, which is supported by both experiment and computer simulation [**21**], the short-range water structure remains upon the presence of DMSO molecules. Owing to the steric constraints of two methyl groups, which prevent the further formation of hydrogen bonds on these sites, the total hydrogen bonds are decreased and the percentage of water molecules that are hydrogen bonded to each other are substantially reduced compared to that in pure water. This allows for interpretation of the reduced n_{HB} values in the mixtures obtained from the dielectric measurement.

Many studies [**14**,**15**] have attributed the increase in the relaxation time with DMSO concentration to hydrophobic hydration caused by the nonpolar methyl groups, analogous with hydrophobic hydration in macromolecules. However, the complete DRS studies here, combined with the neutron diffraction measurements [**8**,**9**], showed that the structure breaking effect of DMSO occurs at dilute concentrations. We think that the energetic parameters, i.e., $\Delta H^{\neq}$ and $\Delta S^{\neq}$, are better criteria for distinguishing the hydrophilic and/or hydrophobic hydration of organic solutes, especially for those having both polar and non-polar groups. By this standard, the structure breaker decreases the activation of enthalpy, and the maker increases $\Delta H^{\neq}$. Fig. **7.7** shows the deviation of the activation enthalpy of the solutions, defined as the difference between that of solution and pure water, $\Delta(\Delta H^{\neq}) = \Delta H^{\neq}_{sol} - \Delta H^{\neq}_{water}$, for several organic solutes: DMSO, tert-butanol, methanol, and dimethyl sulfone. The data for methanol was obtained from literature [**22**].

Positive deviations were obtained for tert-butanol and methanol, which clearly indicate the stabilizing action of these alcohols on water structuring in dilute solutions. In contrast, the negative deviations of $\Delta H^{\neq}$ for DMSO and dimethyl sulfone indicate that they are “water structure breakers”. Tert-butanol has stronger “structure-making” ability than methanol, which is consistent with the TMD measurements [**23**]. The stronger effect comes from the longer carbon chain. Dimethyl sulfone showed stronger “structure-breaking” ability than DMSO, which can be attributed to its larger dipole moment and stronger H-bonding with water.

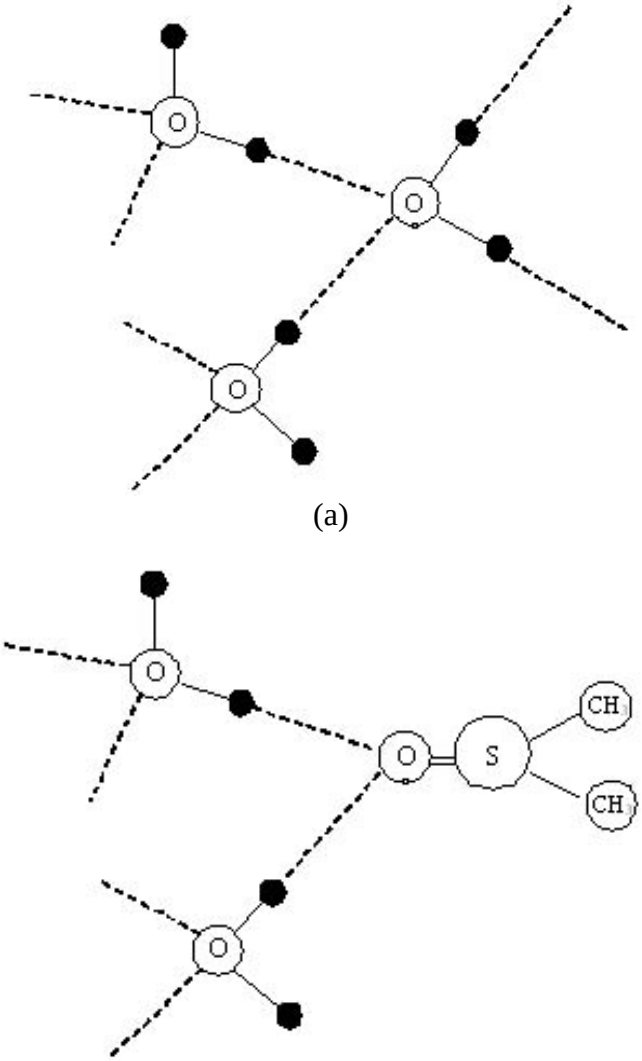

Fig. **7.6**: Schematic view of hydrogen bonding in (a) pure water and (b) DMSO/water mixture. Solid lines represent intramolecular bonds. Dashed lines represent hydrogen bonds.

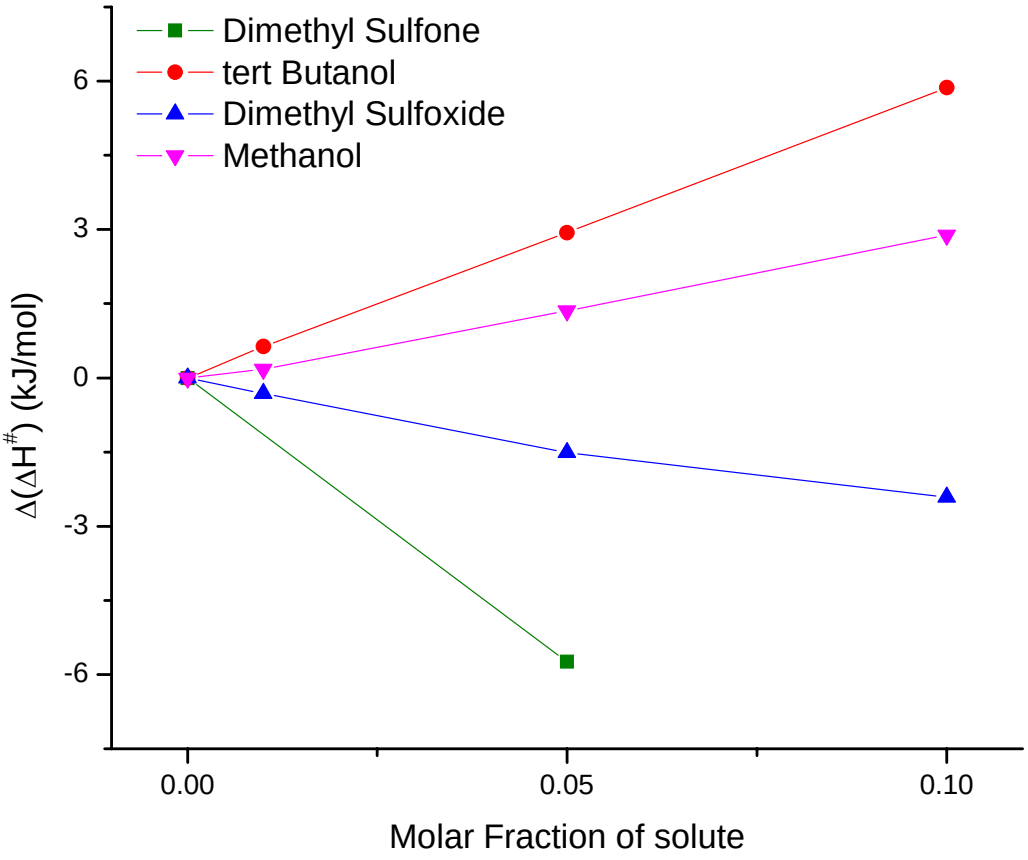

Fig. **7.7**: Concentration dependences of activation enthalpy of dielectric relaxation in aqueous solutions of organic solutes. The data for methanol is cited from reference [**22**]. $\Delta(\Delta H^{\neq}) = \Delta H^{\neq}_{sol} - \Delta H^{\neq}_{water}$.

7.3 Microwave DRS of Nafion 117/DMSO/water system

7.3.1 Equilibrium water sorption

The Naifon 117 membrane, pretreated by 3%H_2O_2 and 0.5M H_2SO_4, was dried under vacuum conditions at 120^oC for 8 hours and then soaked in 20%(volume) DMSO + 80% H_2O for two weeks. The swollen samples were then equilibrated in the controlled water activity using isopiestic sorption method. Fig. **7.8** shows the results of water sorption, expressed as the number of water molecules per sulfonic acid group, λ. Nafion membranes containing DMSO take more water than those samples without such treatment.

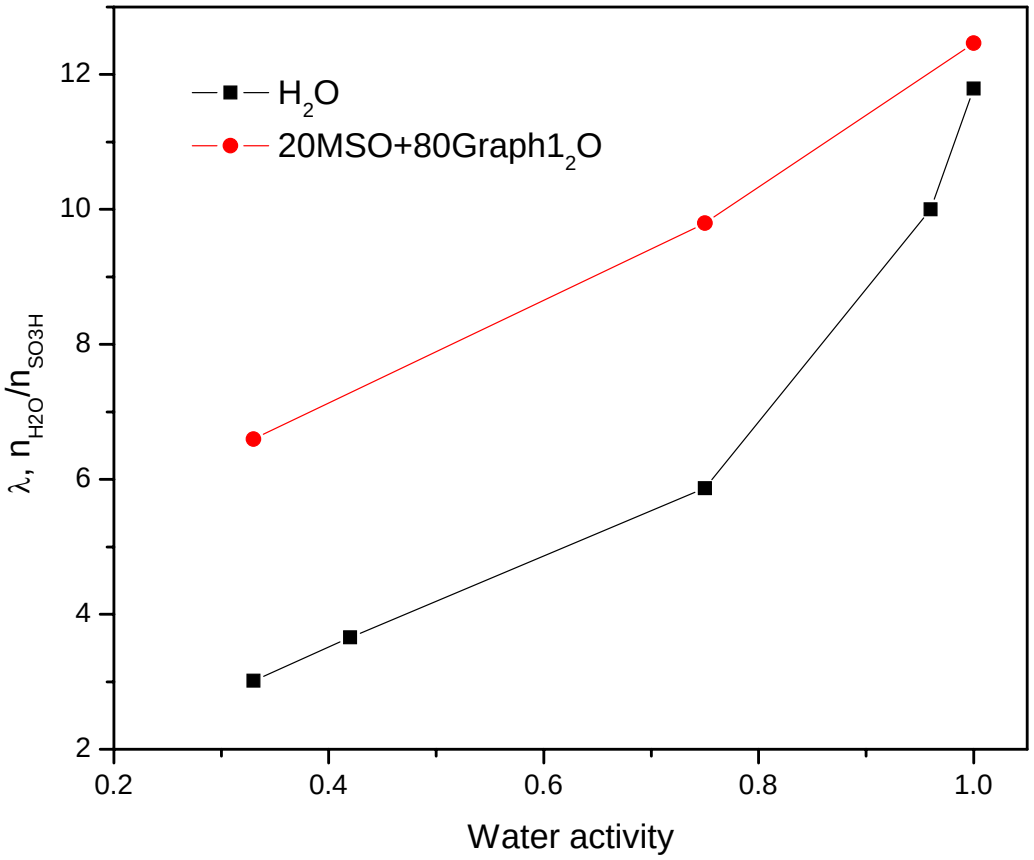

Fig. **7.8**: Isopiestic sorption of water vapor in Flemion SH150 and Nafion 117 membranes at 25°C.

7.3.2 Microwave DRS

The microwave dielectric spectra of the Nafion/DMSO/water system with different water contents have been measured at 25^{o}C. Fig. **7.9** shows the dielectric response for λ = 12.5, 9.8, and 6.6. The dielectric spectra of these membranes were fitted by various dielectric models. The best results are shown in Table **7.2**.

The dielectric spectra of the Nafion/DMSO/water system are best fitted by a sum of two Debye relaxation processes (D2 model). This is in contrast to those of Nafion and Flemion membranes without DMSO, where the spectra were fitted by different dielectric models depending on water contents. An example of the fitting is shown in Fig. **7.10** for λ = 12.5. The relaxation times of these two processes, i.e., 70.74ps and 12.48 ps, correspond to the medium- and high-frequency processes in Nafion membranes without DMSO, thus indicating that the low-frequency process in Nafion membrane disappears after taking DMSO molecules. Fig. **7.11** shows the fitting results for three water contents.

The disappearance of the low-frequency relaxation, which is due to the water molecules associated with the side chains and the polymer backbone in membranes, suggests that DMSO molecules extract this part of water and re-distribute them into the "free" state and/or hydration water of sulfonic acid groups. This is consistent with the dehydration behavior of DPPC caused by DMSO [**11**-**13**].

The "free" water and hydration water in membranes are replaced by the DMSO/water mixtures after the addition of DMSO molecules due to the strong hydrogen bonding between them. Fig. **7.12** shows the fraction of the solvent mixture in the "free" state. Compared to the fraction of "free" water in the Nafion membrane, DMSO

molecules dramatically increase the fraction of the solvent mixture in the “free” state. This increase may be helpful to the proton conduction.

The proton conductivities of DMSO-treated Nafion membranes were measured by the four-probe method at room temperature. Fig. **7.13** shows the results. Compared to the samples without DMSO, the DMSO treatment increases the conductivity at low water content, which may be due to the increase of the fraction of solvent mixture in “free” state. On the other hand, the conductivities of the DMSO-treated samples have lower conductivities at high water content. This can be explained by the longer relaxation times of the DMSO/water mixtures, as shown in Fig. **7.2**. This further suggests that the proton conduction in pure water and aqueous solutions is closely related with the dynamics of the hydrogen bond network, which can be studied by dielectric relaxation spectroscopy.

Table **7.2**: Dielectric parameters of the results of the best fitting for the Nafion/DMSO/water system at 25^{o}C.

λ	Model	$\Delta\varepsilon_1$	τ_1, ps	$\Delta\varepsilon_2$	τ_2, ps	ε_∞	σ, S/cm
12.5	D2	4.22	70.74	4.74	12.48	4.21	0.28
9.8	D2	1.14	73.51	1.25	12.76	3.4	0.16
6.6	D2	0.83	68.47	0.97	12.33	3.2	0.09

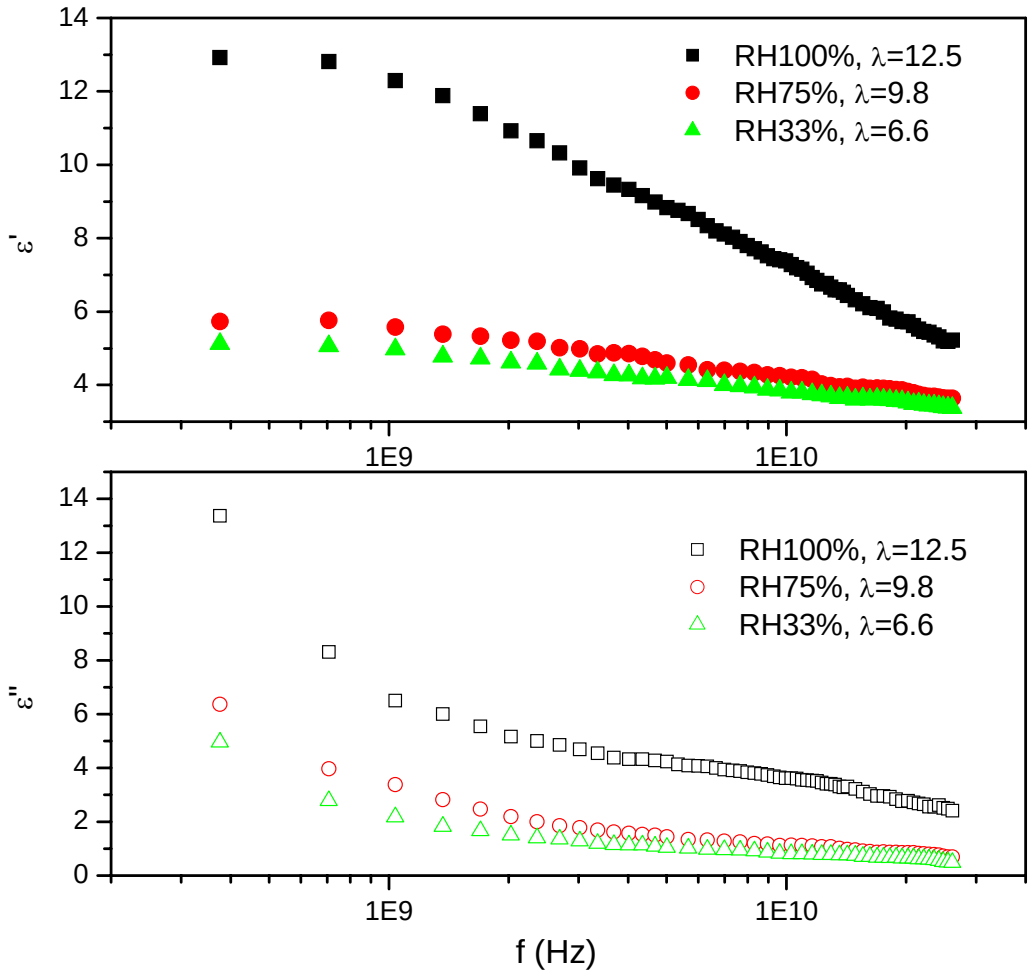

Fig. **7.9**: Measured permittivity, ε′(ω), and absorption, ε″(ω), for Nafio 117 soaked in 20%(vol) DMSO + 80% H2O and then equilibrated in controlled water activities (RH=100%, 75%, and 33%) at 25°C.

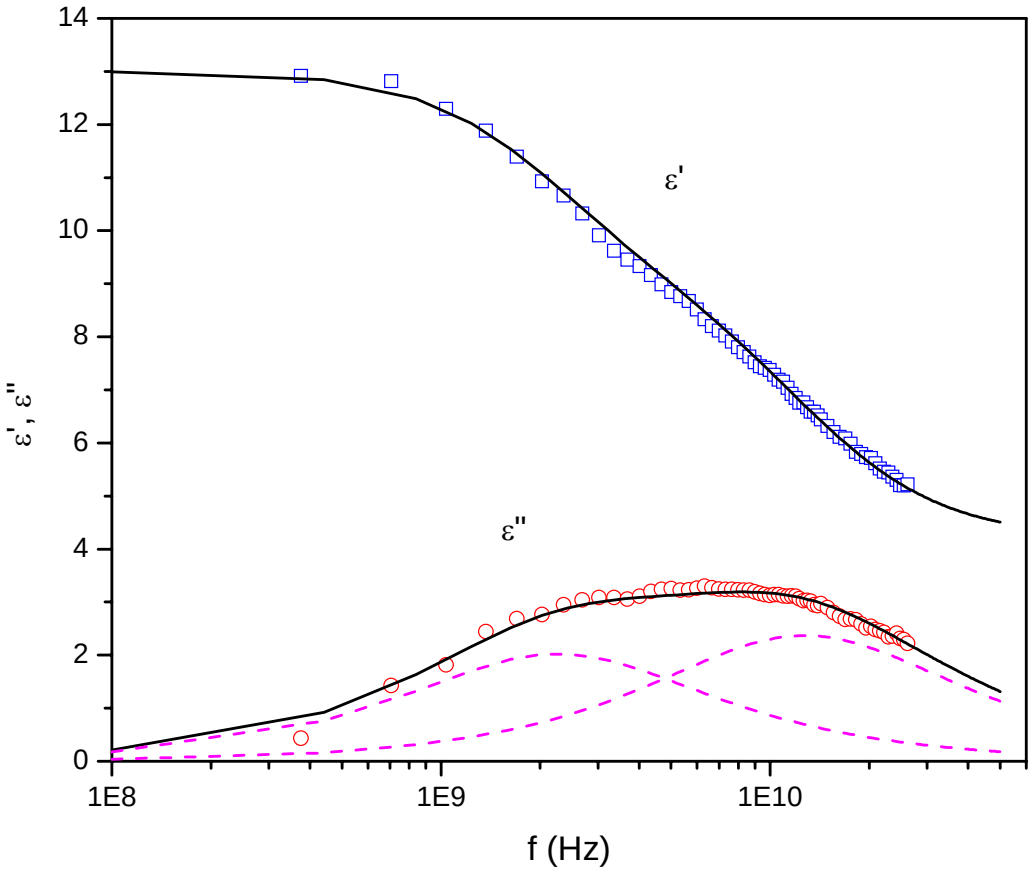

Fig. **7.10**: Permittivity, ε′(ω), and absorption, ε″(ω), for Nafion 117 soaked in 20%(vol) DMSO + 80% H2O and then equilibrated in saturated water vapor (RH=100%, λ = 12.5) measured at 25°C. The contribution from conductivity has been subtracted. The solid lines are the best fitted results and the dash lines represent the three components.

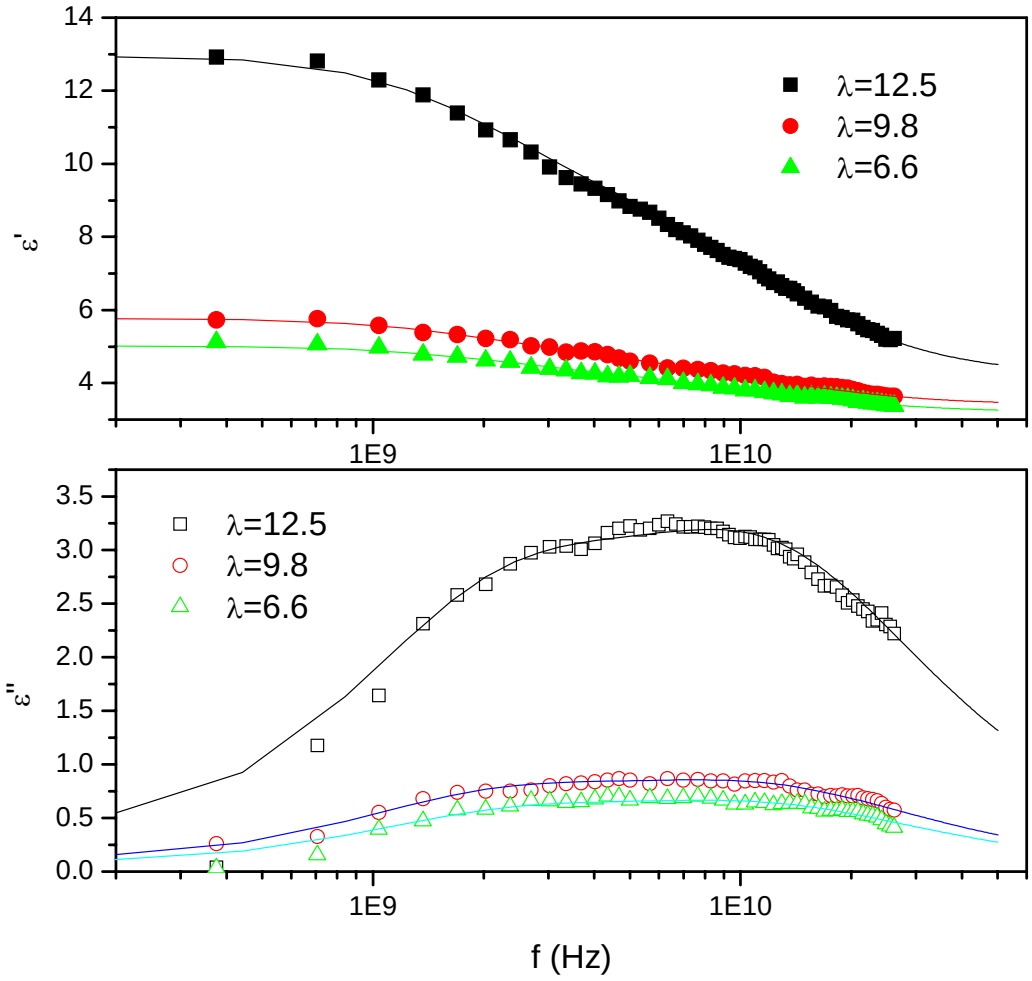

Fig. **7.11**: The effect of water content (λ=12.5, 9.8, and 6.6) on dielectric responses of the Nafion membrane treated with DMSO molecules measured at 25°C. The contribution from dc conductivity has already been subtracted. The solid lines are the best fitted results.

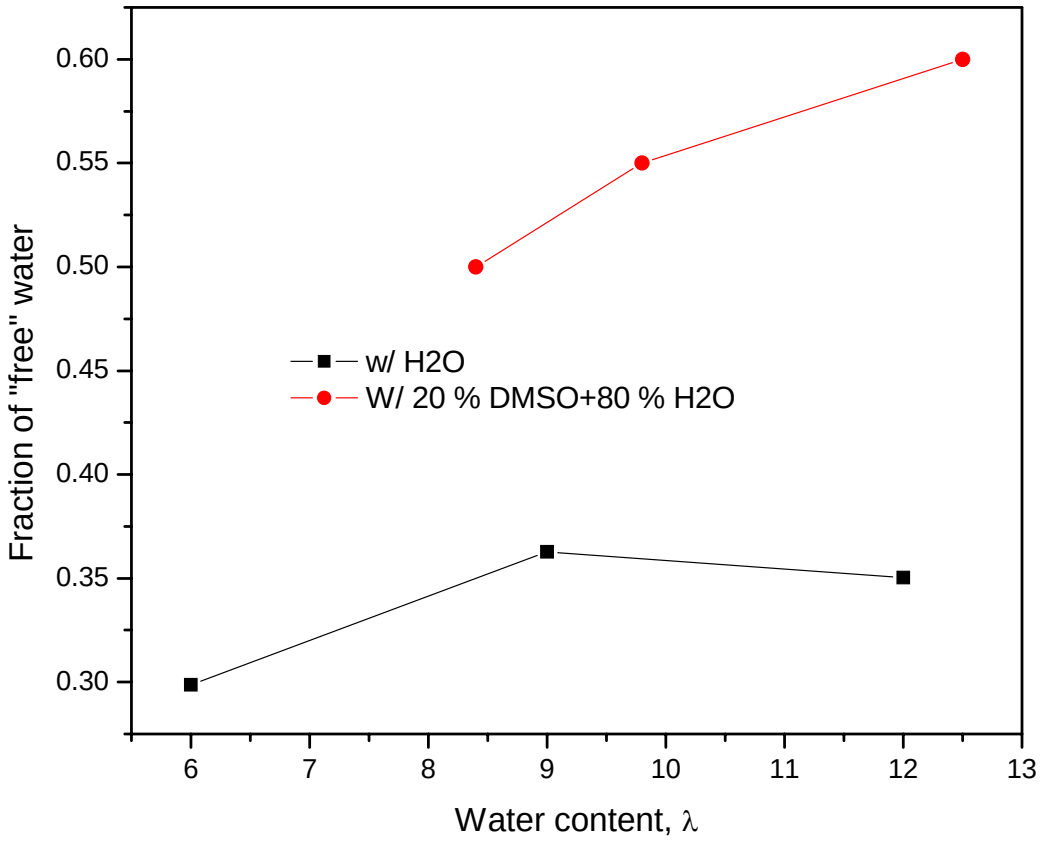

Fig. **7.12**: Comparison of the fraction of “free” solvent, water or DMSO/water mixture in Nafion or Nafion/DMSO respectively, on the addition of DMSO.

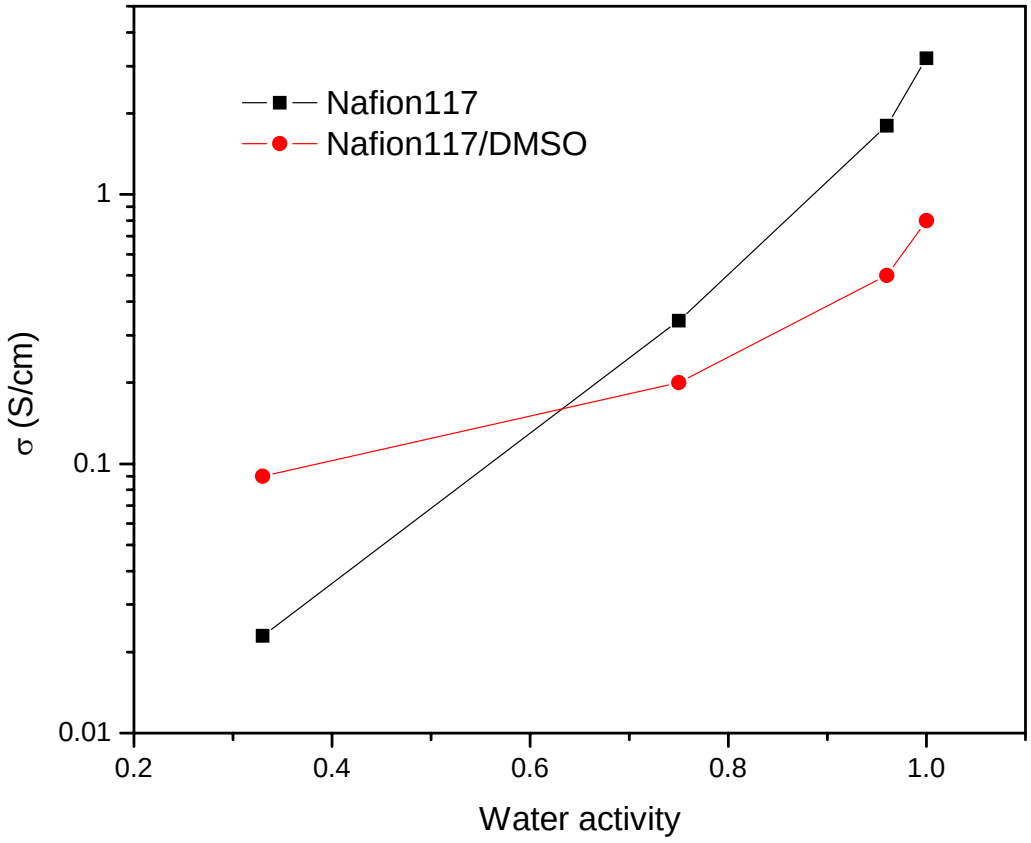

Fig. **7.13**: Ionic conductivity, σ, for the Nafion membrane with and without DMSO versus the water activity in which the sample was equilibrated.

7.4 Summary

Manipulation of dimethyl sulfoxide content was tried to increase the fraction of the “free water” due to its strong ability to form hydrogen bonding with water molecules. The average number of hydrogen bonds per water molecule in DMSO/water mixtures is found to be reduced from that in pure water in the dilute solutions. This effect was caused by the “breaking effect” of DMSO, i.e. the breakdown of the hydrogen bond network of water by DMSO molecules. The dielectric properties of the Nafion/DMSO/water system were also measured at 25^{o}C. Two relaxation processes were observed for the Nafion containing DMSO, which is in contrast to Nafion/water systems. The water molecules associated with the side chains and polymer backbone in the Nafion membrane are removed by addition of DMSO molecules. Also, the fraction of the solvent mixture in the “free” state was shown to be significantly increased compared to the fraction of free water in Nafion membrane. This increase leads to increasing conductivity of Nafion/DMSO at lower water content compared to Nafion. However, the Nafion membrane treated with DMSO has lower conductivity at high water contents. This can be explained by the lower relaxation times for the solvent mixture compared to pure water.

7.5 References

1. E.S. Baker and J. Jones, *J. Phys. Chem.*, **98**, 1730 (1985)

2. G.J. Stafford, P.C. Schaffer, P.S. Leung, G.F. Doebbler, G.W. Brady, E.F.X. Lyden, *J. Chem. Phys.*, **50**, 2140 (1969)

3. H.H. Szmant, in *Biological Actions of Dimethyl Sulfoxide*, S.W. Jacob, Ed., Ann. NY Acad. Sci., Vol. 243 Academic Press, New York, 1975, p20

4. J.M.G. Cowie and P.M. Toporowski, *Can. J. Chem.*, **39**, 2240 (1964)

5. M.F. Fox and K.P. Whittingham, *J. Chem. Soc., Faraday Trans.*, **75**, 1407 (1974)

6. J. Mazurkiewicz and P. Tomasik, *J. Phys. Org. Chem.*, **3**, 493 (1990)

7. U. Kaatze, M. Brai, F.D. Sholle, R. Pottel, *J. Mol. Liquid*, **44**, 197 (1990)

8. A.K. Soper and A. Luzar, *J. Chem. Phys.*, **97**, 1320 (1992)

9. A.K Soper and A. Luzar, *J. Phys. Chem.*, **100**, 1357 (1996)

10. D.D. Macdonald, M.D. Smith, J.B. Hyne, *Can. J. Chem.*, **49**, 2817 (1971)

11. S.N. Shashkov, M.A. Kiselev, S.N. Tioutiounnikov, A.M. Kiselev, P. Lesieur, *Physica B*, **271**, 184 (1999)

12. S. Tristram-Nagle, T. Moore, H. Petraches, J.F. Nagle, *Biochim. Biophys. Acta*, **1369**, 19 (1998)

13. M.A. Kiselev, P. Lesieur, A.M. Kiselev, C. Grabielle-Madelmond, M. Ollioon, *J. Alloys and Compounds*, **286**, 195 (1999)

14. U. Kaatze, R. Pottel, M. Schafer, *J. Phys. Chem.*, **93**, 5623 (1989)

15. A.K. Lyashchenko, A.S. Lileev, T.A. Novskova, V.S. Kharkin, *J. Mol. Liquids*, **93**, 29 (2001)

16. S. Glasstone, L.J. Laidle, H. Eyring, *The Theory of Rate Processes*, McGraw-Hill, New York, 1941

17. R. Buchner, J. Barthel, J. Stauber, *Chem. Phys. Letters*, **306**, 57 (1999)

18. G.E. Walrafen, M.R. Fisher, M.S. Hokmabadi, W.H. Yang, *J. Chem. Phys.*, **85**, 6970 (1985)

19. D.E. Hare and C.M. Sorensen, *J. Chem. Phys.*, **93**, 25 (1990)

20. G. Brink and M. Falk, *J. Mol. Struct.*, **5**, 27 (1970)

21. I.I. Vaisman and M.L. Berkowitz, *J. Am. Chem. Soc.*, **114**, 7889 (1992)

22. T. Sato, A. Chiba, R. Nozaki, *J. Chem. Phys.*, **112**, 2924 (2000)

23. D.D. Macdonald, B.Dolan, J.B. Hyne, *J. Solution Chem.*, **5**, 405 (1976)

Chapter 8

Summary and Future Work

In this work, the physical state and dynamics of water in perfluorosulfonic acid membranes have been studied by using microwave dielectric relaxation spectroscopy, water sorption isotherms, DSC cooling scans, and ^2H NMR T_1 measurements. The following conclusions have been obtained:

1. The dynamic and equilibrium sorption isotherms of Nafion 117 membrane from water vapor over the temperature range 30 to 90^oC were determined. The diffusion process of water in Nafion is Fickian with an average diffusion coefficient in the range of $0.1\text{-}18\times10^{-7}$ cm^2/s. The equilibrium sorption isotherms may be quantitatively analyzed according to the modified BET equation up to water activity of 0.8. The first monolayer capacity, i.e., the first hydration layer of sulfonic acid group, was found to comprise about three water molecules per sulfonate ion. Water clustering was found to occur at water activities above 0.9.

2. DSC cooling scans of the hydrated Nafion membranes indicated two types of water in terms of freezing and non-freezing fractions. The amount of non-freezing water is up to about 10. The ^2H spin lattice relaxation time (T1) of ^2H_2O in Nafion was measured as a function of state of membrane hydration. The first hydration layer of sulfonic acid group was estimated to be about 3 water molecules per sulfonic acid group, which is in agreement with the water sorption isotherms.

3. Dielectric relaxation spectra of Nafion 117 and Flemion SH150 membranes have been measured using the transmission line method over the frequency range of 45 MHz to 26 GHz and over the temperature range of 25-45^{o}C. The spectra were well-fitted by a superposition of one to three Debye relaxation processes, depending on the nature of membrane and water content. The first high-frequency dispersion step, with relaxation time $\tau \approx 8$ ps at 25^{o}C, shows the characteristic dynamics of bulk water and is attributed to the cooperative relaxation of hydrogen bonded networks of "free" water. Free water is assumed to comprise the water molecules at the center of the ion cluster regions or pores. The second step, having a relaxation time of $\tau \approx 30$ ps at 25^{o}C, is attributed to the water molecules in the second hydration shell of sulfonic acid groups. The water molecules in the first hydration shell of SO_3H has a dielectric relaxation at kHz, and can not be detected by the microwave DRS. The remaining relaxation process occurs at low-frequency, having a relaxation time of $\tau \approx 90$ ps, and is postulated to result from the motion of the water molecules associated with the perfluorinated side chains and polymer backbone. The low-frequency relaxation showed negligible activation enthalpies and large negative activation entropies, which may indicate the feature of hydrophobic hydration. The presence of the low-frequency process is found to correspond to the clustering of water and the appearance of the freezing water.

4. The dielectric spectra of hydrated Flemion SH150, which has an equivalent weight of 909, were also been determined to study the effect of equivalent weight on the water state in PSA membrane. Flemion SH150 sorbs more water from water vapor and shows higher static permittivity compared to Nafion 117. Three relaxation processes were found for Flemion SH150 equilibrated in water activity higher than 0.75, while two

relaxation processes were found for samples equilibrated in water activity of 0.33. These relaxation processes are essentially identical to those of Nafion membrane. The “free” and “hydrophobically confined” water are found to start to appear at lower water content in Flemion than in Nafion. These results suggest that Flemion SH150 membrane is likely to form larger and/or more numerous ionic cluster regions.

5. Manipulation of dimethyl sulfoxide content was tried to increase the fraction of the “free water” due to its strong ability to form hydrogen bonding with water molecules. The average number of hydrogen bonds per water molecule in DMSO/water mixtures is found to be reduced from that in pure water in the dilute solutions. This effect was caused by the “breaking effect” of DMSO, i.e. the breakdown of the hydrogen bond network of water by DMSO molecules. The dielectric properties of the Nafion/DMSO/water system were also measured at 25^{o}C. Two relaxation processes were observed for the Nafion containing DMSO, which is in contrast to Nafion/water systems. The water molecules associated with the side chains and polymer backbone in the Nafion membrane are removed by addition of DMSO molecules. Also, the fraction of the solvent mixture in the “free” state was shown to be significantly increased compared to the fraction of free water in Nafion membrane. This increase leads to increasing conductivity of Nafion/DMSO at lower water content compared to Nafion. However, the Nafion membrane treated with DMSO has lower conductivity at high water contents. This can be explained by the lower relaxation times for the solvent mixture compared to pure water.

Considering future work, the following is planned after the completion of this thesis:

1. The hydrogen bonding networks provide a conducting pathway for proton in perfluorosulfonic acid membranes. It is necessary to investigate more systematically the hydrogen bonding structure of water in PEM membranes. The FTIR, Raman spectroscopy, and X-ray or neutron scattering techniques may be used for this purpose.

2. Measurements of the self-diffusion coefficient of water using an NMR method combining the pulsed-field gradient spin-echo (PGSE) technique. By comparing the proton mobility, water self-diffusion coefficient, and dielectric relaxation time, the rate-controlling process for proton transport may be discriminated and the proton conduction mechanism may be established as well.

3. From a practical view, the incorporation of other organic or inorganic molecules which can form hydrogen bonds with water will be systematically investigated. The influence of these molecules on the state and dynamics of water needs to be studied.

VITA

Zijie Lu

Zijie Lu was born on December 2, 1972 in Hubei, China. He matriculated at the Huazhong University of Science and Technology, Wuhan, China, and graduate with a B.S. in Materials Science and Engineering in 1994. He earned his Master's degree in Materials Science and Engineering in 1997 at Institute of Metal Research (IMR), Chinese Academy of Sciences (CAS), Shenyang, China. He was hired as a research engineer in The State Key Laboratory of Corrosion and Protection, Chinese Academy of Sciences in 1997.

Zijie Lu entered the doctoral program in Materials Science and Engineering at The Pennsylvania State University in September 2001, and has presented several papers on his research work.